Phytoplankton variability in the Atlantic and Indian sectors of the Southern Ocean: a biogeochemical approach

IAN J.D. WEIR

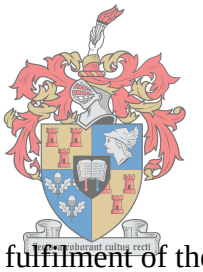

This is submitted in fulfilment of the requirements of a

MASTER OF EARTH SCIENCE DEGREE

December 2018

Department of Earth Science, Stellenbosch University

Supervisor: Dr Susanne Fietz

Declaration

I hereby declare that the entirety of the work contained herein is my own, original work and that I am the authorship owner thereof (unless explicitly otherwise stated). I have not previously submitted in part, or in its entirety, the work presented herein to obtain any qualification. This thesis is submitted in fulfilment of a Master of Science in the department of Earth Science, Stellenbosch University.

Full name: Ian J.D. Weir

Signature: ……

Signed on…… Day of…….2018

Acknowledgements

First and foremost, my most sincere gratitude is extended to my supervisor, Dr. Susanne Fietz for your guidance and mentorship throughout the project. You are an inspiring mentor and someone whom leads by example, qualities which I hold in high regard. You have been a pleasure to work with and I look forward to the continued development of this project through your guidance. To Prof. Alakendra Roychoudhury, your guidance, input and willingness to answer my endless questions played a big role in this project, and for that I am grateful. To Dr Sarah Fawcett and Dr David Walker you were fundamental in bringing this project together and it has been a pleasure getting to know you, I look forward to future collaborations.

I am grateful toward The National Research Foundation (NRF) of South Africa for their financial support, without which, this project would not have been possible. A huge thank you goes out to all those involved in the cruise, Captain Knowledge Bengu and the crew of the SA Agulhas II and most importantly The Stellenbosch University TracEx team – Johan, Ismael, Ryan and Jean. Without a team effort, none of our research is possible and I am greatly indebted to you all for your contribution in bringing this project together.

To my mother, Felicity Henman-Weir and stepfather, Gerhard Diedricks, you started me on this journey a long time ago instilling a love and appreciation for science from a young age. You have always inspired me to follow my interests and for that, I express my most sincere gratitude. To my father, Kim Weir your unquestionable loyalty and the pride you take in my endeavours has provided me with confidence to tackle any challenge. Determination and dedication is something I would not have had without your influence. I would like to thank you all for affording me the opportunity to pursue my dreams and your unwavering support. Lastly, my love goes to my late grandfather, J.D. Weir, to whom this thesis is dedicated.

Abstract

The Southern Ocean is identified as a key component in the global carbon cycle due to a unique combination of physical circulation and biological processes. In light of a predicted changing climate, understanding *in-situ* environmental and biological processes becomes fundamentally important for improving biogeochemical models. Phytoplankton variability in the Indian and Atlantic Southern Ocean are assessed both spatially and temporally, in terms of the unique physical and chemical environments encountered in the major oceanic zones of the Southern Ocean. The approach identified the Polar Front as an important biogeochemical boundary in both summer and winter waters, separating silicic acid replete, diatom-dominated southern waters from northern waters associated with lower silicic acid concentrations and greater flagellate contribution. Summer waters along a 0 °E meridian (Atlantic Southern Ocean) were characterized by high chlorophyll-a (up to 0.56 µg/L) concentrations and bloom conditions at certain stations, which, in some instances were correlated to an influx of trace metals. Studying a suite of trace metal distributions proved to be an important additional variable in understanding phytoplankton variability, as certain metals seemed to be preferentially utilized, possibly driving underutilization of other metals, although it is unclear whether these events were mutually exclusive. Furthermore, it allowed for the association of certain trace metals to specific phytoplankton groups e.g. Zn, Mn distributions were positively correlated with diatoms. Our results indicate a complex relationship between the phytoplankton community and trace metal distribution, as it was unclear whether trace metal distributions drive the community composition or the community composition drives trace metal distributions. . Winter waters along a 30 °E meridian (Indian Southern Ocean) were characterized by deep mixed layers, limited irradiance and cold surface waters with strong vertical mixing. Biomass indicators (biogenic silica, <0.77 µM; chlorophyll-a, <0.37 µg/L) point toward a winter water column that is more productive than previously thought and comparable to both summer (biogenic silica, <2.17 µM; chlorophyll-a, <0.57 µg/L) and spring (<0.36 µg/L) communities. Diatom contribution was shown to be more significant in the winter Antarctic Zone than summer waters, with heavily silicified *Fragilariopis* spp. being the greatest contributor to winter biomass, which may have implications for silicic acid cycling. Picoplankton biomass was also thought to be more important in summer waters than winter waters, which may have implications for micro- and macronutrient cycling, further

demonstrating the importance of understanding seasonal progressions. This study highlighted the use of combining an array of environmental and physical variables in the interpretation of phytoplankton variability, further demonstrating the need for regional and seasonal differentiation in future studies.

Opsomming

Die suidelike oseaan is geïdentifiseer as 'n belangrike komponent in die wêreldwye koolstof siklus, meestal as gevolg van 'n unieke kombinasie van fisiese sirkulasie en biologiese prosesse. In die lig van voorspelde klimaat verandering is ‘n begrip van *in-situ* omgewings- en biologiese prosesse fundamenteel in die verbetering van biogeochemiese modelle. Phytoplankton variasie in die Indiese en Atlantiese Suidelike Oseaan word geografies en oor tyd geassesseer deur verskeidenheid van biogeochemiese veranderlikes te kombineer met veelvuldige parameter lesings. Die benadering help met die karakterisering van beide somer en winter waters in terme van hulle geassosieerde oseaniese sones. Hierdie benadering het die Polêre Front geïdentifiseer as 'n belangrike biogeochemiese grens in beide somer en winter waters. Die suidelike oseaan verskil in terme van sy silika suur, diatoom-dominerende waters teenoor die noordelike waters met laer silika suur konsentrasies en groter flagellate dominasie. Somer waters langs die 0 °E meridiaan (Atlantiese Suidelike Oseaan) was gekenmerk deur hoë chlorofil-a konsentrasies en hoë alge groei toestande by sommige stasies, wat in sommige gevalle korreleer met die teenwoordigheid van spoor metale. Die veelvuldige parameter benadering wat 'n verskeidenheid spoor metale meet is uitgewys as ‘n fundamentele aspek, met sekere metale wat lyk of hul voorkeurig benut word, en heel moontlik die mindere gebruik van ander metale dryf. Die veelvuldige parameter benadering het verder toegelaat vir die assosiasie van sekere spoorelement metale met spesifieke phytoplankton groepe, bv. Zn, Mn verspreidings was gekorreleer met diatome. Ten spyte van die bogenoemde assosiasie was dit onduidelik of spoor metaal verspreidings die gemeenskap samestelling dryf of nie. In vergelyking, was die winter waters parallel met die 30 °E meridiaan (Indiese Suidelike Oseaan) gekenmerk deur diep gemengde lae, beperkte radiasie en koue oppervlak waters met sterk vertikale vermenging. Biomassa indikators verwys na 'n winter water kolom wat meer produktief is as voorheen bekend, en is vergelykbaar met beide somer en lente biomassas. In die Antarktiese Zone blyk die diatoom bydrae as meer beduidend in winter teenoor somer waters, met *Fragilariopis* spp. die mees bydraend tot winter biomassas. In somer waters blyk dit Picoplankton biomassa is meer belangrik as in die winter, met moontlike implikasies vir die biogeochemiese siklus. Die implikasie demonstreer verder die belangrikheid van insig en begrip in seisoenale veranderings. Met die gebruik van veelvuldige parameter veranderlikes in die interpretasie van phytoplankton variasie, het die studie die belangrikheid van geografiese en seisoenale verskille demonstreer.

Table of Contents

List of Figures

List of Tables

List of Abbreviations

ACC – Antarctic Circumpolar Current

bSi – biogenic silica

chla –chlorphyll-a

CTD – conductivity-temperature-depth

HNLC – High Nutrient Low Chlorophyll

ICP-MS – Inductively Coupled Plasma Mass Spectrometry

LNLC – Low Nutrient Low Chlorophyll

MIZ – Marginal Ice Zone

ML – mixed layer

MLD – mixed layer depth

PAR – Photosynthetically Active Radiation

PF – Polar Front

PFZ – Polar Frontal Zone

S. Africa – South Africa

S. Georgia – South Georgia

SACCf – Southern Antarctic Circumpolar front

SAF – Sub-Antarctic Front

SALH – Silicic Acid Leakage Hypothesis

SANAE – South African National Antarctic Expedition

SAZ – Sub-Antarctic Zone

SBdy – Southern Boundary

SIZ – Seasonal Ice Zone

St. – station

STF – Sub-Tropical Front

STZ – Sub-Tropical Zone

WG – Weddell Gyre

Chapter 1

1.1. Introduction

The Southern Ocean is identified as a key component in the global carbon cycle due to a unique combination of physical circulation and biological processes, such as the removal of carbon dioxide (CO_2) by phytoplankton (Deppeler and Davidson, 2017). Global oceans facilitate the fixation of inorganic, atmospheric carbon through different pumps, namely the biological pump and the solubility pump (Sarmiento and Gruber, 2004). The biological pump is driven by phytoplankton that convert inorganic CO_2 into organic matter that may then be exported to the deep ocean, removing CO_2 from upper oceanic and atmospheric inventories (Sarmiento and Gruber, 2004). The Southern Ocean is of particular interest as it accounts for an estimated 40 % of global oceanic uptake of anthropogenic CO_2 (Caldeira and Duffy, 2000). Globally, the efficiency of the biological pump is governed by several factors that stem from phytoplankton's environmental and biogeochemical requirements. Important environmental factors are, for example, seasonal variations in temperature and salinity, irradiance and water column mixing. Additionally, biogeochemical requirements like the availability of macronutrients such as silicic acid ($Si(OH)_4$), nitrate (NO_3^-) and phosphate (PO_4^{3-}) as well as a suite of essential trace metals or micronutrients (such as Fe, Zn, Co etc.) place important controls on productivity and therefore the efficiency of the biological pump.

The significance of macro- and micronutrient availability is highlighted by the fact that large areas of the Southern Ocean are characterised by an unusual phenomenon where high concentrations of macronutrients are coupled with low chlorophyll-a (chla) concentrations (Sunda, 1991). This phenomenon is known as the Southern Ocean paradox (Sunda, 1991), defining the Southern Ocean as a High Nutrient Low Chlorophyll (HNLC) region. Numerous studies have attributed the HNLC waters of the Southern Ocean to a scarcity of micronutrients, in particular iron, which are essential in phytoplankton's metabolic functions (Sunda and Huntsman, 1995; Moffett and Ho, 1996; Takeda, 1998; Frew et al., 2001). It is therefore important to study the links between phytoplankton communities and biogeochemical variables, such as macro- and micronutrients concentrations, across different oceanic zones to better understand factors driving phytoplankton variability in the Southern Ocean.

In addition to the large spatial variability, the Southern Ocean reflects large seasonal and environmental fluctuations in productivity (Deppeler and Davidson, 2017). Satellite imaging and *in-situ* measurements conducted in the summer and spring periods indicate that these seasons support a profusion of phytoplankton biomass, making summer and spring the focal points of most biogeochemical studies (e.g. Antoine et al., 1996; Fiala et al., 1998; Gibberd et al., 2013). Consequently, the comparatively large data set generated from these seasons is used in the compilation of oceanic and climate prediction models, thereby creating the potential for seasonal bias. Winter biogeochemical studies are scant, as winter is deemed largely unproductive and further overlooked due to logistical constraints, although, almost 30 years ago, Prog et al. (1987) found winter waters to be more productive than previously thought. In light of a changing climate, some regions in Antarctica, such as the West Antarctic Peninsula, are experiencing rapid warming (Vaughan et al., 2003) while others have experienced an increase in winter sea ice extent (Turner et al., 2009), likely inducing changes in planktonic responses and biogeochemical cycles. Therefore, to fully understand current and future biogeochemical cycling in the Southern Ocean, understanding seasonal progressions, including the winter period, becomes fundamentally important in providing accurate input for climate prediction models.

To investigate such spatial and seasonal variabilities, a multi-variable approach, which included biological, chemical and physical variables, was implemented in this study to assess phytoplankton variability across a latitudinal gradient. The overall aim is to better understand the environmental conditions driving the *in-situ* phytoplankton community. Diatoms, a dominant Southern Ocean phytoplankton group, are documented as a major contributor to nutrient cycling and carbon export (e.g. Buesseler et al., 2005; Romero and Armand, 2010) and are a focal point of this study. Therefore, a combination of analytical techniques, including microscopy and the chemical analysis of seawater, are utilized to better understand *in-situ* summer and winter phytoplankton communities across the Southern Ocean.

The first objective of this project is to characterise the relationship between the surface phytoplankton community, macronutrients and essential micronutrients across the different oceanic zones of the summer Atlantic Southern Ocean. This includes an assessment of the phytoplankton community using characteristic marker pigments and group-specific indicators such as biogenic silica (bSi). The second objective of this project focusses on environmental

drivers and biogeochemical consequences of diatom and bSi distributions across the winter Indian Southern Ocean. The final objective is to compare summer and winter phytoplankton communities and their associated environments. The first two objectives are addressed in this thesis in the form of two separate manuscripts, which have been edited to fit the chapter format of this thesis, with concluding remarks addressing the third objective, and recommendations for future research at the end of this thesis. The two manuscripts are as follows:

I. Weir, I.J., Viljoen J.J., Fietz, S., Cloete, R., Loock, J.C., Philibert, R., Roychoudhury, A.N. Links between phytoplankton community composition, macronutrient and trace metal distribution in the surface waters of the Atlantic Southern Ocean. *Prepared for submission to Limnology and Oceanography.*

II. Weir, I.J., Fawcett, S., Walker, D., Bornman, T., Fietz, S. Winter biogenic silica and diatom distribution in the Indian Sector, Southern Ocean. *Prepared for submission to Deep Sea Research I.*

1.2. Background

1.2.1. Introduction

Marine biogeochemistry is the study of chemical, physical, geological and biological processes and reactions that govern the chemical composition of the marine environment. Of particular interest in the oceans are the processes relating to- and cycling of, carbon due to its role in the greenhouse effect on our climate. Global oceans are documented as a large anthropogenic CO_2 sink, accounting for an estimated 30 % of anthropogenic CO_2 removal (Falkowski and Raven, 2007). It is estimated that of this global 30 %, the Southern Ocean alone accounts for 40 % of absorption of oceanic anthropogenic CO_2 storage (Caldeira and Duffy, 2000). In the ocean, CO_2 is regulated by a number of processes, namely the solubility pump, biological pump and carbonate counter-pump (Caldeira and Duffy, 2000). The solubility pump controls the processes of dissolution and dissociation of CO_2 between the atmosphere and oceans (Ito and Follows, 2003). This pump demonstrates the temperature dependence of CO_2 solubility, with the CO_2

molecules being more than twice as soluble in cold, high latitude waters (Weiss, 1974) than warmer, low latitude waters. The carbonate counter-pump is a biological mechanism driven by calcareous photosynthetic organisms in which the calcium carbonate shells they produce are remineralized and CO_2 is incorporated back into the oceanic and atmospheric inventories (Sarmiento and Gruber, 2004). The biological pump is of particular significance in this study, due to the involvement of photosynthetic organisms, such as phytoplankton, which are responsible for the fixation of dissolved inorganic carbon into organic matter. Carbon, in the form of organic matter, is then exported to the deep ocean as settling faecal pellets and dead biota, where it may be stored on the ocean floor for centuries (Ducklow et al., 2001). Figure 1.1 illustrates the complex interplay between biotic and abiotic factors, which govern carbon cycling and export to the deep ocean. In terms of carbon cycling and export, the Southern Ocean is of particular significance (Deppeler and Davidson, 2017) and will further be discussed in sections to follow.

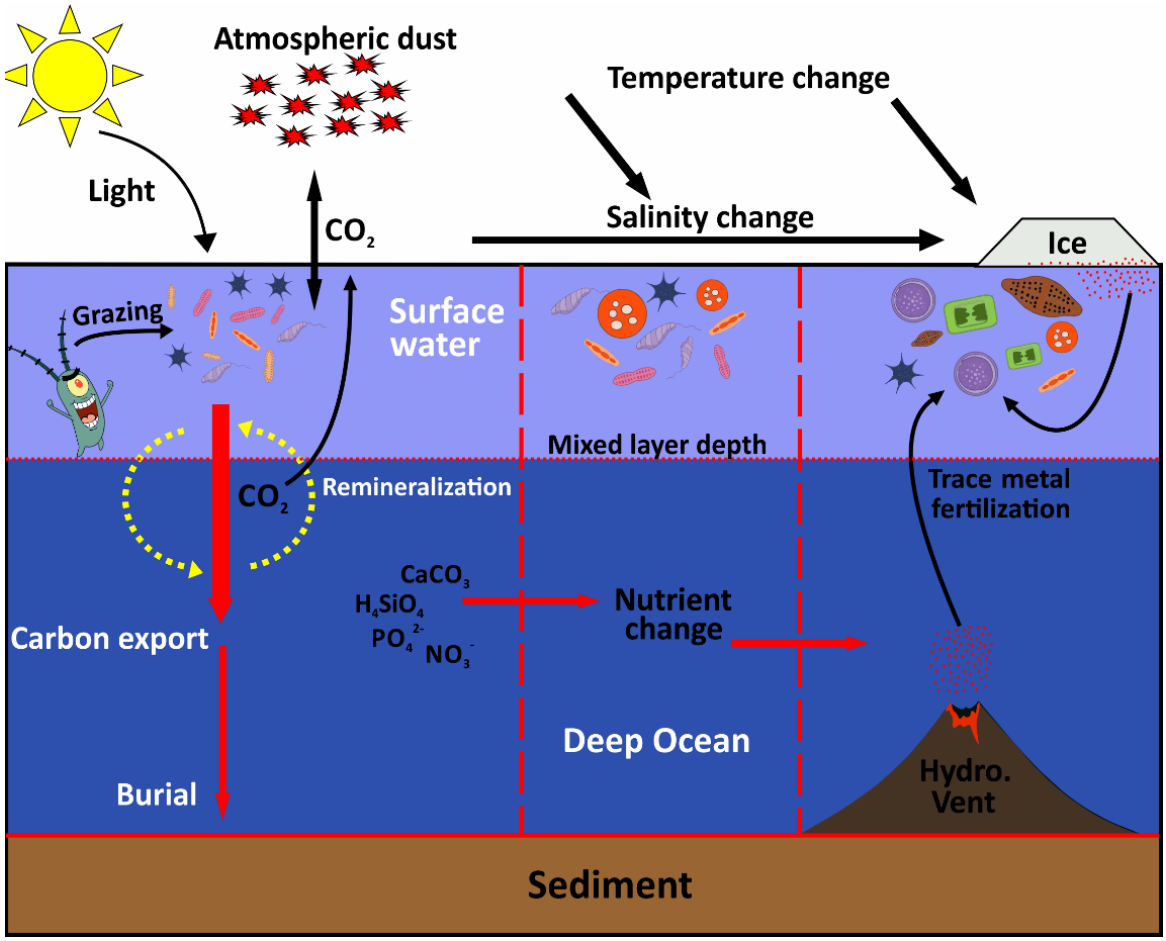

Figure 1.1 Schematic illustrating the biological carbon pump and biotic and abiotic factors which govern the cycling of macro- and micronutrients (trace metals) in the ocean.

1.2.2. Southern Ocean

The Southern Ocean, also known as the Antarctic Ocean, forms part of the Pacific, Atlantic and Indian ocean basins as well as the tributary seas, such as the Ross Sea, surrounding Antarctica (Rintoul et al., 2001). The Southern Ocean plays a fundamental role in driving, modifying and regulating global climate change, largely due to a combination of cold deep water masses and the presence of the world's largest ocean current, the Antarctic Circumpolar Current (ACC). The ACC is unhindered by land and therefore laterally continuous, connecting the three ocean basins mentioned above (Rintoul et al., 2001). This interbasin connection allows for global overturning circulation to exist, permitting for the transfer of heat, freshwater, nutrients, and CO_2 (Rintoul et al., 2001). The ACC is comprised of three major fronts, the Polar Front (PF), Subantarctic Front (SAF) and Polar Front (PF; Fig 1.2), which form important biogeochemical boundaries. The fronts separate four distinct water masses or zones on the basis of differences in physical and chemical properties; the Antarctic Zone (AAZ), Polar Frontal Zone (PFZ), Subantarctic Zone (SAZ) and the Subtropical Zone (SAZ).

As such, these oceanic zones can be very different from one another, not only in terms of their physical and chemical properties, but also in terms of the resulting biology. The PF exemplifies such a relationship, separating LNLC/oligotrophic subtropical waters to the north from HNLC waters to the south (Bowie et al., 2011). These low chlorophyll waters to the south of the PF are typically characterized by phytoplankton communities dominated by diatoms (Smetacek et al., 1997; Gibberd et al., 2013) and high concentrations of macronutrients; nitrate, phosphate and silicic acid. Whereas waters north of the PF have been shown to have a greater flagellate contribution (Fiala et al., 1998; Becquevort et al., 2000). The unusual phenomenon whereby high macronutrient concentrations persist south of the PF, albeit relatively low biomass is known as the Southern Ocean paradox. Several studies have postulated that low biomass encountered in macronutrient-replete waters of the Southern Ocean arise due to a limitation of essential micronutrients or trace metals (Martin et al., 1990; Sunda, 1991; Frew et al., 2001), this concept will be further expanded on in Section 1.2.3.

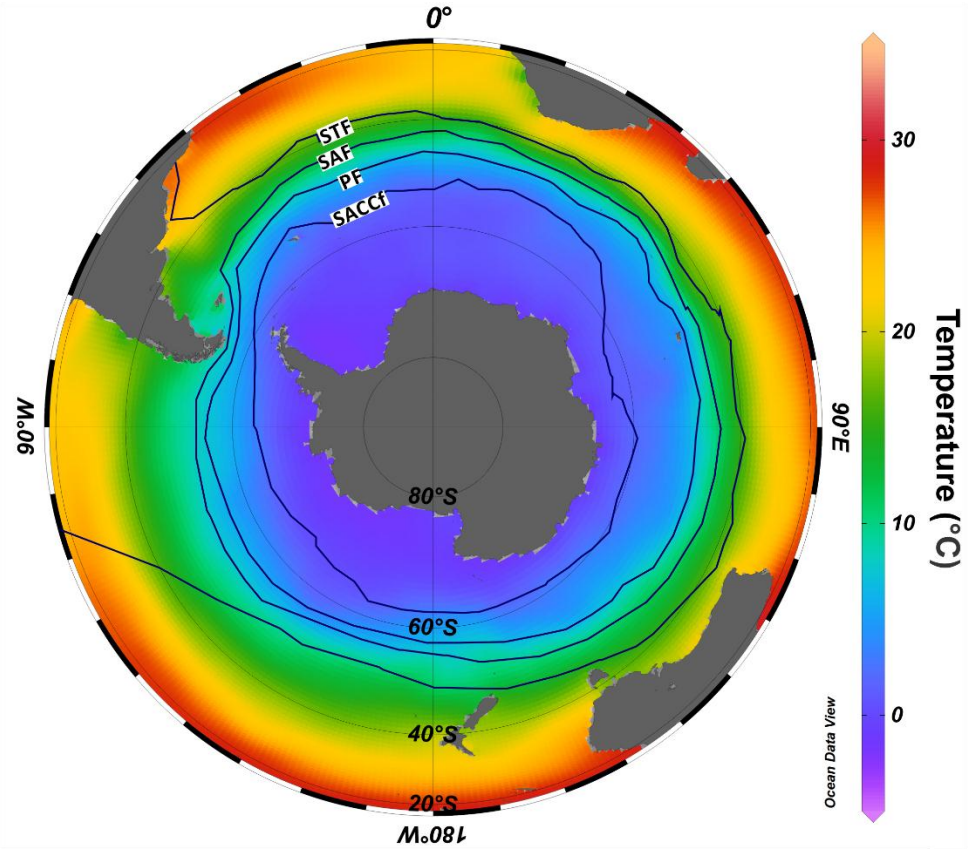

Figure 1.2 Schematic illustration of frontal locations and average sea surface temperature in the Southern Ocean. SACCf, Southern Antarctic Circumpolar Front; PF, Polar Front; SAF, Subantarctic Front; STF, Subtropical Front. The figure was constructed on Ocean Data View (ODV**;** Schiltzer, 2018) using the World Ocean Database for average sea surface temperature.

1.2.3. Macro- and micronutrients

The Southern Ocean paradox arises as in addition to macronutrients, phytoplankton require micronutrients or trace metals in particular proportions, which are defined by the extended Redfield Ratio (180C: 23N: 1P: $5x10^{-3}$Fe: $2x10^{-3}$Zn: $1x10^{-3}$Mn: $5x10^{-4}$Ni: $4x10^{-4}$Cd: $2x10^{-4}$Cu: $4x10^{-5}$Co; Ito and Follows, 2003). The presence of replete macronutrient concentrations in the Southern Ocean coupled with low phytoplankton biomass suggests macronutrients are inefficiently utilized, thereby decreasing the efficiency of the biological pump. Micronutrients have been recorded in the nano- to picomolar range throughout the Southern Ocean (e.g. Croot et al., 2011; Klunder et al., 2011; Abouchami et al., 2014) and are known to be an important factor, in conjunction with light, that limits phytoplankton productivity. Micronutrients are responsible for an array of metabolic functions and play an essential role in algal physiology (Twining and Baines, 2013). For instance, iron is required in the enzyme that catalyses carbon and nitrogen fixation, zinc is part of the carbonic anhydrase, responsible for the hydration and dehydration of

CO_2, while manganese is essential for oxygen-evolving enzymes, responsible for the oxidation of water during photosynthesis (Twining and Baines, 2013). Metal requirements differ between phytoplankton groups and can fluctuate in response to changes in environmental conditions (e.g. Viljoen et al. *submitted*).

Environmental changes brought about by seasonality, such as changes in temperature, can greatly influence macro- and micronutrient distributions, and in turn the phytoplankton community in the Southern Ocean. Due to the replete nature of macronutrient concentrations in large areas of the Southern Ocean, seasonal changes in micronutrient concentrations are more pronounced. It is well documented that the mixed layer depth shoals in summer waters (70 – 100 m in the SAZ for example), while mixed layer depths in winter have been recorded as deep as 600 m in some instances (Alexander et al., 2000; Deppeler and Davidson, 2017). Wind and temperature driven deep winter mixed layers have access to deeper reservoirs of micro- and macronutrients, resupplying the depleted pre-existing summer waters (Swart et al., 2015). For example, a recent study done by Cloete et al. (*submitted*), comparing summer and winter water columns, established that winter waters were characterized by higher concentrations of copper, zinc and nickel in the mixed layer than summer waters. Further seasonal influences such as the extent and melting of sea ice, influence micronutrient distributions. For instance, melting of sea ice during the summer period is documented as an important micronutrient source and is often associated with phytoplankton blooms (Martin et al., 1990; Fitzwater et al., 2000;). Therefore, micronutrient distributions are one of many variables that shape the phytoplankton community composition and are an essential additional biogeochemical variable in understanding phytoplankton community distribution.

1.2.4. Phytoplankton communities

In addition to macro- and micronutrients, other environmental variables such as light, salinity, temperature and the mixed layer depth (Arrigo, 1999) shape the community composition. Such variables also fluctuate seasonally, as summer waters are exposed to greater irradiance and higher sea surface temperatures (SST) than winter waters. For instance, coccolithophores in the Australian Sector of the Southern Ocean are generally reported in an optimum temperature range of 2 – 15.7 °C (Findlay and Giraudeau, 2000). Sea surface temperatures that do not fall in this range will not favour coccolithophore growth. Diatoms have been shown to dominate waters

with highly stratified water columns associated with shallower mixed layers, while *Phaeocystis antarctica* dominate communities of deep mixed layers (Arrigo et al., 1999).

The HNLC waters of the Southern Ocean are, broadly speaking, dominated by diatoms and flagellates (e.g. *Phaeocystis*) as seen by Figure 1.3 (Alvain et al., 2011). Flagellates dominate the pico- and nano-phytoplankton size fraction, while the micro-phytoplankton size range is typically dominated by large, heavily silicified diatoms (Smetacek et al., 1997; Gibberd et al., 2013). Localized summer and spring phytoplankton blooms are triggered by localized trace metal inputs, and are often associated with diatoms and flagellates, which have high nutrient requirements and faster growth rates (Arrigo et al., 1999).

Therefore, to fully understand phytoplankton variability across a latitudinal gradient a number of physical, environmental, biological and chemical factors need to be considered. This reiterates the notion of studying phytoplankton communities in terms of their associated oceanic zones, as in light of predicted changing ocean dynamics (Deppeler and Davidson, 2017), the community response is expected to differ in the distinct oceanic zones of the Southern Ocean. As such, community variability will be assessed across a latitudinal gradient in the Atlantic Southern Ocean (Chapter 2) and the Indian Southern Ocean (Chapter 3).

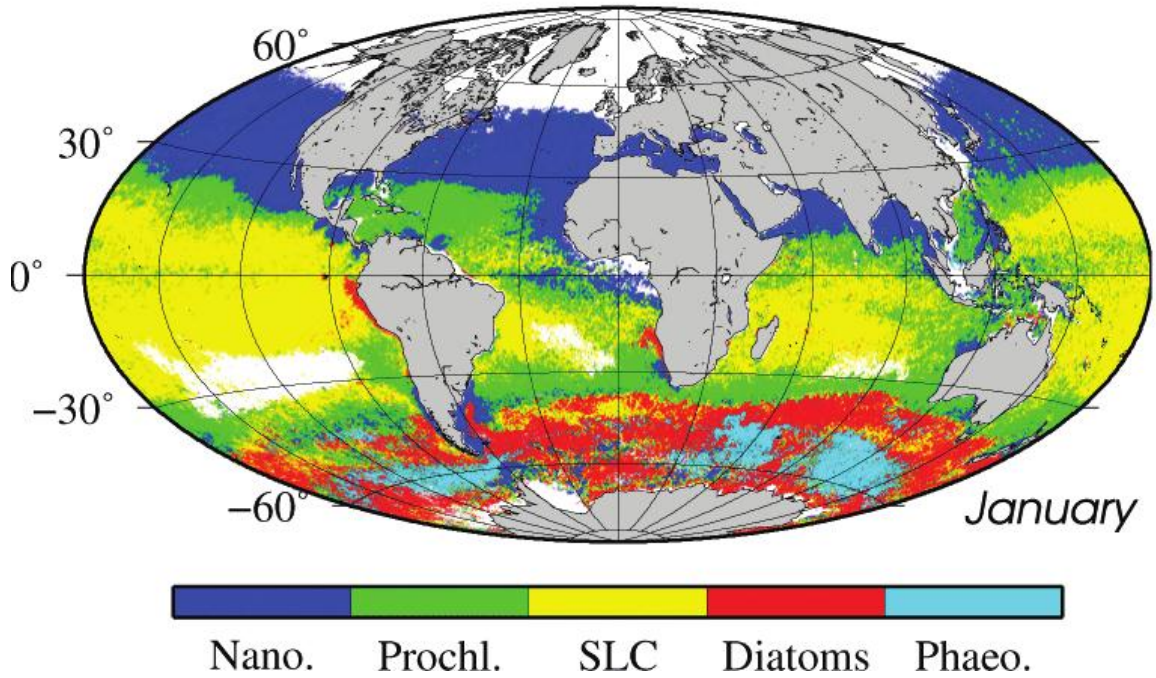

Figure 1.3 Climatology maps (1997 – 2008, SeaWiFS) of the dominant phytoplankton groups in January, projected using PHYSAT. Nano., nanophytoplankton; Prochl., Prochlorococcus; SLC, Synechococcus-like cyanobacteria; Phaeo., Phaeocystis (Alvain et al., 2011).

References

Abouchami, W., Galer, S.J.G., de Baar, H.J.W., Middag, R., Vance, D., Zhao, Y., Klunder, M., Mezger, K., Feldmann, H., Andreae, M.O., 2014. Biogeochemical cycling of cadmium isotopes in the Southern Ocean along the Zero Meridian. Geochim. Cosmochim. Acta 127, 348–367. https://doi.org/10.1016/J.GCA.2013.10.022

Alexander, M.A., Scott, J.D., Deser, C., 2000. Processes that influence sea surface temperature and ocean mixed layer depth variability in a coupled model. J. Geophys. Res. Ocean. 105, 16823–16842. https://doi.org/10.1029/2000JC900074

Alvain, S., Duforêt-Gaurier, L. Loisel, H., 2011. Observation of ocean colour beyond chlorophyll-a, in Handbook of Satellite Remote Sensing Image Interpretation: Applications for Marine Living Resources Conservation and Management, viewed 29 August 2018, from http://www.ioccg.org/handbook/casestudy5_alvain_etal.pdf

Antoine, D., André, J.-M., Morel, A., 1996. Oceanic primary production: 2. Estimation at global scale from satellite (Coastal Zone Color Scanner) chlorophyll. Global Biogeochem. Cycles 10, 57–69. https://doi.org/10.1029/95GB02832

Arrigo, K.R., Robinson, D.H., Worthen, D.L., Dunbar, R.B., DiTullio, G.R., VanWoert, M., Lizotte, M.P., 1999. Phytoplankton community structure and the drawdown of nutrients and CO2 in the Southern Ocean. Science 283, 365–367. https://doi.org/10.1126/SCIENCE.283.5400.365

Bowie, A.R., Brian Griffiths, F., Dehairs, F., Trull, T.W., 2011. Oceanography of the subantarctic and Polar Frontal Zones south of Australia during summer: Setting for the SAZ-Sense study. Deep Sea Res. Part II Top. Stud. Oceanogr. 58, 2059–2070. https://doi.org/10.1016/j.dsr2.2011.05.033

Buesseler, K.O., Andrews, J.E., Pike, S.M., Charette, M.A., Goldson, L.E., Brzezinski, M.A., Lance, V.P., 2005. Particle export during the Southern Ocean Iron Experiment (SOFeX). Limnol. Oceanogr. 50, 311–327. https://doi.org/10.4319/lo.2005.50.1.0311

Caldeira, K., Duffy, P.B., 2000. The Role of the Southern Ocean in Uptake and Storage of Anthropogenic Carbon Dioxide. Science 287, 620–622. https://doi.org/10.1126/science.287.5453.620

Cloete, R., Loock, J.C., Mtshali, T.N., Fietz, S., Roychoudhury, A.N., *submitted*. Winter and summer distributions of Copper, Zinc and Nickel along the International GEOTRACES section GIPY05: Insights into deep winter mixing. Chem. Geol.

Croot, P.L., Baars, O., Streu, P., 2011. The distribution of dissolved zinc in the Atlantic sector of the Southern Ocean. Deep Sea Res. Part II Top. Stud. Oceanogr. 58, 2707–2719. https://doi.org/10.1016/j.dsr2.2010.10.041

Deppeler, S.L., Davidson, A.T., 2017. Southern Ocean Phytoplankton in a Changing Climate. Front. Mar. Sci. 4, 40. https://doi.org/10.3389/fmars.2017.00040

Ducklow, H.W., Steinberg, D.K., Buesseler, K.O., 2001. Upper Ocean Carbon Export and the Biological Pump. Oceanogr.

Falkowski, P.G., Raven, J.A., 2007. Photosynthesis and primary production in nature, in: Chapter 9 in Aquatic Photosynthesis, 2nd ed, Princeton University Press, Princeton.

Fiala, M., Semeneh, M., Oriol, L., 1998. Size-fractionated phytoplankton biomass and species composition in the Indian sector of the Southern Ocean during austral summer. J. Mar. Syst. 17, 179–194. https://doi.org/10.1016/S0924-7963(98)00037-2

Findlay, C.S., Giraudeau, J., 2000. Extant calcareous nannoplankton in the Australian Sector of the Southern Ocean (austral summers 1994 and 1995). Mar. Micropaleontol. 40, 417–439. https://doi.org/10.1016/S0377-8398(00)00046-3

Fitzwater, S.E., Johnson, K.S., Gordon, R.M., Coale, K.H., Smith, W.O., 2000. Trace metal concentrations in the Ross Sea and their relationship with nutrients and phytoplankton growth. Deep Sea Res. Part II Top. Stud. Oceanogr. 47, 3159–3179. https://doi.org/10.1016/S0967-0645(00)00063-1

Frew, R., Bowie, A., Croot, P., Pickmere, S., 2001. Macronutrient and trace-metal geochemistry of an in-situ iron-induced Southern Ocean bloom. Deep Sea Res. Part II Top. Stud. Oceanogr. 48, 2467–2481. https://doi.org/10.1016/S0967-0645(01)00004-2

Gibberd, M.J., Kean, E., Barlow, R., Thomalla, S., Lucas, M., 2013. Phytoplankton chemotaxonomy in the Atlantic sector of the Southern Ocean during late summer 2009. Deep Sea Res. Part I Oceanogr. Res. Pap. 78, 70–78. https://doi.org/10.1016/j.dsr.2013.04.007

Ito, T., Follows, M.J., 2003. Upper ocean control on the solubility pump of CO_2. J. Mar. Res. 61, 465–489. https://doi.org/10.1357/002224003322384898

Klunder, M.B., Laan, P., Middag, R., de Baar, H.J.W., van Ooijen, J.C., 2011. Dissolved iron in the Southern Ocean (Atlantic sector). Deep Sea Res. Part II 58, 2678–2694. https://doi.org/10.1016/j.dsr2.2010.10.042

Martin, J.H., Gordon, R.M., Fitzwater, S.E., 1990. Iron in Antarctic waters. Nature 345, 156–158. https://doi.org/10.1038/345156a0

Moffett, J.W., Ho, J., 1996. Oxidation of cobalt and manganese in seawater via a common microbially catalyzed pathway. Geochim. Cosmochim. Acta 60, 3415–3424. https://doi.org/10.1016/0016-7037(96)00176-7

Prog, S., Kottmeier, S.T., Sullivan, C.W., 1987. Late winter primary production and bacterial production in sea ice and seawater west of the Antarctic Peninsula. Mar. Ecol. Prog. Ser. 36, 287-298.

Rintoul, S., Hughes, C., Olbers, D., 2001. The Antarctic Circumpolar Current System, Ocean Circulation and Climate. Int. Geophys. Ser 77, 271-302.

Romero, O.E., Armand, L.K., 2010. Marine diatoms as indicators of modern changes in oceanographic conditions. The diatoms: applications for the environmental and earth sciences, 2nd ed, 373–400, Cambridge University Press, London, Editors: Smol J.P. and Stoermer E.F.

Sarmiento, J.L., Gruber, N., 2004. Ocean Biogeochemical Dynamics Chapter 10: Oceanic carbon cycle, atmospheric CO2, and climate. Princeton University Press, Princeton.

Smetacek, V., De Baar, H.J.W., Bathmann, U.V., Lochte, K., Rutgers Van Der Loeff, M.M., 1997. Ecology and biogeochemistry of the antarctic circumpolar current during austral spring: a summary of Southern Ocean JGOFS cruise ANT X/6 of R.V. Polarstern. Deep Sea Res. Part II Top. Stud. Oceanogr. 44, 1–21. https://doi.org/10.1016/S0967-0645(96)00100-2

Sunda, W.G., 1991. Trace Metal Interactions with Marine Phytoplankton. Biol. Oceanogr. 6, 411–442.

Sunda, W.G., Huntsman, S.A., 1995. Iron uptake and growth limitation in oceanic and coastal phytoplankton. Mar. Chem. 50, 189–206.

Swart, S., Thomalla, S.J., Monteiro, P.M.S., 2015. The seasonal cycle of mixed layer dynamics and phytoplankton biomass in the Sub-Antarctic Zone: A high-resolution glider experiment. J. Mar. Syst. 147, 103–115. https://doi.org/10.1016/j.jmarsys.2014.06.002

Takeda, S., 1998. Influence of iron availability on nutrient consumption ratio of diatoms in oceanic waters. Nature 393, 774–777. https://doi.org/10.1038/31674

Turner, J., Comiso, J.C., Marshall, G.J., Lachlan-Cope, T.A., Bracegirdle, T., Maksym, T., Meredith, M.P., Wang, Z., Orr, A., 2009. Non-annular atmospheric circulation change induced by stratospheric ozone depletion and its role in the recent increase of Antarctic sea ice extent. Geophys. Res. Lett. 36, L08502. https://doi.org/10.1029/2009GL037524

Twining, B.S., Baines, S.B., 2013. The Trace Metal Composition of Marine Phytoplankton. Ann. Rev. Mar. Sci. 5, 191–215. https://doi.org/10.1146/annurev-marine-121211-172322

Vaughan, D.G., Marshall, G.J., Connolley, W.M., Parkinson, C., Mulvaney, R., Hodgson, D.A., King, J.C., Pudsey, C.J., Turner, J., 2003. Recent Rapid Regional Climate Warming on the Antarctic Peninsula. Clim. Change 60, 243–274. https://doi.org/10.1023/A:1026021217991

Viljoen, J.J., Philibert, R., van Horsten, N., Mtshali, T., Roychoudhury, R.N., Thomalla, S., Fietz, S., *submitted*. Phytoplankton response in growth, photophysiology and community structure to iron and light in polar frontal and Antarctic waters. Oceanogr. Limnol.

Weiss, R.F., 1974. Carbon dioxide in water and seawater: the solubility of a non-ideal gas. Mar. Chem. 2, 203–215. https://doi.org/10.1016/0304-4203(74)90015-2

Chapter 2

Manuscript prepared for submission to Limnology and Oceanography

Links between phytoplankton community composition, macronutrients and trace metal distribution in the surface waters of the Atlantic Southern Ocean

Ian Weir[1§], Johan Viljoen[1§], Susanne Fietz[1]*, Ryan Cloete[1], Jean Loock[1], Raissa Philibert[1¥], Alakendra N. Roychoudhury[1]

[1]*Centre for Trace Metal and Experimental Biogeochemistry, Department of Earth Sciences, University of Stellenbosch, 7600 Stellenbosch, South Africa*

[¥]*Current address: Coastal Ocean Research Institute, Vancouver, British Columbia*

[§]*These authors contributed equally to the manuscript*

*Corresponding author: Department of Earth Sciences, Stellenbosch University, 7600 Stellenbosch, South Africa, sfietz@sun.ac.za, +27218083117

Keywords: GEOTRACES; hydrothermal plume; biogenic silica; pigments; bioactive trace metals

Geographic bounding coordinates: 70.14 °S 03 °W: 33.93 °S 16.64 °E

I.J. Weir contribution to manuscript: I.J. Weir and J.J. Viljoen share equal contribution as first authors on this manuscript. In terms of analysis, I.J. Weir was responsible for the SEM analysis and diatom identification as well as biogenic silica analysis. In terms of the written component, I.J. Weir wrote about biogenic silica, macronutrient and trace metal distribution in the Results section. I.J. Weir contributed to the writing of the Abstract, Methods and Conclusion. Furthermore, I.J. Weir compiled the discussion of the paper.

Abstract

Phytoplankton and trace metal distribution are intrinsically linked in the ocean by metabolic requirements and uptake. Traditionally, the relationship between phytoplankton and trace metals has been addressed through incubation studies in which species are commonly studied in isolation and/or in terms of selected trace metals. This study assesses *in-situ* phytoplankton community variability in terms of trace metal distribution in summer surface waters of the Atlantic Southern Ocean along the GEOTRACES GIPY_05 transect. A multi-variable approach, which included both chemical and environmental variables, was implemented to address phytoplankton community variability both spatially and temporally in the five major oceanic zones, the Weddell Gyre region, Antarctic Zone, Polar Frontal Zone, Subantarctic Zone and Subtropical Zone, across the transect. Diatoms were the dominant phytoplankton group south of the Polar Front in the Antarctic Zone and Weddell Gyre, where silicic acid concentrations greatly increased, with notable *Phaeocystis* and coccolithophore contribution. Zinc and manganese were most strongly correlated ($p < 0.01$, $R^2 > 0.7$) with silicic acid in this region, indicative of a community simultaneously utilizing these metals and silicic acid, such as diatoms. North of the Polar Front, in the Polar Frontal Zone, Subantarctic Zone and Subtropical Zone, communities were *Phaeocystis*-dominated with notable diatom contribution and important cyanobacteria contribution in the Subtropical Zone which may be linked with unusual cobalt depletion. *Phaeocystis* dominance north of the Polar Front is most likely attributed to limiting silicic acid concentrations and deep mixed layers, while the abundance of smaller phytoplankton groups may be related to warmer, higher salinity waters. Seasonally, the highest chlorophyll-a concentrations in the study area were encountered in January, and on the reoccupation of selected stations there was an obvious shift in community structure and macronutrient ratios between months. Our findings indicate that an influx or abundance of trace metals linked to hydrothermal plume activity and ice melt is closely related to increasing biomass and community diversification. Such a diversification in community structure could not be explained by macronutrients and physical variables. The timing of such trace metal fluxes also proved to be a pivotal factor, particularly for iron in some instances, which seemed to be preferentially depleted to near-limiting concentrations and may have driven under-utilization of certain metals such as nickel. The study highlights the importance of considering a suite of trace metals as an additional variable when accounting for phytoplankton variability in the open ocean,

although it is unclear whether trace metal distributions drive the community composition or the community composition drives trace metal distributions.

2.1. Introduction

The fundamental role macronutrients play in marine algal photosynthesis has been well-documented (Redfield, 1958; Arrigo, 1999). However, our understanding of the relationship between micronutrients (essential trace metals) and phytoplankton communities is traditionally hindered by a lack of parallel trace metal and community composition data. Due to group-specific nutrient requirements, the phytoplankton community composition greatly influences biogeochemical cycles, including those of trace elements. In turn, availability of nutrients, including essential trace nutrients, will drive the phytoplankton community composition because of group and taxa-specific requirements of essential nutrients. Accordingly, current initiatives aim at providing more robust data sets focused on trace metal, macronutrient and community assemblages. Trace metals are essential micronutrients responsible for an array of photosynthetic and metabolic functions in marine phytoplankton. For instance, iron (Fe) is required in the enzyme that catalyses carbon and nitrogen fixation, zinc (Zn) is part of the carbonic anhydrase, responsible for the hydration and dehydration of carbon dioxide (CO_2), while manganese (Mn) is essential for oxygen-evolving enzymes, responsible for the oxidation of water during photosynthesis (Twining and Baines, 2013). Metal requirements differ between taxa and can fluctuate in response to changes in environmental conditions, such as light. The extended Redfield ratio describes the proportions with which phytoplankton utilise major nutrients and is defined as 180C: 23N: 1P: $5x10^{-3}$Fe: $2x10^{-3}$Zn: $1x10^{-3}$Mn: $5x10^{-4}$Ni: $4x10^{-4}$Cd: $2x10^{-4}$Cu: $4x10^{-5}$Co. It follows that trace metal distribution exerts a strong control on primary production, and which groups of phytoplankton constitute that production.

Phytoplankton form the base of the marine food web and are of particular importance in the Southern Ocean, especially in the summer and spring period when large blooms develop, supporting a profusion of Antarctic life. Furthermore, phytoplankton play a critical role in biogeochemical cycles, which mediate the global climate (Deppeler and Davidson, 2017). The Southern Ocean, in particular, accounts for ca. 40 % of anthropogenic CO_2 taken up by oceans (Deppeler and Davidson, 2017). Those global carbon fluxes into the ocean are largely driven by phytoplankton growth and the subsequent sinking to the deep ocean and sequestration of the

phytoplankton organic matter. Different phytoplankton groups have diverse roles in the food web as well as variable CO_2 requirements. For example, studies have shown that nutrient requirements differ between dinoflagellates and diatoms with certain species of dinoflagellates requiring greater volumes of CO_2 than diatoms (Chitari and Anil, 2017). Therefore, understanding factors that impart dominance of certain taxa is fundamental for improving oceanic biogeochemical models.

Few studies have been done to assess the driving factors of phytoplankton productivity and community structure across different zones in the Southern Ocean that include both macronutrients and essential trace metals (Wright et al., 2010; Gibberd et al., 2013). Seasonal studies from the Ross Sea, for example, show that phytoplankton community assemblages heavily influence biogeochemical characteristics and cycles in this region, demonstrating that changes in the dominant groups and taxa impart distinctive nutrient removal ratios in the residing water mass (Arrigo, 1999; Smith and Asper, 2001). This paper presents an analysis on the surface distribution and structure of the phytoplankton community on the GEOTRACES GIPY-05 transect in the Atlantic Southern Ocean. This transect includes the crossing of a mid-ocean ridge and the marginal ice zone. The over-arching aim of this study is to assess the relationship between micro- and macronutrient distributions and the phytoplankton community assemblage to better understand the planktonic community response to changing environmental conditions.

2.2. Methods

2.2.1. Cruise Track

This study focuses on sampling conducted on the R/V SA Agulhas II during the South African National Antarctic Expedition (SANAE) 54 from December 2014 to February 2015 along the GEOTRACES GIPY_05 transect in the Atlantic Southern Ocean (Fig. 2.1). This cruise was conducted over a period of ten weeks. The first leg went from Cape Town, South Africa, to the Antarctic shelf following the Bonus Good Hope monitoring line (05/12/2014 – 16/12/2014; herein referred to as “December”). A section not further discussed here followed north-westward to South Georgia and from South Georgia north-east to reach the Good Hope Line again at 46 °S (29/12/2014 – 6/1/2015). The third leg started at 46 °S and followed the Good Hope Line

southward (6/1/2015 – 23/1/2015; herein referred to as "January") and the fourth leg returned north along the same line (7/2/2015 – 15/2/2015; herein referred to as "February"). Three major fronts of the Antarctic Circumpolar Current (ACC) were crossed, Sub-Tropical Front (STF; 40.4 °S), Sub-Antarctic Front (SAF; 44.1 °S) and Polar Front (PF; 50.4 °S; Fig. 2.1). The Southern Boundary (SBdy) of the ACC was located at ca. 55.44 °S. The frontal positions at the time of this study were identified from the fourth leg of the cruise based on temperature data from the eXpendable BathyThermographs (XBT) transects AX25 (NOAA, 2015) using criteria in Orsi et al. (1995). Using the fronts and the SBdy, we classified the Southern Ocean surface waters in our study into five distinctive zones: Sub-Tropical Zone (STZ), Sub-Antarctic Zone (SAZ), Polar Frontal Zone (PFZ), Antarctic Zone (AAZ) and Weddell Gyre (WG; Fig. 2.1).

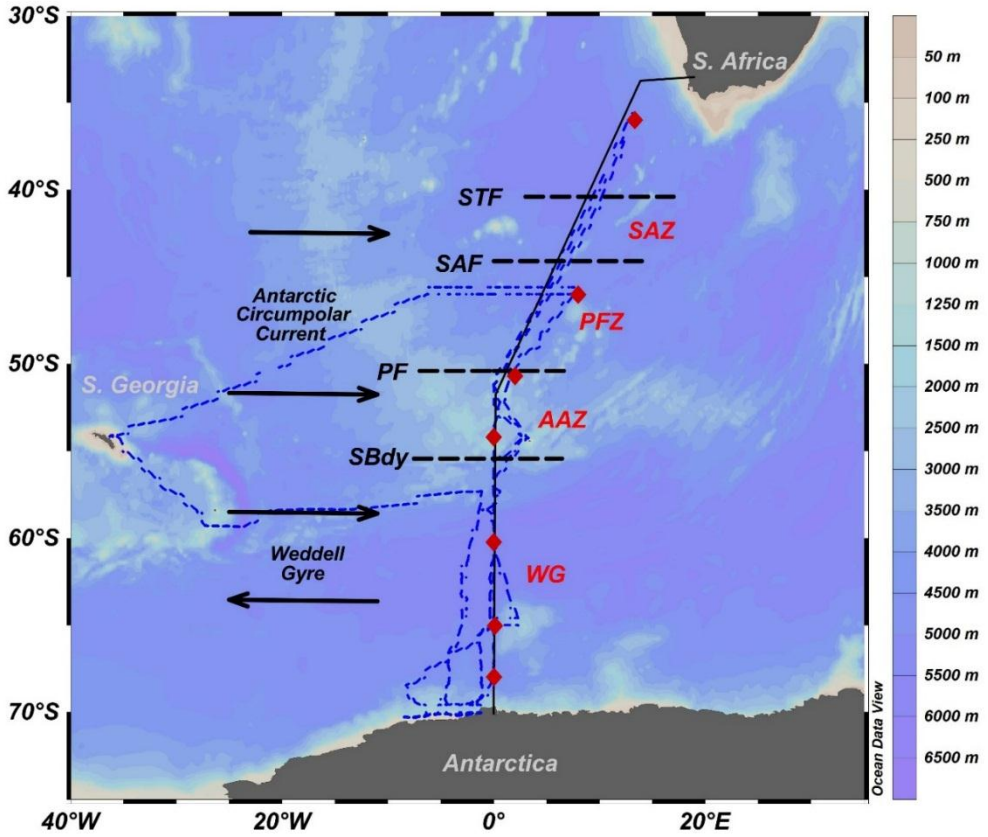

Figure 2.1 SANAE 54 cruise track, all samples are collected along the Bonus Goodhope line between Cape Town and Antarctica (as indicated by the solid black line). The dotted blue line indicates the cruise track the ship took throughout the entire SANAE 54 voyage. The horizontal black dotted lines indicate the frontal positions, the oceanic zones are indicated by red text and trace metal sampling stations are indicated by red diamonds. Ocean bathymetry is specified by the colour bar on the right of the figure. Abbreviations in alphabetical order: AAZ, Antarctic zone; PF, Polar Front; PFZ, Polar Frontal Zone; S. Africa, South Africa; S. Georgia, South Georgia; STF, Subtropical Front; SAF, Subantarctic Front; SAZ, Subantarctic Zone; SBdy, Southern Boundary; WG, Weddell Gyre.

2.2.2. Sampling and analysis

Three sampling strategies were adopted in this study: 1) temperature and salinity data were recorded continuously at 10-minute intervals by the ship's on-board system from the underway supply located at around 5-6 m water depth at the ship's bow; 2) samples for all other variables except for trace metals were taken from the underway supply at lower resolution (details follow below); 3) water samples for trace metals were collected using a GoFlo bottle array according to GEOTRACES trace metal clean standards at six stations (details follow below).

i. Pigments and determination of phytoplankton community composition

Seawater was collected for chlorophyll-a (chl-a) and accessory pigment analysis from the continuous underway supply at around 5-6 m water depth from the ship's bow. Water was collected approximately at every degree south and additionally when approaching a conductivity-temperature-salinity (CTD) trace metal station. The resulting sample set contained 33 samples representing surface phytoplankton communities across all major water masses (STZ, SAZ, PFZ, AAZ and WG). These surface pigment samples were taken as single samples due to logistical constraints of an extremely tight time schedule aboard. The water was filtered under dim light through Whatmann® GF/F glass fibre filters (0.7 µm nominal pore size) and filters were immediately stored at -80 °C until analysis after the cruise. Freeze-dried filters were extracted and analysed for phytoplankton pigments by High-Performance Liquid Chromatography (HPLC) at Laboratoire d'Océanographie de Villefranche/Mer (LOV – CNRS) as described by Ras et al. (2008). The calculation of phytoplankton community composition using the pigment data was done using CHEMTAX software (Mackey et al. 1996; Wright et al. 2010; details provided in Supplementary Methods, S2.1). The degradation (phaeo-) pigments, phaeophorbid-a and phaeophytin-a and the photoprotective pigments diadinoxanthin (DD) and diatoxanthin (DT) were used to assess degradation and photophysiology.

ii. Macronutrient, biogenic silica and SEM imagery

Surface water was also collected from the continuous underway supply for the analysis of dissolved nutrients (NO_3^-, NO_2^-, $Si(OH)_4$ and PO_4^{3-}). Samples were frozen at -20 °C immediately after sampling and analysed within one to two months after sampling. A Lachat Quick-Chem Flow injection autoanalyzer, housed at the University of Cape Town, was used for the analysis of NO_3^-, NO_2^- and $Si(OH)_4$ (Egan, 2008; Wolters, 2002). Phosphate was analysed manually

according to methods described by Grasshoff et al. (1983). The analytical error of the NO_3^- + NO_2^-, PO_4^{3-} , and $Si(OH)_4$ quantification is ± 0.04 µM, ± 0.06 µM and ± 0.02 µM, respectively (Grasshoff et al., 1983). Samples collected for particulate silica analysis were collected underway when approaching a CTD cast station or departing the station. Approximately 1L of seawater was filtered onto a 0.45 µm Omnipore Membrane filter through the bow intake of the ship while underway. The filter was then oven-dried for at least 12 hrs at 60 °C. Biogenic silica (bSi) was determined using the NaOH digestion method described by Ragueneau and Tréguer (1994). Biogenic silica is hydrolysed by a hot NaOH solution and analysed for silicic acid using the modified colorimetric detection method of Grasshoff et al. (1983). Details of adjustments from the Grasshoff et al. (1983) colorimetric detection are provided in Supplementary Methods (S2.2). The reduced silicomolybdic acid species was measured on a Genesys 10-S UV Spectrophotometer at 810nm. A blank filter interference of 0.04 ±0.002 µM and 0.12 µM limit of detection is reported for the NaOH digestion. Other analytical errors, such as instrumental errors, associated with the NaOH digestion were reported to be < 4 %. Samples were further collected for Scanning Electron Microscope (SEM) imaging, to aid in the identification of phytoplankton with mineralized skeletons. This work supported our phytoplankton community composition determination described above.

iii. Dissolved trace metals

Trace metal samples were collected from six CTD stations (Fig. 2.1) using GoFlo bottles on a titanium frame, and sub-sampling in a certified class 100 clean container on board. All sampling and material cleaning procedures strictly followed GEOTRACES standards outlined in Cutter et al. (2014). Only dissolved trace metals are reported here, sampled in low density polyethylene (LDPE) bottles after online filtration through 0.2 µm Sartobran filters. Prior to analysis, samples were pre-concentrated using a seaFAST-pico SC-4 DX module (Elemental Scientific Inc.) in the certified class 100 laboratory at Stellenbosch University. Pre-concentrated samples were then analysed using an Inductively Coupled Plasma Mass Spectrometry (Agilent 7900 ICP-MS) at Stellenbosch University. Details on materials used, washing procedures, instrument calibration and method validation can be found in Cloete et al. (*submitted*) and Loock et al. (*submitted*). Full depth profiles for a suite of bioactive trace metals (Cu, Zn, Ni, Co, Mn and Cd) are also provided by those authors. Here, we focus on the surface phytoplankton community and nutrient concentrations. The shallowest depth of the vertical trace metal profiles (ca. 15 m) was used as

surface concentrations. All concentrations referred to in this study are of dissolved metal species, except for Co, where lack of UV radiation during sample processing means that the analysed Co only encompassed the labile fraction (Loock et al., *submitted*).

iv. Data analysis

Several statistical correlation techniques were implemented to determine i) nutrient-type behaviour of trace metals ii) which trace metals and phytoplankton groups behaved similarly across the transect and iii) the relationship between phytoplankton groups and macro- and micronutrients. Nutrient-type behaviour of trace metals is defined as, in this paper, trace metals which behave in a similar fashion to macronutrients in a typical depth-related profile. A typical nutrient profile is described as biological uptake in the surface followed by remineralization below surface waters and consistent concentrations at depth. Nutrient-type behaviour of trace metals and macronutrients is inferred by the Pearson's Correlation Coefficient (*p*-value) and the Coefficient of Determination (R-value), whereby depth profiles of individual trace metals and macronutrient concentrations are plotted against one another. A p-value < 0.05 and R-value > 0.7 are deemed significant, both criteria must be met to infer nutrient-type behaviour of a trace metal. A Principal Component Analysis (PCA) was performed to assess which a) trace metals behaviour similarly and b) phytoplankton groups are most related across the transect. Variance among selected variables (trace metals and phytoplankton groups) as well as the proportion of variance is explained by three principal underlying. A PCA cannot identify the component itself. The PCA was performed in SPSS software with rotation method varimax and Kaiser normalization. Finally, a non-parametric rank correlation Kendall-tau was calculated in SPSS to assess the strength of the relation between phytoplankton group's chla concentrations and macro- or micronutrients. The null hypothesis was that there is no correlation between these variables.

2.3. Results

Temperature and salinity: As expected, sea surface temperatures (SSTs) generally decreased from north to south with sub-zero temperatures in proximity of the Antarctic shelf (Fig. 2.2). Salinity also decreased from north to south, especially through the STZ and SAZ (Fig. 2.2). Higher variability was observed in close proximity to the fronts and to the ice shelf. Seasonal

progression towards warmer waters from December to February was observed, while little seasonal variation in salinity was observed (Fig. 2.2).

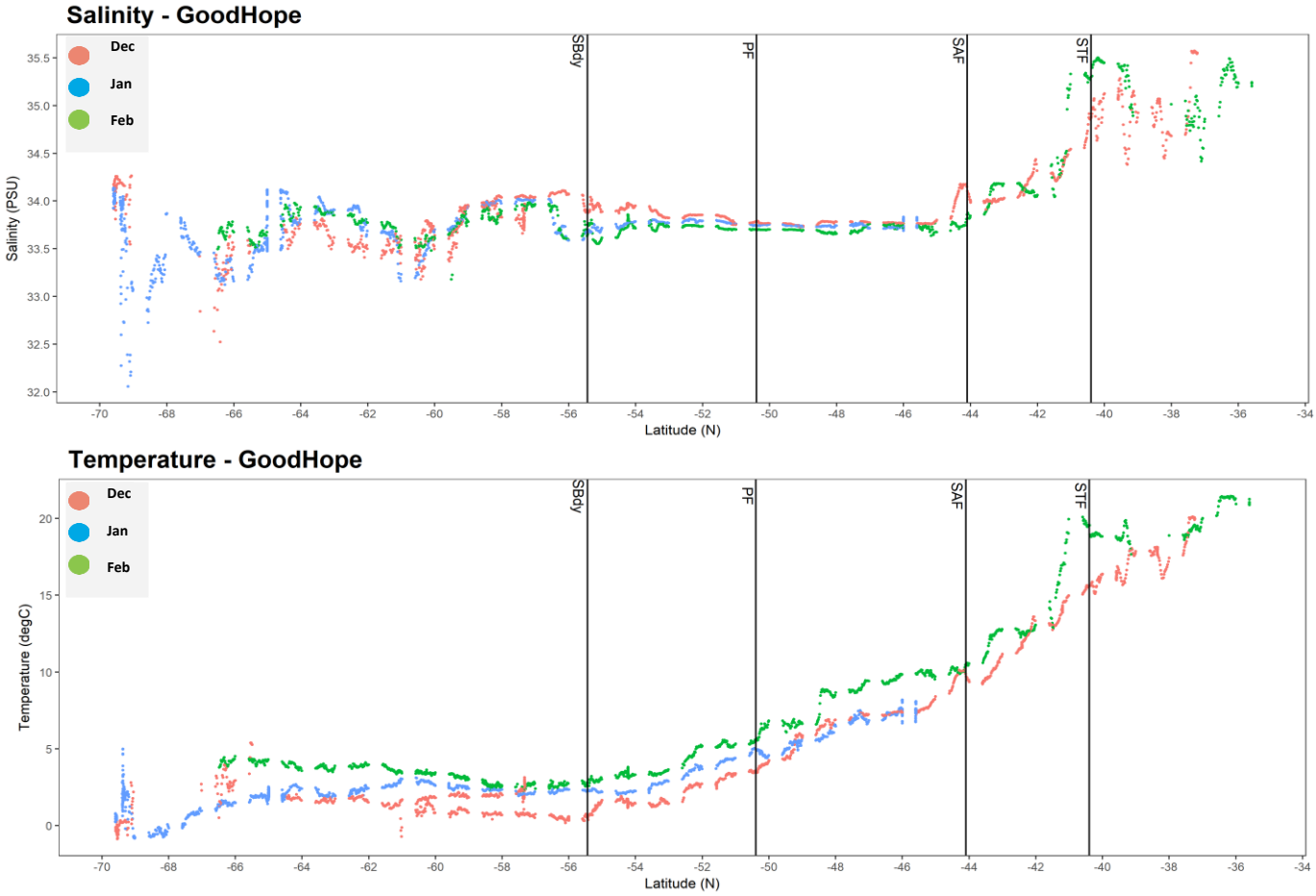

Figure 2.2 Surface (ca. 5-6m) salinity and temperature along the Good Hope Line during the first (05/12/2014 – 16/12/2014; "December"), third (29/12/2014 – 6/1/2015; "January") and fourth (7/2/2015 – 15/2/2015; "February") legs of voyage SANAE54 on board R/V SA Agulhas II. Red dots represent temperature and salinity encountered in "December", blue dots "January" and green dots "February." Frontal positions are calculated from leg four ("February") of the cruise.

Macronutrients: Nitrate surface concentrations were low throughout the STZ in December (avg. 1.3 µM), while displaying a southward increase to 25 µM in the SAZ and ca. 30 µM in the PFZ and AAZ (Fig. 2.3a, Table S2.1). South of 55 °S (i.e. the SBdy), nitrate concentrations decreased again to < 25 µM. Average nitrate concentrations in the PFZ and northern AAZ showed large depletion in January and February (ca. 18 µM). Phosphate gradually increased southward from < 0.5 µM in the STZ reaching values > 3 µM in certain sections of the WG in December (Fig.

2.3b). As a consequence, nitrate to phosphate (N/P) ratios were low in the STZ and WG, but elevated in the SAZ, PFZ and AAZ, i.e. between the STF and the SBdy (Fig. 2.3, Table S2.1). January and February phosphate concentrations indicated depletion with seasonal progression, but followed a similar north-south trend as observed in December. For example, January surface phosphate concentrations averaged 1.1 µM in the PFZ, but increased south across the AAZ to > 2.5 µM at ca. 67 °S (Fig. 2.3b, Table S2.1). Consequently, the N/P ratios varied only slightly across the water masses (Fig. 2.3, Table S2.1). Relatively low concentrations of silicic acid (avg. < 3 µM) persisted throughout the STZ, SAZ and PFZ in December, followed by a sharp rise at the PF to about 15 µM (Fig. 2.3c, Table S2.1). Silicic acid concentrations rapidly increased south of the PF reaching concentrations as high as 87 µM upon approaching the Antarctic Shelf. Ratios of silicic acid versus nitrate and phosphate (Si/N and Si/P), showed similar trends with high Si/N and Si/P ratios in the STZ, very low ratios in the SAZ and PFZ, increasing ratios in the AAZ, and highest ratios in the WG (Fig. 2.3, Table S2.1). In January and February, low concentrations of silicic acid (avg. 2.7 µM) also prevailed in the STZ, SAZ and PFZ, that increased south of the PF in the AAZ (avg. 11.5 µM), and WG (53 µM). However, as in December, silicic acid concentrations declined in the proximity of the Antarctic shelf (ca. 70 °S; Fig. 2.3c).

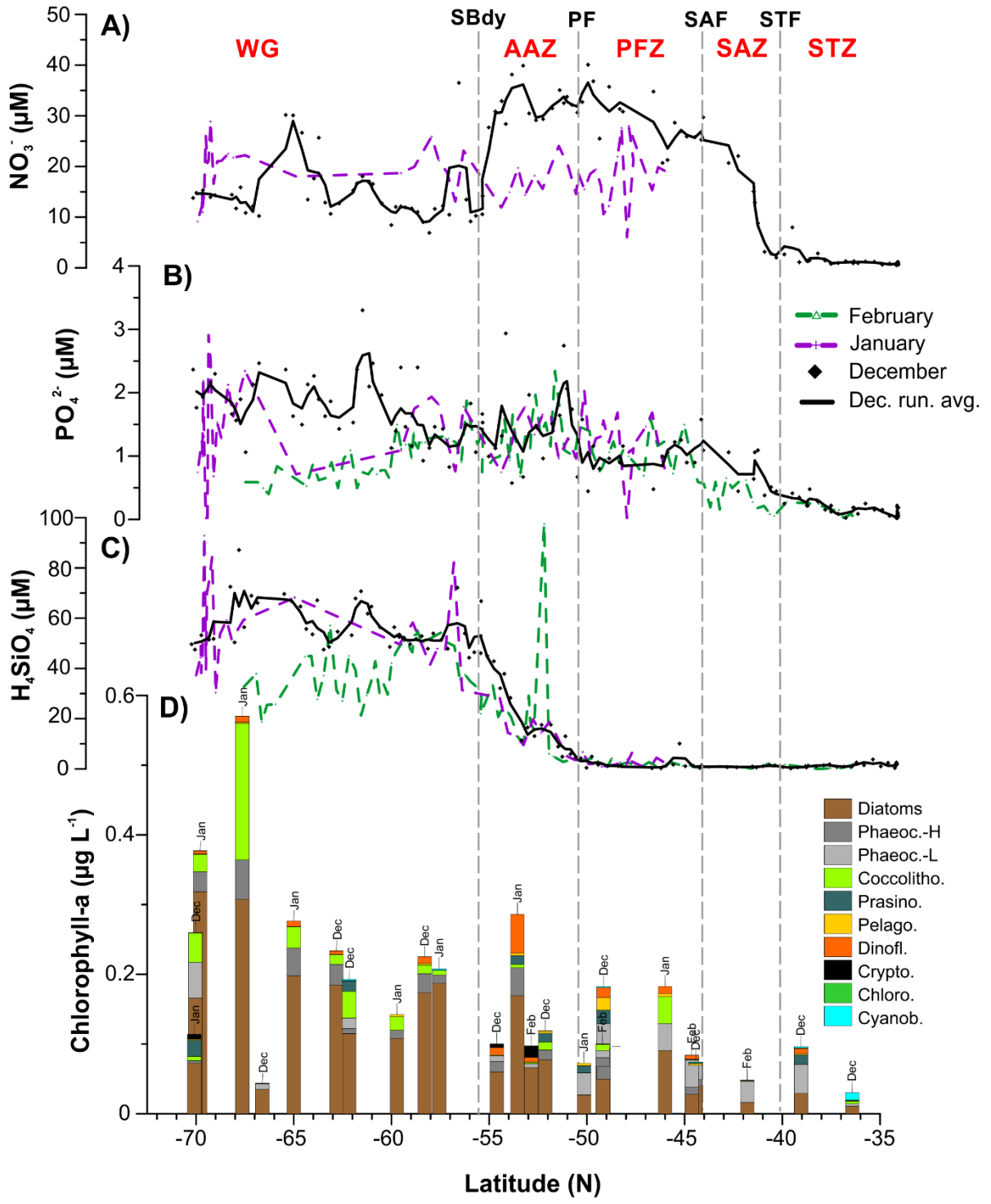

Figure 2.3 Macronutrients (nitrate, NO_3^- (**A**); phosphate, PO_4^{2-} (**B**), silicic acid, H_4SiO_4 (**C**)) and the phytoplankton community composition (**D**) as determined by CHEMTAX from all sampling legs of the cruise (December, January, February). The dotted grey line indicates frontal positions. Phaeoc.-H, Phaeocystis-H; Phaeoc.-L, Phaeocystis-L; Coccolitho., Coccolithophore; Prasino., Prasinophyte; Pelago., Pelagophyte; Dinofl., Dinoflagellate; Crypto., Cryptophytes; Chloro., Chlorophyte; Cyano., Cyanobacteria.

Dissolved trace nutrients: Sampling for determination of dissolved trace metal concentration only occurred at six stations during the fourth leg of SANAE54, in January 2015 (Fig. 2.1). The main dissolved trace metals investigated here showed very different surface water profiles along the transect (Table 2.1). Three principal components accounted for almost all (98 %) the variance in the trace metal distribution (Table 2.2a). Both, Cu and Ni followed a comparable trend to that of nitrate and were correlated negatively with the first factor of the PCA, which accounted for 40.8% of the variance, and positively with the second factor, which accounted for 34.9% of the variance (Table 2.2a, Fig. S2.1a). Low concentrations of Cu and Ni were recorded in the STZ, with concentrations increasing southwards (Fig. 2.4) from 0.5 to 1.8 nM and from 2.4 to 6.0 nM for Cu and Ni, respectively (Table 2.1a). Copper and Ni both showed nutrient-type depth profiles (i.e. depth profiles significantly positively correlated to nitrate and phosphate) at all stations (Table 2.1b) pointing to biological uptake at the surface.

Zinc and Mn showed maximum concentrations at 36 °S (9.4 and 0.96 nM, respectively; Table 2.1a), strongly decreased across the PFZ, AAZ and most of the WG, while increasing again close to the ice shelf at 68 °S (Fig. 2.4c). Both Zn and Mn correlated well with the first component, but only weakly with the second (Table 2.2a, Fig. S2.1a). The Zn and Mn maximum observed at surface at 36 °S coincides with the observation that neither Zn nor Mn show nutrient-type depth profile at this station (Table 2.1b). Indeed, Mn only showed nutrient-type depth profiles at two stations, ca. 50 °S and ca. 60 °S (Table 2.1b).

Iron, Co and Cd showed different surface profiles, with increasing concentrations from the STZ to the PFZ, decreasing concentrations across the PFZ, AAZ and most of the WG (Fig. 2.4b). However, while Co and Cd correlated strongly with the second component, Fe was not correlated to either the first or the second component, but strongly correlated to a third component, which accounted for 22.2% of the observed variance (Table 2.2a). The most prominent distinction between the transect profiles was the drastic increase in Co and Cd closest to the ice shelf, while Fe decreased (Fig. 2.4b). Out of these three metals, only Cd showed nutrient-type depth profiles at all measured stations (Table 2.1b). Iron depth profiles differed from typical nutrient-type profiles at ca. 54 °S and at ca. 60 °S and cobalt only showed nutrient-type depth profiles at 36 °S and 50 °S, indicating that Co was only utilized in the surface at those two stations.

Table 2.1 A) Trace metal concentrations (in nM) determined at six stations across the Atlantic sector of the Southern Ocean measured during the fourth (February) leg of voyage SANAE54 (see Fig. 2.1 for cruise map). **B**) Assessment of nutrient-type behaviour considering depth profile. Nutrient-type behaviour is assumed herein if correlation between depths profiles for metal and nitrate and phosphate were significantly and positively correlated.

A)

			concentrations at surface (µM)						
Date	**Latitude (N)**	**Longitude (E)**	**Cd**	**Cu**	**Fe**	**Zn**	**Ni**	**Mn**	**Co**
5/2/2015	-36.00	13.35	0.01	0.50	0.17	9.37	2.37	0.96	0.008
12/1/2015	-46.03	8.00	0.25	1.00	0.38	1.46	5.07	0.24	0.033
14/1/2015	-50.71	2.03	0.25	0.94	0.23	1.27	4.98	0.13	0.020
15/1/2015	-54.22	0.00	0.34	1.45	0.25	1.55	5.42	0.21	0.024
16/1/2015	-60.25	0.01	0.22	1.49	0.14	1.33	5.98	0.03	0.014
18/1/2015	-65.04	0.12	0.12	1.29	0.22	1.02	4.65	0.04	0.009
19/1/2015	-67.98	0.05	0.69	1.83	0.11	4.56	6.02	0.26	0.030

B)

			depth profile significantly, positively correlated to N and P (i.e. nutrient-type)						
Date	**Latitude (N)**	**Longitude (E)**	**Cd**	**Cu**	**Fe**	**Zn**	**Ni**	**Mn**	**Co**
5/2/2015	-36.00	13.35	y	y	y	no	y	no	y
12/1/2015	-46.03	8.00	y	y	y	y	y	no	no
14/1/2015	-50.71	2.03	y	y	y	y	y	y	y
15/1/2015	-54.22	0.00	y	y	no	y	y	no	no
16/1/2015	-60.25	0.01	y	y	no	y	y	y	no
18/1/2015	-65.04	0.12	y	y	y	y	y	no	no
19/1/2015	-67.98	0.05	y	y	y	y	y	no	no

Table 2.2 Rotated component matrices derived from Principal Component Analysis for **A**) trace metal concentrations. **B**) Phytoplankton group chla concentrations. Highlighted correlation coefficients indicate significant correlation at 95 % confidence interval.

A)

	Components		
	1	**2**	**3**
% of variance	40.8	34.9	22.2
Cd	-0.17	**0.94**	-0.27
Cu	-0.58	0.62	-0.48
Fe	-0.13	-0.03	**0.98**
Zn	**0.95**	-0.08	-0.28
Ni	-0.77	0.60	-0.14
Mn	**0.98**	-0.17	-0.01
Co	-0.14	**0.89**	0.44

B)

	Component			
	1	**2**	**3**	**4**
% of variance	26.1	19.5	18.8	13.0
Cyano.	-0.12	**0.96**	-0.01	0.04
Prasino.	-0.27	-0.10	**0.74**	-0.02
Dinoflag.	0.32	-0.06	**0.66**	-0.21
Crypto.	-0.33	-0.15	-0.03	-0.77
Phaeocy-H	**0.84**	-0.09	0.44	-0.01
Phaeocy-L	-0.50	-0.17	0.04	**0.71**
Cocco.	**0.74**	-0.09	-0.18	0.17
Pelago.	-0.04	-0.04	**0.80**	0.36
Chloro.	-0.14	**0.95**	-0.16	-0.01
Diatoms	**0.89**	-0.21	-0.11	-0.10

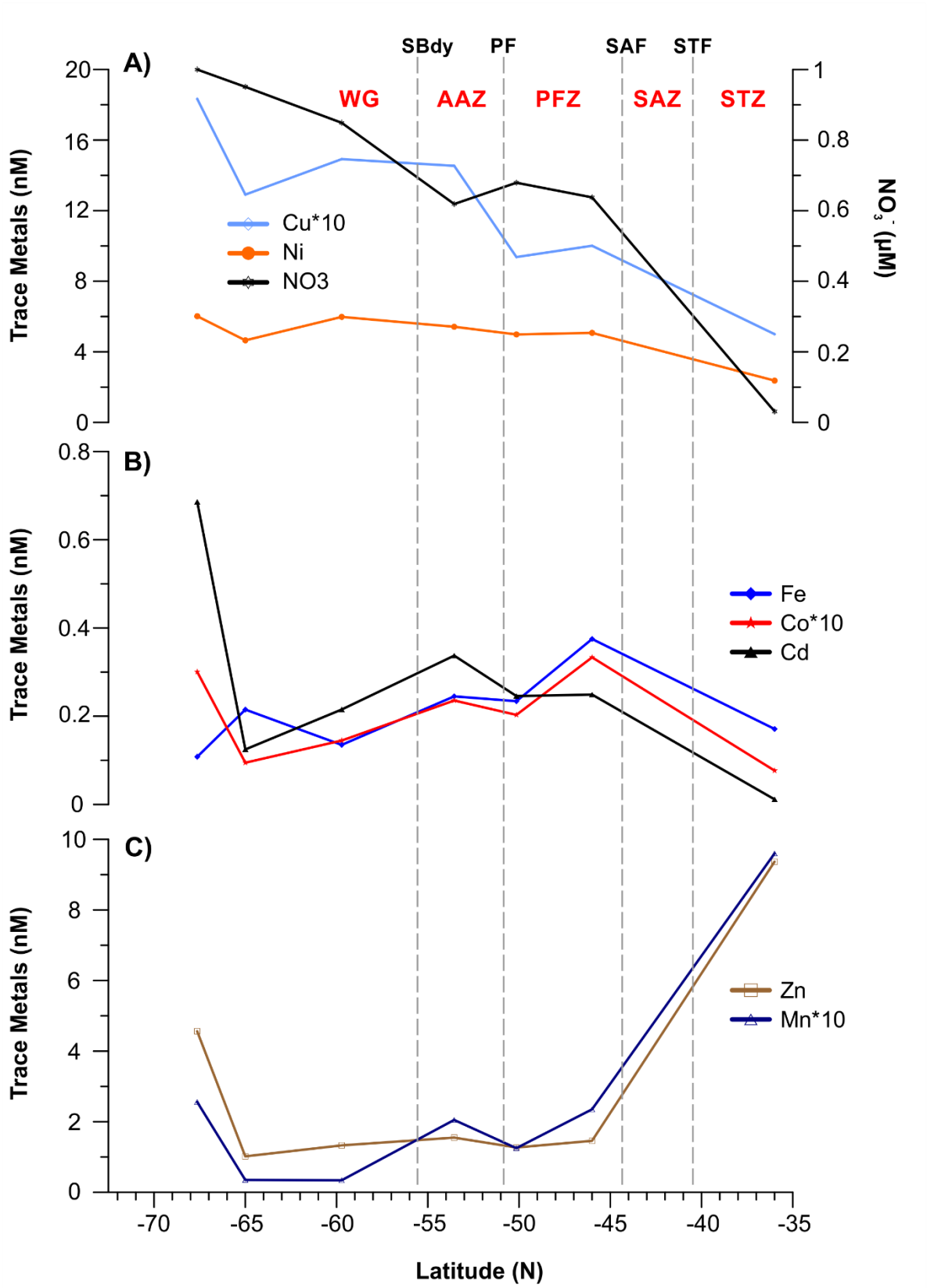

Figure 2.4 Surface dissolved trace metal distribution along the transect. **A**) Cu (*10) and Ni; note that nitrate concentrations are shown in this panel to illustrate the similar trends of some trace metals. **B**) Fe, Co (*10) and Cd. C) Zn and Mn (*10).

Phytoplankton community: The total chla concentrations generally increased from north to south, ranging from 0.03 to 0.57 µg $L^{-1}$with higher chla concentrations seen close to the ice edge (Fig. 2.3d). Strongest correlation with regard to macronutrients was found between chla and silicic acid concentration, even though total chla was also correlated (at 90 % confidence interval) with nitrate and phosphate (Table 2.3a). Total chla was furthermore weakly (at 90 % confidence interval) correlated to Cu and Zn (Table 2.3b). No significant correlation was found between the surface chla concentrations and the mixed-layer depth (MLD; not shown). Phaeopigments were not detected in the STZ, SAZ and PFZ, indicating low grazing pressure and cell degradation (Carreto et al., 2016; Jeffrey et al., 1997; Wright et al., 2010). However, pheophorbide A and pheophytin both occurred south of the PF with maximum concentrations of 0.03 and 0.008 µg L^{-1}, respectively (Fig. S2.2a). Maximum pheopigment:chla ratio (0.2 µg:µg) was observed at 65 °S (Fig. S2.2a).

Two principal components explain 46 % of the variance in phytoplankton distribution (Table 2.2, Fig. S2.1b). The first component correlated with high diatom chla concentrations (Table 2.2). Contribution of diatoms to total chla generally increased from north to south ranging from ca. 30 to 90 %, with diatom chla concentrations ranging from ca. 0.01 to 0.3 µgL^{-1} (Fig. S2.3d, Table S2.4), but decreased south of 69 °S within proximity of the ice. Diatom chla concentrations were significantly correlated with silicic acid, phosphate and Cu concentrations (Table 2.3). No significant correlation was found between the surface diatom community (or any other phytoplankton group investigated here), chla concentrations and the MLD (not shown). Scanning electron micrographs at 36 °S indicated a low cell abundance (at least of mineralized species), which comprised predominantly small centric diatoms (< 3 µm), which reaffirm low chla concentrations (0.03 µgL^{-1}) as the station was dominated by diatoms. The surface bSi concentrations also increased from 0.35 µM at 36 °S to 4.6 µM at 50 °S, and remained similarly high until 60 °S. Scanning electron micrographs from station 53.6 °S, in the AAZ, indicated diatoms were medium to large in size (ca. 7-55 µm) and comprised *Chaetoceros spp.*, *Thalassioisira spp*. and *Fragilairiopsis spp*. Noticeably lower bSi values (< 0.76 µM) were encountered within proximity of the ice (Table 2.4). However, a very prominent peak in bSi of 13.8 µM was observed at 65 °S that did not correspond to a peak in diatom chla (Table 2.4). The bSi:diatom-chla ratio (µmol:µg) ranged between 2 and 6 throughout most of the transect, with the exception of a prominent peak in the ratio at 50 °S and very low ratios close to the ice edge

(Table 2.4). The contribution of haptophyte, *Phaeocystis antarctica* to total chla increased from 36 °S to reach its maximum of 63 % at 42 °S, but decreased southwards thereafter (Fig. S2.3d, Table S2.4). The *P. antarctica* chla was not correlated to any macronutrient and only showed weak correlation with Mn and Cd (Table 2.3). Two forms of *P. antarctica* can be differentiated based on their composition of photo-protective versus light-harvesting pigments ratios, regulated according to the availability of dissolved iron (DiTullio et al., 2007; Wright et al., 2010). Along our transect, the two forms showed generally opposite trends (Fig. S2.3d, Table S2.4). The chla concentration from *P. antarctica* with the characteristic pigmentation pattern of iron replete conditions increased southwards, while chla concentration from *P. antarctica* with the characteristic pigmentation pattern of iron depleted conditions decreased southwards (Fig. S2.3d, Table S2.4). As a consequence, the chla concentration from *P. antarctica* with the characteristic pigmentation pattern of iron replete conditions correlated with principal component one, similarly to diatom chla, while chla concentration from *P. antarctica* with the characteristic pigmentation pattern of iron depleted conditions correlated with a separate component, distinct to all other groups investigated in this study (Table 2.2). Neither form was correlated to Fe concentration nor any other trace metal investigated (not shown).

Coccolithophore chla concentrations were correlated to the first principal component along with diatoms and iron-replete forms of *P. antarctica* (Table 2.2). Coccolith platelets have been observed from SEM micrographs at station 53.6 °S, most likely belonging to the species *Emiliania huxleyi*, reaffirming the presence of coccolithophores in this region. Coccolithophore chla ranged between 0.0004 and 0.04 μgL^{-1}, showing a general increase from north to south. However, coccolithophores showed a sudden increase to ca. 34 % of total chla (i.e. ca. 0.20 μgL^{-1}) at ca. 67 °S within the WG (Fig. S2.3, Table S2.4). This coccolithophore increase encountered at ca. 67 °S coincided with the maximum chla concentration of the total community (Fig. 2.3d).

Some pigments, such as diadinoxanthin and diatoxanthin, generally found in diatoms and haptophytes including *Phaeocystis* and coccolithophores, can be used as indicators of photoacclimation (Alderkamp et al., 2011; Brunet et al., 2011). Photoprotective pigments (diadino- and diatoxanthin) were not detected in the STZ, but concentrations increased southwards, except close to the ice edge (Fig. S2.2b). Consequently, the ratio of the photoprotective (diadino- and diatoxanthin) versus light-harvesting (fucoxanthin and 19′-hex-

fucoxanthin) pigments was lowest close to the ice edge (0.07 µg:µg), but ranged between 0.09 and 0.2 across all other water masses (except in the STZ; Fig. S2.2b).

Other phytoplankton groups showed only minor contributions to total chla (< 20 %) and few general north-south trends. Cyanobacteria and chlorophytes correlated with a second principal component (Fig. S2.1b), but neither was correlated to macro- or micronutrient concentrations (not shown). Cyanobacteria, for example, dominated the phytoplankton community with a contribution of ca 36 % in the STZ at 36 °S, but contributed < 2 % southwards (Fig. 2.3d). All other groups correlated best with the third principal component (Table 2.2b) and their occurrence did not show trends across the water masses. For instance, sudden peaks in contribution to total chla by dinoflagellates (19 %) and cryptophytes (17 %) were observed at 55.3 °S and 52.8 °S, respectively, while prasinophytes showed a prominent peak close to the Antarctic ice at 70 °S (Fig. 2.3d). Interestingly, a correlation between pelagophyte chla concentration and Fe was found as well as a weak correlation with Co (Table 2.3).

Several sample sites were revisited on different legs of the SANAE54 expedition, allowing for an evaluation of seasonal progression. The community structure at 44 °S for example, was very similar between December and January. At 49 °S, the December community contained important contributions of picophytoplankton, such as flagellate eukaryotes and cyanobacteria, not seen in February at this station. Three samples were taken in close proximity to 70 °S in December and January. One sample was collected at 70 °S on 16 December, one at 69.7 °S on 20 January, and a third at 70.1 °S on 23 January. The December community showed a chla concentration of 0.26 μgL^{-1} in the range of the two January communities (0.38 and 0.11 μgL^{-1}). Diatoms dominated all three communities with around 63-64 % contribution to total chla, while contributions of coccolithophores (16 %) and *P.antarctica* in its low-iron acclimated state (20 %) were higher in December compared to the January communities.

Table 2.3 Kendall-Tau correlation between selected phytoplankton group chla concentrations and **A)** macronutrients, where sample size was n=24 and **B)** dissolved trace nutrients, where sample size was n=6. Only phytoplankton groups with at least one significant correlation are included in this table. Bold correlation coefficients indicate significant correlation at least at 90 % confidence interval. * indicates significant correlation at 95 % confidence interval and ** at 99 %.

A)		total chla	Diatoms	Phaeoc.	Cocco.	Pelago.
N	Correlation Coefficient	**0.28**	0.22	0.16	0.12	0.23
	Sig. (2-tailed)	**0.05**	0.14	0.28	0.41	0.12
P	Correlation Coefficient	**0.28**	**0.29***	0.07	0.20	0.02
	Sig. (2-tailed)	**0.06**	**0.04**	0.64	0.17	0.92
Si	Correlation Coefficient	**0.44****	**0.54****	-0.12	**0.46****	-0.22
	Sig. (2-tailed)	**0.00**	**0.00**	0.43	**0.00**	0.14

B)		total chla	Diatoms	Phaeoc.	Cocco.	Pelago.
Cu	Correlation Coefficient	**0.60**	**0.60**	0.47	0.33	-0.33
	Sig. (2-tailed)	**0.09**	**0.09**	0.19	0.35	0.35
Ni	Correlation Coefficient	0.33	0.33	0.20	0.33	-0.07
	Sig. (2-tailed)	0.35	0.35	0.57	0.35	0.85
Zn	Correlation Coefficient	**0.60**	0.33	0.47	0.33	0.20
	Sig. (2-tailed)	**0.09**	0.35	0.19	0.35	0.57
Mn	Correlation Coefficient	0.47	0.20	**0.60**	0.47	0.33
	Sig. (2-tailed)	0.19	0.57	**0.09**	0.19	0.35
Cd	Correlation Coefficient	0.47	0.20	**0.60**	0.20	0.33
	Sig. (2-tailed)	0.19	0.57	**0.09**	0.57	0.35
Co	Correlation Coefficient	0.20	-0.07	0.33	0.20	**0.60**
	Sig. (2-tailed)	0.57	0.85	0.35	0.57	**0.09**
Fe	Correlation Coefficient	-0.20	-0.47	-0.07	-0.20	**0.73***
	Sig. (2-tailed)	0.57	0.19	0.85	0.57	**0.04**

Table 2.4 Biogenic silica concentration and ratio of bSi versus diatom-chla concentration determined at eight stations across the Atlantic sector of the Southern Ocean (see Fig. 2.1 for cruise map).

Date	Latitude (N)	Longitude (E)	BSi (µM)	BSi/ (diatom chla) (µmol:µg)
5/2/2015	-36.00	13.35	0.35	32
12/1/2015	-46.03	8.00	1.20	13
14/1/2015	-50.71	2.03	4.61	171
15/1/2015	-54.22	0.00	3.72	22
16/1/2015	-60.25	0.01	3.59	33
18/1/2015	-65.04	0.12	13.8	69
19/1/2015	-67.98	0.05	0.38	1.2
20/1/2015	-69.79	-1.94	0.69	2.2
23/1/2015	-70.09	-1.59	0.17	2.4

2.4. Discussion

Our mutli-variable approach contributes to understanding the dynamics of phytoplankton community composition in the Atlantic Southern Ocean. In the absence of a single, predominant nutrient driving the community composition across all water masses in our study, variable and potentially interacting nutrient drivers will first be addressed here. Various possible phytoplankton community composition drivers will be discussed for each of the major oceanic zones individually (STZ, SAZ, PFZ, AAZ and WG), highlighting the dominant changes observed within these biogeochemically distinct zones. The potential impact of other driving factors, such as changes in temperature and light regimes will also be discussed.

2.4.1. STZ

The STZ was characterized by low chla concentrations, especially at the northern-most station (ca. 36 °S). Here the community was dominated by diatoms and cyanobacteria, with both contributing equal proportions. At 39 ° S, the contribution of cyanobacteria to total chla dropped to less than 2 %. However, diatoms did not dominate, but a rather diverse community was found with important contributions by prasinophytes and dinoflagellates. Low diatom contribution to the community was accompanied by low bSi concentration, but relatively high bSi:diatom chla

ratios, indicative of smaller cells. Higher contribution of smaller phytoplankton groups in the STZ might be a result of the warmer waters (Mendes et al., 2015; Schlüter et al., 2011; Van Leeuwe et al., 2015) or due to the particularly low nitrate and phosphate concentrations (Hudson and Morel, 1990; van Leeuwe et al., 2015). Additionally, low silicic acid concentrations may have been driving lower diatom contribution, allowing higher contribution of other phytoplankton groups. Our community structure data only encompassed early December conditions at 36 °S, but based on the observed low nutrient concentrations and ratios, a similar community composition could also be assumed for February. Important contribution of cyanobacteria in February, for example, is supported by trace metal data. At 36 °S, Co concentrations are heavily depleted in the surface displaying a strong positive correlation between Co and phosphate in the upper 1000 m, indicative of typical nutrient-like behaviour of Co (Loock et al. *submitted*). The strong Co uptake is accompanied by a depletion in Cu, Ni, Cd and Fe, but weak surface depletion of other bioactive trace elements (Zn, Mn). Cyanobacteria, abundant at this particular STZ station, demonstrate an absolute requirement for Co (Saito and Moffett, 2002). Their dominance may therefore explain the observed unusual strong depletion in Co at station 36 °S.

2.4.2. SAZ

The SAZ community, determined in February, was characterized by a low chla concentration, similar to the STZ, and dominated by *Phaeocystis* (63.4 %) with a noteworthy diatom contribution. *Phaeocystis*-dominated waters in February have been reported in the SAZ by Gibberd et al. (2013), albeit at much higher total chla concentrations (ca. 0.45 µg L^{-1}) and ca. 2.5 fold higher nitrate and phosphate concentrations. This suggests that lower chla concentrations reported herein may be linked to a more depleted February nitrate and phosphate pool. Substantial nitrate removal (-81 %) accompanied by an increase in the Si/N ratio, was evident from December to February. Despite this increase, the Si/N ratios < 1 are likely to inhibit diatom growth (Brzezinski, 1985), lessening diatom competition for other nutrients and allowing other groups such as *Phaeocystis* to dominate the community structure.

2.4.3. PFZ

The majority of communities encountered in the PFZ comprised predominantly diatoms and *Phaeocystis*. High nitrate concentrations (30 µM), noticeably higher than global averages (19

µM), are reported for this region (Garcia et al., 2013). Furthermore, high N/P molar ratios (35:1) were observed in December. It is unlikely that the high nitrate concentrations were driven by spring ice melt and northward transport of nutrient-rich meltwaters, as one would expect to see equally elevated phosphate and silicate concentrations. Klausmeier et al. (2004) have shown that under exponential growth (i.e. growth during the bloom season), N/P molar ratios exceeding 35:1 are a result of either limiting irradiance, nitrate, phosphate or a combination. On the same cruise, Viljoen et al. (*submitted*) established that, within the deep mixed layers (ML), which characterize the PFZ, the residing community was predominantly affected by light limitation with iron as a co-limiting factor. The under-utilization of nitrate in the PFZ was therefore possibly caused by light and iron co-limitation, along with limiting silicic acid concentrations. The nitrate was, however, largely removed between December and February (-68 %), possibly as a result of shifts in the community structure. For example, the December community at 44 °S was diatom-dominated, but shifted to *Phaeocystis* dominance in February.

Trace nutrient data were available in the PFZ at 46 °S. The community at 46 °S was diatom-dominated with large contributions from *Phaeocystis* and coccolithophores. While *Phaeocystis* was already a major contributor to the total chla across the STZ and SAZ, coccolithophore contributions were negligible. Coccolithophores can occur within a range of 2 – 15.7 °C (Findlay and Giraudeau (2000) and the decrease of water temperatures south of the STF to below 15 °C may have been favourable for coccolithophore growth in the PFZ. Biogenic silica concentrations were higher than at 36 °S and the N/P ratios (ca. 14:1) at this station correspond with diatom-dominated waters (Smith and Asper, 2001). The Si/N (0.3:1) and Si/P (3:1) ratios, in contrast, suggest diatom productivity was still limited by silicic acid. Copper and Zn showed typical nutrient-like behaviour and bio-utilization *(*Cloete et al. *submitted*). Surface Zn concentrations decreased drastically from the STZ to the PFZ, showing strongest depth profile correlation with silicic acid (compared to correlations with nitrate and phosphate). This points to simultaneous uptake of Zn and silicic acid, thus a community dependant on silicic acid and Zn, such as diatoms. Copper also showed strongest depth profile correlation with silicic acid (Cloete et al. *submitted*). Cadmium, in contrast, showed typical nutrient behaviour, but strongest correlation with nitrate and phosphate, possibly indicating preferential uptake by groups other than diatoms, e.g. *Phaeocystis* and coccolithophores. Manganese and Co, in contrast, did not indicate surface depletion. This is surprising as coccolithophores have a requirement for Co, which can be

replaced by Zn in Co-limited environments (Xu et al., 2007). Surface Fe at 46 °S was the highest encountered at all stations but was not accompanied by high chla concentration. This dissolved Fe pool might not be fully accessible for biological uptake and as a result, may in fact be limiting. For example, pigment composition indicated dominance of the *Phaeocystis* form acclimated to low-iron availability across the STZ and SAZ and PFZ. As mentioned above, alternatively, Viljoen et al. (*submitted)* have shown that at this particular station macro- and micronutrient under-utilization is possibly related to light limitation.

At 49 °S (December) and 50 °S (January), the communities were *Phaeocystis*-dominated, with large contributions of diatoms, and smaller contributions from other picoplankton. Macronutrient concentrations and ratios differed greatly between the two sites. At both stations, nitrate appeared to be largely under-utilized while low, possibly limiting, silicic acid concentrations prevailed. The deepest ML on the transect (102m) was observed at 50 °S, which might explain *Phaeocystis* dominance at this station (Arrigo 1999). *Phaeocystis* have been shown to be more abundant in deeply mixed waters due to photosynthetic properties that allow for efficient light usage under varying light conditions (Alderkamp et al., 2012) and their ability to form colonies that are more resistant to turbulent water (Rousseau et al., 2007; Schoemann et al., 2005). The station at 49 °S was revisited in February, revealing a shift to a diatom-dominated community. February N/P molar ratios (ca. 14:1) agree with a shift to more diatom-dominated waters (Smith and Asper, 2001). An increase in SST from December and February (5.8 °C to 6.5 °C) may potentially destabilize the water column, resulting in a more stratified water column and shallower ML favouring diatom growth (Arrigo, 1999). Silicic acid concentrations increased slightly and phosphate concentrations remained similar from December to February, while nitrate has seen large depletion to near-limiting concentrations, which is suggestive of a late summer community removing nitrate at a much more rapid rate than other macronutrients. Low chla concentrations, coupled with rapid, preferential, nitrate removal suggests that there might be another factor, such as heterotrophic bacterial uptake (Kirchman and Wheeler, 1998) responsible for the large nitrate removal with seasonal progression. Alternatively, near-limiting concentrations of essential trace metals such as Fe could also result in the low chla encountered at 50 °S. This station is one of the two stations where surface depletion and nutrient-type depth profiles were found for Mn and Co (Loock et al., *submitted*). Cobalt was more strongly correlated with phosphate and nitrate than silicic acid which may suggest that the majority of Co

is not taken up by diatoms but other, prominent groups such as *Phaeocystis* (Sunda and Huntsman, 1995).

2.4.4. AAZ

Waters in the AAZ, between the Polar Front and the Southern Boundary of the ACC, are characterized by a relatively diverse community structure dominated by diatoms with notable coccolithophore, haptophyte, pelagophyte and prasinophyte contributions. Nitrate concentrations were still high in December and silicic acid concentrations increased drastically southward across the AAZ. In late summer (February), nitrate concentrations were considerably lower than in December while phosphate and silicic acid concentrations remained largely unchanged. A relatively deep ML (100 m) was encountered at station 53.6 °S, accompanied by relatively high surface concentration of all trace metals (compared to other stations along the transect). Hot spots of increased Mn and Zn concentrations were also observed in the sub-surface in the vicinity of a seamount. Elevated trace metal concentrations have been previously reported in the region around 54 °S and may be attributed to the Bouvet Triple Junction (52 – 56 °S) hydrothermal plume activity (Klunder et al., 2011). The abundance of trace metals may have induced the higher biomass and diversification as well as led to enhanced and preferential uptake of nitrate. Degradation pigments were detected at 53.6 °S that were absent north of the PF, which point to a possibly mature community. Therefore, it is thought that a trace metal influx prior to our trace metal sampling may have caused an early stage local bloom and that our occupation of this station reflects waning bloom conditions. The lower phytoplankton productivity observed in December and February in the same area also supports the concept of a short lived phytoplankton bloom in January caused by a periodic trace metal influx.

Loock et al. (*submitted)* and Cloete et al. (*submitted*) showed that Co, Cd and Zn were more strongly utilized in the surface than Cu and Ni, most likely because phytoplankton have a smaller requirement for Cu and Ni compared to Fe and Zn (Twining and Baines, 2013). Copper might have been utilized by diatom species *Thalassiosira*, which has been shown to have a greater Cu requirement under Fe limitation (Peers and Price, 2006), but the absence or low contribution of typical Cu-utilising groups, such as cyanobacteria, cholorophytes and prasinophytes may be driving under-utilization of Cu. Nickel may also be more important for cyanobacteria and picoeukaryotes than other algal groups in the community (Dupont et al., 2010). Iron limitation

may further decrease the Ni requirement of diatoms by halting urease activity in order to prevent further iron stress (Dupont et al., 2010).

2.4.5. WG

The community structure in the WG was characterized by the highest chla concentration in the study area, although with lower community diversity. High silicic acid concentrations as well as a shoaling of the ML, are environmental factors that favour diatom productivity at the expense of the community (Sedwick et al., 2007). Pigment data further suggests diatom-dominance throughout the season, which is strongly supported by average Si/N and N/P ratios in this region (Arrigo, 1999; Smith and Asper, 2001). High bSi concentration and high bSi to diatom chla ratio at 65 °S further suggest that we encountered diatom bloom conditions, at least at some stations. Nevertheless, coccolithophores and *Phaeocystis* also largely contribute to total chla. Temperatures in the WG fall on the low end of the temperature range reported for coccolithophores (Findlay and Giraudeau, 2000). Gibberd et al. (2013) showed negligible coccolithophore contribution in the WG region in 2008/2009 under similar macronutrient but lower SST conditions. We speculate here that the higher SST observed in 2014/2015 may have led to coccolithophore growth in the WG. Throughout most of the WG, *Phaeocystis* was dominant in its state acclimated to high iron conditions, even though the Fe concentrations were low, possibly limiting. This may be a result of acclimation to earlier high Fe surface concentrations released from ice melt approximately a week prior to our sampling. Highest phaeopigment:chl-a ratios were recorded in the WG indicative of post-bloom communities at the time of sampling at least at some stations. Although our dataset does not encompass any variable to account for zooplankton grazing, we recognise this as an important factor which can also shape the phytoplankton community composition (Gibberd et al., 2013).

At 60 °S and 65 °S, for example, a low salinity feature and a temperature inversion is observed at these stations, accompanied by a shoaling of the ML (50 m), most likely a result of low density waters from ice melt producing stratified waters in this region (Wright et al., 2010). The shoaling of the ML may possibly create a stratified water column potentially driving diatom dominance in this region. Water column stratification caused by melt waters could have acted as a hydrographic barrier and may have limited vertical resupply of nutrients. Depth profiles at station 60 °S and 65 °S both showed large surface depletion of bio-utilized trace metals

(excluding Ni and Cu) and of macronutrients in the water column. Iron, for example, showed near-limiting concentrations (Moore et al., 2013) and was possibly a key factor controlling the low chla concentration (Moore et al., 2013; Viljoen et al., *submitted*). Furthermore, Viljoen et al. (*submitted)* have shown through incubation experiments that iron is limiting at 65 °S. In addition, co-limitation with other trace metals may have played a role. For example, the strong Mn depletion may be related to the importance of Mn in iron deficient waters as Fe-deficient conditions increase the Mn demand (Peers and Price, 2004). Loock et al. (*submitted*) furthermore highlighted large Co surface depletion and have attributed this to bloom conditions depleting a range of micronutrients, thereby creating a selection pressure which may promote Co substitution through removal of primary enzymatic nutrients.

Conditions south of 68 °S, close to the ice edge, changed drastically and with it the community. For example, at station 68 °S the highest biomass, and some of the highest surface trace metal concentrations were encountered, with the highest coccolithophore contribution (34 %) to any community structure in the study area. The large coccolithophore biomass and greater contribution to the community structure may be linked with trace metal concentrations, particularly Fe, Co and Cd. *Emiliania huxleyi,* for example, have been shown to have a lower cellular requirement for Fe than diatoms (Brand, 1991; Sunda and Huntsman, 1995; Muggli and Harrison, 1996). Furthermore, various studies have hypothesized that *Emiliania huxleyi's* low Fe requirement allows it to grow in regions where diatoms are limited by Fe (Brand, 1991; Muggli and Harrison, 1997). Ho et al. (2003) have further shown coccolithophores to have a higher quota for Co and Cd than diatoms. Therefore, large coccolithophore contribution in these waters may be related to iron approaching limiting concentrations, inhibiting further diatom growth as well as an abundance of essential metals, particularly Co and Cd, essential in coccolithophore metabolic functions.

The presence of the high iron acclimated form of *Phaeocystis* indicates that there was possibly high availability of Fe prior to the sampling as it has been documented that they take at least two days to fully acclimate to high iron conditions by adjusting their photosynthetic pigments (Sedwick et al., 2007; Viljoen et al., *submitted*). Therefore, we assume a recent ice melt accompanied by augmented trace metal supply in which Fe is preferentially utilized to near limiting concentrations. Elevated trace metal surface concentrations in this region are partly attributed to ice melt and subsequent input of associated trace metals into the surface waters

(Grotti et al., 2001). Extensive iron utilization was coupled with limited bio-utilization of other metals probably due to highest phytoplankton requirements for Fe (Twining and Baines, 2013).

2.5. Conclusion

In this study, as in previous studies within the Atlantic Southern Ocean, we have seen a variety of physical (temperature, salinity, mixed-layer depth and the resulting water column structure) and chemical (macronutrients) properties shape and influence phytoplankton abundance and community structure. It is well established that certain factors that differ regionally, like macronutrients and temperature, shape the phytoplankton community and the relative contribution of groups to the community. However, differences in phytoplankton abundance and community structure are not accounted for when considering each of these variables on their own. Herein, lies the advantage of a multi-variable *in-situ* observational approach, which incorporates essential trace metals, to address phytoplankton community variability both spatially and temporally. Additional variables, particularly biological variables such as grazing, were not considered in this study, although we acknowledge that biological interactions are definite driver of phytoplankton variability and warrant further investigation.

Micronutrients are a vital, additional variable which can account for such variability when physical and macronutrients observations cannot. Zinc and Mn were most strongly correlated with silicic acid south of the PF, indicative of a diatom-dominated community that was dependent on both silicic acid and these metals. The importance of considering the influence of a suite of trace metals has also been shown in this study when localised blooms could not be explained by the other variables, or iron alone. Our findings suggest that an influx or abundance of a suite of trace metals linked to hydrothermal plume activity and ice melt is closely related to increasing biomass and community diversification. Although, in some instances, it is unclear whether trace metal distributions drive the community composition, or the composition of the community drives observed trace metal distributions. Our findings corroborate the importance of Fe as an essential trace metal. Iron concentrations appeared to affect the community composition (most notably illustrated by acclimation state of *Phaeocystis*) as well as trace metal distributions, in some instances. For example, at station 68 °S, preferential iron utilization to near-limiting concentrations may have driven under-utilization of other essential trace metals.

Lastly, the timing of trace metal fluxes brought about by summer ice melt and potential hydrothermal inputs proved to be a pivotal factor in the community interpretation. Therefore, when making inferences about the community structure and trace metal distribution we strongly recommend future studies to consider timing (if possible) of such influx events.

Acknowledgements

The work leading to these results received funding from the National Research Foundation (NRF) under the SA/Norway Collaboration Program and the South African National Antarctic Program, grant numbers 91313 and 110731 awarded to S. Fietz. I.J. Weir acknowledges the financial assistance of the NRF through the South African National Antarctic Program grant number 110731. The authors furthermore thank the crew of the R/V SA Agulhas II, Department of Environmental Affairs (DEA), and all the scientific cruise participants of SANAE 54.

References

Alderkamp, A.C., Garcon, V., de Baar, H.J.W., Arrigo, K.R., 2011. Short-term photoacclimation effects on photoinhibition of phytoplankton in the Drake Passage (Southern Ocean). Deep Sea Res. Part I Oceanogr. Res. Pap. 58, 943–955. https://doi.org/10.1016/j.dsr.2011.07.001

Alderkamp, A.C., Kulk, G., Buma, A.G.J., Visser, R.J.W., Van Dijken, G.L., Mills, M.M., Arrigo, K.R., 2012. The effect of iron limitation on the photophysiology of *Phaeocystis antarctica* (prymnesiophyceae) and *Fragilariopsis cylindrus* (bacillariophyceae) under dynamic irradiance. J. Phycol. 48, 45–59. https://doi.org/10.1111/j.1529-8817.2011.01098.x

Arrigo, K.R., 1999. Phytoplankton community structure and the drawdown of nutrients and CO_2 in the Southern Ocean. Science 283, 365–367. https://doi.org/10.1126/science.283.5400.365

Brand, L.E., 1991. Minimum iron requirements of marine phytoplankton and the implications for the biogeochemical control of new production. Limnol. Oceanogr. 36, 1756–1771. https://doi.org/10.4319/lo.1991.36.8.1756

Brunet, C., Johnsen, G., Lavaud, J., Roy, S., 2011. Pigments and photoacclimation processes, in: Roy, S., Llewellyn, C., Egeland, E.S., Johnsen, G. (Eds.), Phytoplankton Pigments: Characterization, Chemotaxonomy and Applications in Oceanography. Cambridge University Press, New York, pp. 445–471. https://doi.org/10.1017/CBO9780511732263.017

Brzezinski, M.A., 1985. The Si:C:N ratio of marine diatoms: interspecific variability and the effect of some environmental variables. J. Phycol. 21, 347–357. https://doi.org/10.1111/j.0022-3646.1985.00347.x

Carreto, J.I., Montoya, N.G., Carignan, M.O., Akselman, R., Acha, E.M., Derisio, C., 2016. Environmental and biological factors controlling the spring phytoplankton bloom at the Patagonian shelf-break front – Degraded fucoxanthin pigments and the importance of microzooplankton grazing. Prog. Oceanogr. 146, 1–21. https://doi.org/10.1016/j.pocean.2016.05.002

Chitari, R.R., Anil, A.C., 2017. Estimation of diatom and dinoflagellate cell volumes from surface waters of the Northern Indian Ocean. Oceanologia 59, 389–395. https://doi.org/10.1016/j.oceano.2017.03.001

Cloete, R., Loock, J.C., Mtshali, T.N., Fietz, S., Roychoudhury, A.N., *submitted*. Winter and summer distributions of Copper, Zinc and Nickel along the International GEOTRACES section GIPY05: Insights into deep winter mixing. Chem. Geol.

Cutter, G., Codispoti, L., Croot, P., Francois, R., Lohan, M., Rutgers Van Der Loeff, M., 2014. Sampling and Sample-handling Protocols for GEOTRACES Cruises [http://www.geotraces.org/libraries/documents/Intercalibration/Cookbook.pdf].

Deppeler, S.L., Davidson, A.T., 2017. Southern Ocean Phytoplankton in a Changing Climate. Front. Mar. Sci. 4, 40. https://doi.org/10.3389/fmars.2017.00040

DiTullio, G.R., Garcia, N., Riseman, S.F., Sedwick, P.N., 2007. Effects of iron concentration on pigment composition in *Phaeocystis antarctica* grown at low irradiance. Biogeochemistry 83, 71–81. https://doi.org/10.1007/978-1-4020-6214-8_7

Dupont, C.L., Buck, K.N., Palenik, B., Barbeau, K., 2010. Nickel utilization in phytoplankton assemblages from contrasting oceanic regimes. Deep Sea Res. Part I Oceanogr. Res. Pap. 57, 553–566. https://doi.org/10.1016/J.DSR.2009.12.014

Egan, L., 2008. Determination of nitrate and/or nitrite in brackish or seawater by flow injection analysis. Quickchem method® 31-107-04-1-C. Lachat Instruments, USA.

Findlay, C.S., Giraudeau, J., 2000. Extant calcareous nannoplankton in the Australian Sector of the Southern Ocean (austral summers 1994 and 1995). Mar. Micropaleontol. 40, 417–439. https://doi.org/10.1016/S0377-8398(00)00046-3

Garcia, H.E., Locarnini, R.A., Boyer, T.P., Antonov, J.I., Baranova, O.K., Zweng, M.M., Reagan, J.R., Johnson, D.R., 2013. World Ocean Atlas 2013. Vol. 4: Dissolved Inorganic Nutrients (phosphate, nitrate, silicate). S. Levitus, Ed.; A. Mishonov, Tech. Ed. NOAA Atlas NESDIS 76, 25. https://doi.org/10.1182/blood-2011-06-357442

Gibberd, M.J., Kean, E., Barlow, R., Thomalla, S., Lucas, M., 2013. Phytoplankton chemotaxonomy in the Atlantic sector of the Southern Ocean during late summer 2009. Deep Sea Res. Part I Oceanogr. Res. Pap. 78, 70–78. https://doi.org/10.1016/j.dsr.2013.04.007

Grasshoff, K., Kremling, K., Ehrhardt, M., 1983. Methods of Seawater Analysis. Verlag Chemie, Weinheim, Germany.

Grotti, M., Soggia, F., Abelmoschi, M.L., Rivaro, P., Magi, E., Frache, R., 2001. Temporal distribution of trace metals in Antarctic coastal waters. Mar. Chem. 76, 189–209. https://doi.org/10.1016/S0304-4203(01)00063-9

Ho, T.Y., Quigg, A., Finkel, Z. V., Milligan, A.J., Wyman, K., Falkowski, P.G., Morel, F.M.M., 2003. The elemental composition of some marine phytoplankton. J. Phycol. 39, 1145–1159. https://doi.org/10.1111/j.0022-3646.2003.03-090.x

Hudson, R.J.M., Morel, F.M.M., 1990. lron transport in marine phytoplankton: Kinetics of cellular and medium coordination reactions. Limnol. Oceanogr. 35, 1002–1020. https://doi.org/10.4319/lo.1990.35.5.1002

Jeffrey, S.W., Mantoura, R.F.C., Wright, S.W., 1997. Phytoplankton pigments in oceanography: guidelines to modern oceanography. UNESCO Publishing. United Nations Educational, Scientific and Cultural Organization, Paris. https://doi.org/10.1023/A:1007168802525

Kirchman, D.L., Wheeler, P.A., 1998. Uptake of ammonium and nitrate by heterotrophic bacteria and phytoplankton in the sub-Arctic Pacific. Deep Sea Res. Part I Oceanogr. Res. Pap. 45, 347–365. https://doi.org/10.1016/S0967-0637(97)00075-7

Klausmeier, C.A., Litchman, E., Daufresne, T., Levin, S.A., 2004. Optimal nitrogen-to phosphorus stoichiometry of phytoplankton. Nature 429, 171–174. https://doi.org/1.1029/2001GL014649

Klunder, M.B., Laan, P., Middag, R., De Baar, H.J.W., van Ooijen, J.C., 2011. Dissolved iron in the Southern Ocean (Atlantic sector). Deep Sea Res. Part II Top. Stud. Oceanogr. 58, 2678–2694. https://doi.org/10.1016/j.dsr2.2010.10.042

Loock, J., Cloete, R., Mtshali, T., Fietz, S., Roychoudhury, A., *submitted*. The biogeochemistry of Co, Mn and Cd on a seasonal re-occupation of the Southern Ocean. Chem. Geol.

Mackey, M., Mackey, D., Higgins, H., Wright, S., 1996. CHEMTAX - a program for estimating class abundances from chemical markers:application to HPLC measurements of phytoplankton. Mar. Ecol. Prog. Ser. 144, 265–283. https://doi.org/10.3354/meps144265

Mendes, C.R.B., Kerr, R., Tavano, V.M., Cavalheiro, F.A., Garcia, C.A.E., Gauns Dessai, D.R., Anilkumar, N., 2015. Cross-front phytoplankton pigments and chemotaxonomic groups in the Indian sector of the Southern Ocean. Deep Sea Res. Part II Top. Stud. Oceanogr. 118, 221–232. https://doi.org/10.1016/j.dsr2.2015.01.003

Moore, C.M., Mills, M.M., Arrigo, K.R., Berman-Frank, I., Bopp, L., Boyd, P.W., Galbraith, E.D., Geider, R.J., Guieu, C., Jaccard, S.L., Jickells, T.D., La Roche, J., Lenton, T.M., Mahowald, N.M., Maranon, E., Marinov, I., Moore, J.K., Nakatsuka, T., Oschlies, A., Saito, M.A., Thingstad, T.F., Tsuda, A., Ulloa, O., 2013. Processes and patterns of oceanic nutrient limitation. Nat. Geosci 6, 701–710. https://doi.org/10.1038/ngeo1765

Muggli, D., Harrison, P., 1996. Effects of nitrogen source on the physiology and metal nutrition of *Emiliania huxleyi* grown under different iron and light conditions. Mar. Ecol. Prog. Ser. 130, 255–267. https://doi.org/10.3354/meps130255

Muggli, D.L., Harrison, P.J., 1997. Effects of iron on two oceanic phytoplankters grown in natural NE subarctic pacific seawater with no artificial chelators present. J. Exp. Mar. Bio. Ecol. 212, 225–237.

NOAA, 2015. High density XBT transects: AX25 [http://www.aoml.noaa.gov/phod/hdenxbt/ax_home.php?ax=25].

Orsi, A.H., Whitworth, T., Nowlin, W.D., 1995. On the meridional extent and fronts of the Antarctic Circumpolar Current. Deep Sea Res. Part I Oceanogr. Res. Pap. 42, 641–673. https://doi.org/10.1016/0967-0637(95)00021-W

Peers, G., Price, N.M., 2004. A role for manganese in superoxide dismutases and growth of iron-deficient diatoms. Limnol. Oceanogr. 49, 1774–1783. https://doi.org/10.4319/lo.2004.49.5.1774

Peers, G., Price, N.M., 2006. Copper-containing plastocyanin used for electron transport by an oceanic diatom. Nature 441, 341–344. https://doi.org/10.1038/nature04630

Ragueneau, O., Tréguer, P., 1994. Determination of biogenic silica in coastal waters: applicability and limits of the alkaline digestion method. Mar. Chem. 45, 43–51. https://doi.org/10.1016/0304-4203(94)90090-6

Ras, J., Claustre, H., Uitz, J., 2008. Spatial variability of phytoplankton pigment distributions in the Subtropical South Pacific Ocean: comparison between in-situ and predicted data. Biogeosciences 5, 353–369.

Redfield, A.C., 1958. The biological control of chemical factors in the environment. Am. Sci. 46, 230. https://doi.org/10.2307/27827150

Rousseau, V., Chrétiennot-Dinet, M.-J., Jacobsen, A., Verity, P., Whipple, S., 2007. The life cycle of Phaeocystis: state of knowledge and presumptive role in ecology. Biogeochemistry 83, 29–47. https://doi.org/10.1007/s10533-007-9085-3

Saito, M.A., Moffett, J.W., 2002. Temporal and spatial variability of cobalt in the Atlantic Ocean. Geochim. Cosmochim. Acta 66, 1943–1953.

Schlüter, L., Henriksen, P., Nielsen, T.G., Jakobsen, H.H., 2011. Phytoplankton composition and biomass across the southern Indian Ocean. Deep Sea Res. Part I Oceanogr. Res. Pap. 58, 546–556. https://doi.org/10.1016/j.dsr.2011.02.007

Schoemann, V., Becquevort, S., Stefels, J., Rousseau, V., Lancelot, C., 2005. *Phaeocystis* blooms in the global ocean and their controlling mechanisms: a review. J. Sea Res. 53, 43–66. https://doi.org/10.1016/j.seares.2004.01.008

Sedwick, P.N., Garcia, N.S., Riseman, S.F., Marsay, C.M., DiTullio, G.R., 2007. Evidence for high iron requirements of colonial *Phaeocystis antarctica* at low irradiance. Biogeochemistry 83, 83–97. https://doi.org/10.1007/s10533-007-9081-7

Smith, W.O., Asper, V.L., 2001. The influence of phytoplankton assemblage composition on biogeochemical characteristics and cycles in the southern Ross Sea, Antarctica. Deep Sea Res. Part I Oceanogr. Res. Pap. 48, 137–161. https://doi.org/10.1016/S0967-0637(00)00045-5

Sunda, W.G., Huntsman, S.A., 1995. Cobalt and zinc interreplacement in marine phytoplankton: Biological and geochemical implications. Limnol. Oceanogr. 40, 1404–1417. https://doi.org/10.4319/lo.1995.40.8.1404

Twining, B.S., Baines, S.B., 2013. The Trace Metal Composition of Marine Phytoplankton. Ann. Rev. Mar. Sci. 5, 191–215. https://doi.org/10.1146/annurev-marine-121211-172322

van Leeuwe, M.A., Kattner, G., van Oijen, T., de Jong, J.T.M., de Baar, H.J.W., 2015. Phytoplankton and pigment patterns across frontal zones in the Atlantic sector of the Southern Ocean. Mar. Chem. 177, 510–517. https://doi.org/10.1016/j.marchem.2015.08.003

Viljoen, J.J., Philibert, R., van Horsten, N., Mtshali, T., Roychoudhury, R.N., Thomalla, S., Fietz, S., *submitted*. Phytoplankton response in growth, photophysiology and community structure to iron and light in polar frontal and Antarctic waters. Limnol. Oceanogr.

Wolters, M., 2002. Determination of silicate in brackish or seawater by flow injection analysis. QuickChem® method 31-114-24-1-D. Lachat Instruments, USA.

Wright, S.W., van den Enden, R.L., Pearce, I., Davidson, A.T., Scott, F.J., Westwood, K.J., 2010. Phytoplankton community structure and stocks in the Southern Ocean (30-80E) determined by CHEMTAX analysis of HPLC pigment signatures. Deep Sea Res. Part II Top. Stud. Oceanogr. 57, 758–778. https://doi.org/10.1016/j.dsr2.2009.06.015

Xu, Y., Tang, D., Shaked, Y., Morel, F.M.M., 2007. Zinc, cadmium, and cobalt interreplacement and relative use efficiencies in the coccolithophore *Emiliania huxleyi*. Limnol. Oceanogr. 52, 2294–2305. https://doi.org/10.4319/lo.2007.52.5.2294

Supplementary to Chapter 2

Links between phytoplankton community composition and trace metal distribution in the surface waters of the Atlantic Southern Ocean

Ian Weir[1§], Johan Viljoen[1§], Susanne Fietz[1]*, Ryan Cloete[1], Jean Loock[1], Raissa Philibert[1¥], Alakendra N. Roychoudhury[1]

S2. Supplementary Methods

S2.1. Details regarding the choice of specific pigments and phytoplankton groups in the CHEMTAX processing for S54 cruise Good Hope transect.

The interpretation of HPLC pigment data for the assessment of phytoplankton community composition can be difficult due to pigment markers that are present in several groups. However, with the use of the CHEMTAX v1.95 chemical taxonomy software (Mackey et al., 1996), the HPLC-pigment concentration data sets can be used to calculate the contribution of individual phytoplankton functional groups to total chlorophyll-a (used here as a proxy for biomass). The CHEMTAX phytoplankton community composition estimates are based on the relative abundance of a suite of marker pigments to total chla, initial ratios, in water of close proximity to the current study area, determined by previous studies (Wright et al., 2010). The software makes use of the idea that each group has a characteristic set of accessory pigments, but all phytoplankton groups contain chla responsible for the contribution to the total chla of a community. The CHEMTAX matrix factorisation is therefore based on the ratios between at least two, often various accessory pigments and chla per group (Mackey et al., 1996; Wright et al., 2010). These ratios are loaded into the program along with the pigment concentrations determined by HPLC analysis, where after it goes through a suite of iterations and provides an estimate of the group contribution to the total chla. For the results of the CHEMTAX software to be reliable and as accurate as possible, knowledge on the phytoplankton communities present in the study area is needed in the form of pigment ratios per phytoplankton group (Schlüter et al., 2011). Below we briefly describe the set-up of the CHEMTAX software (choices of groups and their accessory pigments) to process the respective pigment data for the identification of phytoplankton functional groups and determination of their relative abundances for each surface

sample taken. We also provide additional explanations on less typical selections of groups and "marker" pigments.

Choice of groups: The main phytoplankton groups to be included into the initial ratio matrix that were used by the CHEMTAX processing were selected based on literature data published for the Atlantic Southern Ocean and nearby regions (Gibberd et al., 2013; Mendes et al., 2015; Wright et al., 2010). Ten phytoplankton groups were chosen: cyanobacteria, prasinophytes, dinoflagellates, cryptophytes, *Phaeocystis*-H (High iron-acclimated state of *Phaeocystis antarctica*), *Phaeocystis*-L (Low iron-acclimated state of *P. antarctica*), coccolithophores (haptophytes-6), pelagophytes (pelago-1), chlorophytes and diatoms. *Phaeocystis*-H and -L here refer exclusively to *P. antarctica* (Wright et al., 2010) but were separated into functional forms acclimated to low and high iron due to the ability of *P. antarctica* to adjust their pigment ratios to various ambient iron concentration and conditions, iron enriched vs. iron depleted conditions (DiTullio et al., 2007). Although it would be ideal, no separate bins were created according to depth or regional differences as with different zones. This was due to the limitation of samples and HPLC data as that only represents surface communities. Therefore, all HPLC pigment data was set to be processed within one run. The optimised ratios after the CHEMTAX analyses can be found in Table S2.3. Below we provide further details regarding the choice of specific pigments for the CHEMTAX.

Choice of pigments: The following pigments were included in our analysis: Chl-c3; Chl-c1c2; peridinin (Peri); 19'-butanoyloxyfucoxanthin (19-But); fucoxanthin (Fuco); neoxanthin (Neo); prasinoxanthin (Pras); 19'-hexanoyloxyfucoxanthin (19-Hex); alloxanthin (Allox); zeaxanthin (Zea); Chl-b (Table S2.2). From the detected pigments, these pigments were selected as two or more of them together are indicative of the identified phytoplankton groups in certain ranges of ratios versus chla. Since the published optimised ratios from Wright et al. (Wright et al., 2010) for the Southern Ocean do not contain zeaxanthin values and no other literature was found that reports zeaxanthin ratios for phytoplankton studies that include pelagophytes and coccolithophores in the same initial pigment ratio set, ratios for the Indian SAZ from Mendes et al. (Mendes et al., 2015) were used in our study. Some pigments known to be prominent and suitable marker pigments in other oceanic regions, such as lutein, for example, were below detection limit in our Atlantic Southern Ocean study. In contrast to Viljoen et al. (submitted),

Allox was detected and was included as it was an indication of the presence of the cryptophyte group. However, to ensure that the number of pigments used for the CHEMTAX analyses is higher than the number of phytoplankton groups (i.e. ten; Mackey et al. 1996), we added the pigment pair Chl-c1c2 to the suite of marker pigments used in our CHEMTAX processing. This Chl-c1c2 ratio is a combined signal of the Chl-c1 and Chl-c2 pigments, which could not be separated by the HPLC system used. The Chl-c1c2 was included as it was the only pigment left within our HPLC-pigment data set that is not drastically influenced by degradation or photo-acclimation (Appendix A - Supplemental information of Viljoen et al. submitted; section 1.1.5). The CHEMTAX software does not allow the number of phytoplankton groups to be equal or more than the number of pigments used in the calculations. To adhere to this, diatoms were grouped as total diatoms to reduce the number of phytoplankton and due to the need of both Chl-c3 and Chl-c1 separate from Chl-c2 to distinguish two separate group of diatoms with the use of pigments (Wright et al., 2010).

Pelagophytes (pelago-1), which are not commonly reported in Atlantic Southern Ocean CHEMTAX studies (Gibberd et al., 2013), were included as their presence in our samples was supported by the presence of their dominant marker pigment 19'-butanoyloxyfucoxanthin (Schlüter et al., 2011). This proved valuable, since the CHEMTAX results showed they were present in noticeable contributions within a reasonable amount of our samples, especially in the PFZ and AAZ. For all 19-But ratios, the latest and geographically, closest available ratios optimised for the Indian SAZ were used (Mendes et al., 2015).

S2.2. Modified colorimetric detection of silicic acid

Concentrations of certain reagents differed slightly from the original method described by Grasshoff (1983). Following the modified method, sulphuric acid (3.6 M) was added to a solution of ammonium molybdate terathydrate (20g/100ml) as opposed to sulphuric acid (4.5 M) and ammonium molybdate tetrahydrate (12.7g/100ml) as recommended by Grasshoff (1983). A modified solution of ascorbic acid (1.75g/100ml) was also used, which differed from the 2.8g/100ml recommended by Grasshoff (1983).

S2. Supplementary Figures

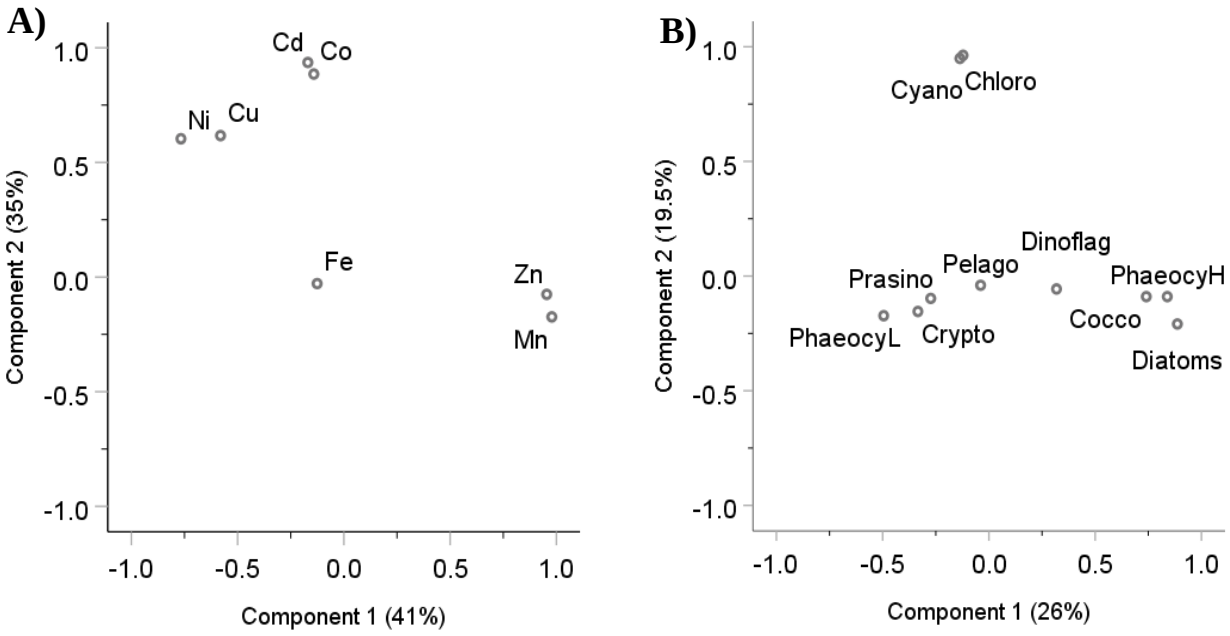

Figure S2.1 Principal component analysis (PCA) for dissolved trace metal and phytoplankton composition. Visual display of Table 2.2 to aid in providing a better overview trace metal variance and phytoplankton group variance. **A)** PCA loading plot of trace metal distribution, where component 1 explains 41 % and component 2 35 % of the variance. A third component accounts for 22 % of the variance. **B)** PCA loading plot of phytoplankton groups, where component 1 explains 26 % and component 2 19.5 % of the variance.

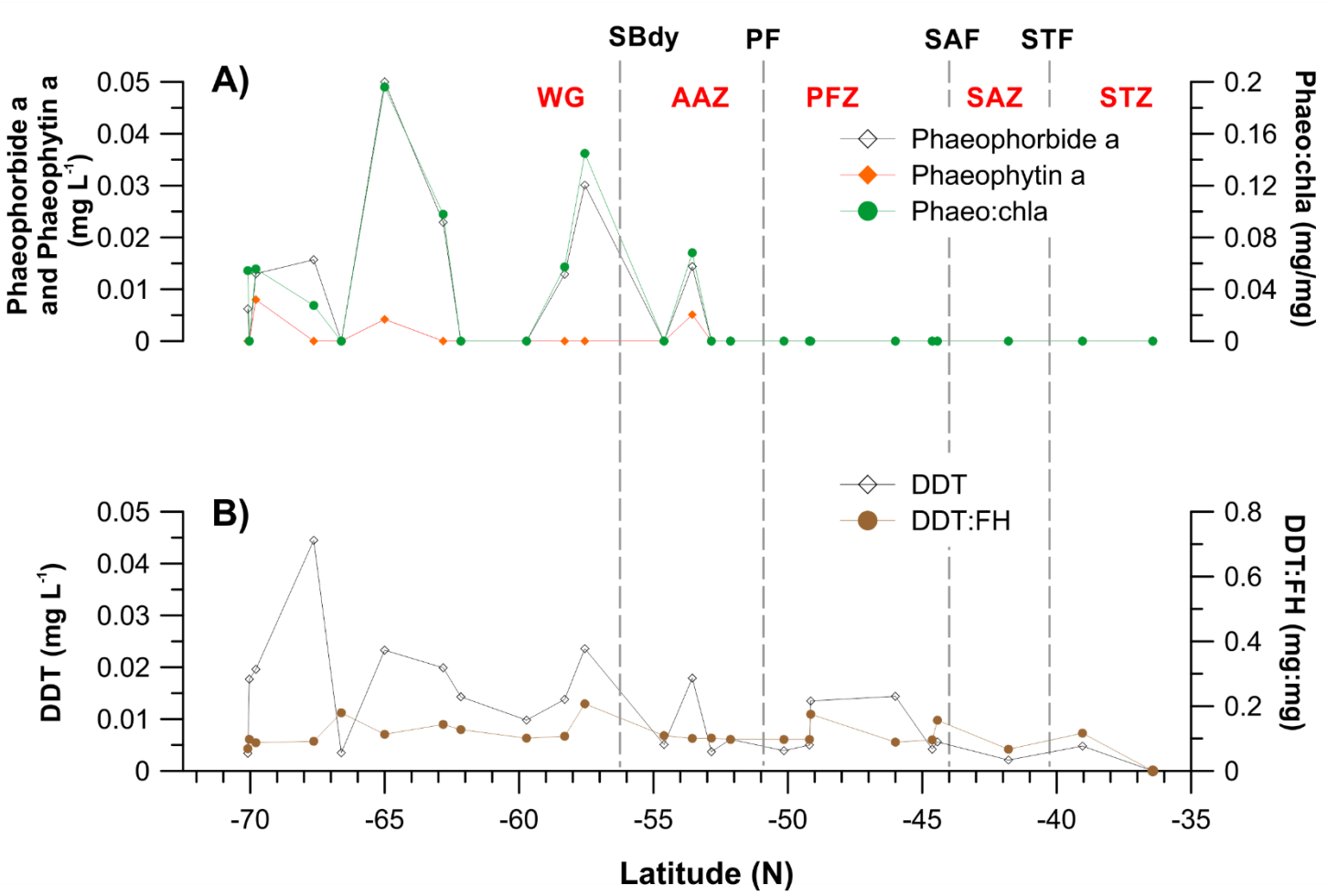

Figure S2.2 Transect profiles of pigments indicative of degradation and photo-acclimation to determine potential grazing and bloom conditions. **A)** Phaeopigments (Pheophorbide a and Pheophytin a) concentrations, and ratio of phaeopigment (sum of phaeophorbide plus phaeophytin) versus chl-a (Phaeo:chla); **B)** Sum of diadinoxanthin and diatoxanthin concentrations (DDT), and ratio of DDT versus sum of Fucoxanthin + 19'-hexanoyloxyfucoxanthin, (DDT:FH).

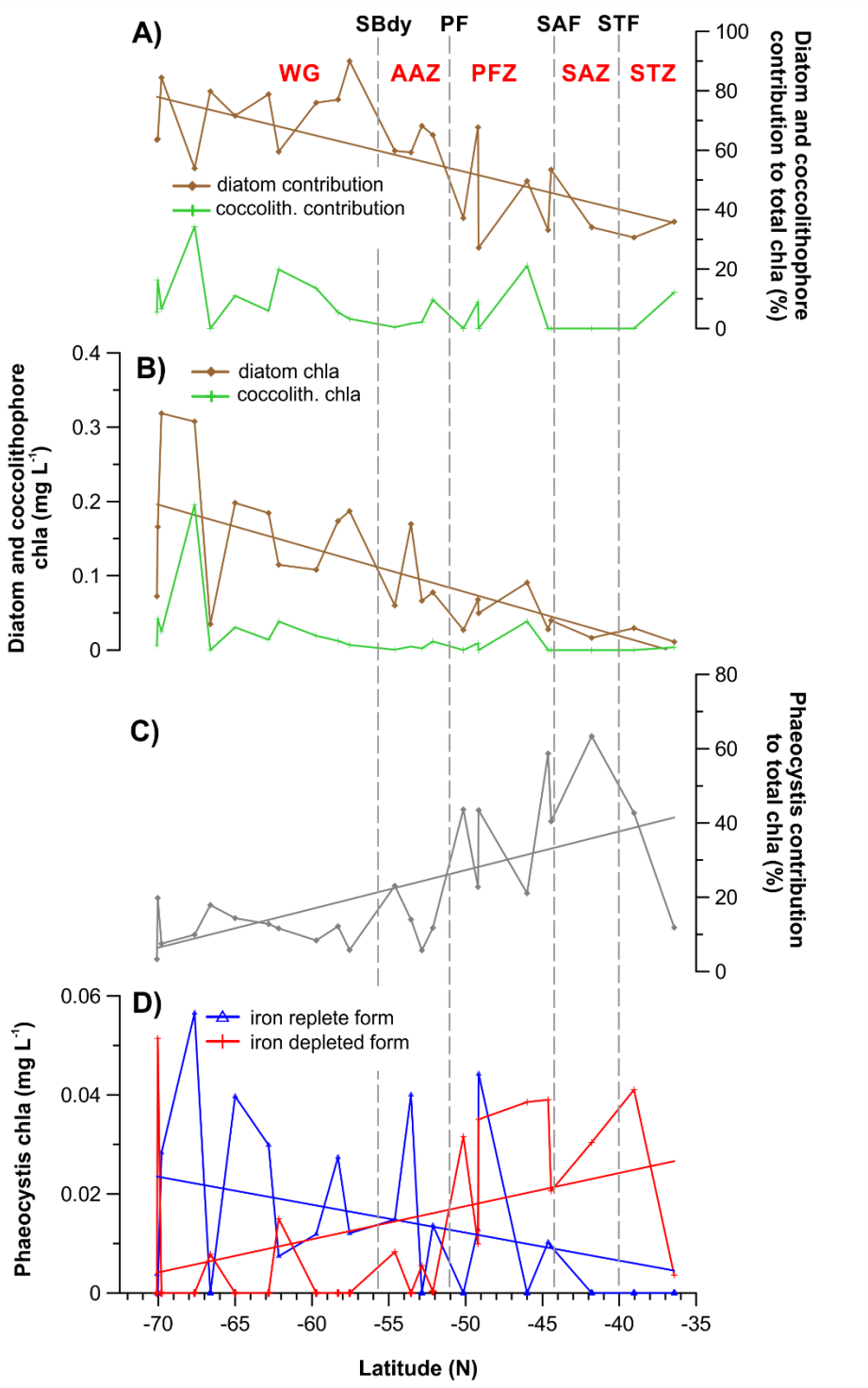

Figure S2.3 Trends in diatom (**A**, **B**) and *Phaeocystis antarctica* (**C**, **D**) distribution along Good Hope Line transect. The two groups are the dominant phytoplankton across the transect, therefore understanding their distribution is important. The trends in contribution and in group-specific chl-a are estimated based on the marker pigments composition using CHEMTAX matrix factorisation software (Mackey et al., 1996; Wright et al., 2010). (**A**) diatom contribution to total chl-a, **B**) chl-a derived from diatoms, **C**) *Phaeocystis* contribution to total chl-a, **D**) chl-a derived from *Phaeocystis*, which can be distinguished into forms acclimated to high iron concentrations and forms acclimated to low iron concentrations (Wright et al. 2010). The coefficient of

S2. Supplementary Tables

Table S2.1 Averages and ranges of macronutrient **A**) concentrations and **B**) ratios in the four distinguished water masses across the Atlantic sector of the Southern Ocean measured during the first (December), third (January) and fourth (February) leg of voyage SANAE54 (see Fig. 2.1 for cruise map). The table provides an overview of nutrient regimes in each oceanic zone and monthly changes in concentrations and ratios. Nutrient concentration profiles are shown in Figure 2.3. Avg. – average, N.D. – not determined.

A)	Zone	H_4SiO_4 (µM)		NO_3^- (µM)		PO_4^{2-} (µM)	
		Range	Avg.	Range	Avg.	Range	Avg.
	STZ (34 - 40.4°S)	(0.2-3.8)	1.5	(1.3-7.9)	1.3	(0.00-0.46)	0.2
	SAZ (40.41 - 44°S)	(0.3-10.1)	1.7	(2.7-40.2)	24	(0.36-1.57)	0.9
Dec	PFZ (44.1 - 50.4°S)	(0.3-10.1)	2.1	(20.7-40.2)	30	(0.42-1.57)	1.0
	AAZ (50.4 - 55.4°S)	(4.5-66.8)	24	(10.5-40.1)	30	(0.6-2.9)	1.5
	WG (55.4-70°S)	(37.5-87)	56	(6.8-36.6)	14	0.57-3.3)	1.7
	STZ (34 - 40.4°S)	N.D.	N.D.	N.D.	N.D.	N.D.	N.D.
	SAZ (40.41 - 44°S)	N.D.	N.D.	N.D.	N.D.	N.D.	N.D.
Jan	PFZ (44.1 - 50.4°S)	(0.7-6.7)	2.7	(5.9-28)	16	(0.03-2.02)	1.1
	AAZ (50.4 - 55.4°S)	(3.6-19.8)	12	(14.3-24)	18	(0.95-1.77)	1.3
	WG (55.4-70°S)	(28.2-84.3)	53	(11.8-25.9)	19	(0.66-2.4)	1.4
	STZ (34 - 40.4°S)	(0-1.7)	0.6	(0.2-0.7)	0.4	(0-0.25)	0.1
	SAZ (40.41 - 44°S)	(0.6-4.3)	0.9	(0.3-8.8)	4.5	(0.06-0.63)	0.4
Feb	PFZ (44.1 - 50.4°S)	(0.6-4.3)	2.2	(4.9-13.4)	9.5	(0.57-1.6)	1.0
	AAZ (50.4 - 55.4°S)	(2.8-98)	24	(12.7-22.1)	17	(0.66-2.4)	1.3
	WG (55.4-70°S)	(18.7-57.1)	41	(6.9-34.4)	13	(0.34-1.86)	1.0

B)	Zone	Si/P (µmol:µmol)		Si/N (µmol:µmol)		N/P (µmol:µmol)	
		Range	Avg.	Range	Avg.	Range	Avg.
	STZ (34 - 40.4°S)	(0-53)	11	(0.03-3.89)	1.8	(0-31.3)	7.8
	SAZ (40.41 - 44°S)	(0.6-3.3)	1.8	(0.03-0.76)	0.2	94.4-52)	18
Dec	PFZ (44.1 - 50.4°S)	(0.2-8.1)	1.9	(0.01-0.37)	0.1	(16.2-94.9)	35
	AAZ (50.4 - 55.4°S)	(1.7-51)	20	(0.2-4.7)	1.1	(6.3-69)	26
	WG (55.4-70°S)	(21.4-78.5)	37	(2-7.05)	4.2	(3.9-31)	9.5
	STZ (34 - 40.4°S)	N.D.	N.D.	N.D.	N.D.	N.D.	N.D.
	SAZ (40.41 - 44°S)	N.D.	N.D.	N.D.	N.D.	N.D.	N.D.
Jan	PFZ (44.1 - 50.4°S)	(0.5-6.9)	2.5	(0.04-0.44)	0.2	(6.8-32.4)	15
	AAZ (50.4 - 55.4°S)	(3-14.9)	8.7	(0.2-1.01)	0.7	(8-25.4)	14
	WG (55.4-70°S)	(17.7-127)	43	(1.35-6.31)	3.0	(9.5-26)	15
	STZ (34 - 40.4°S)	(0-32.4)	8.8	0.1-4.13	1.8	(0-10)	3.7
	SAZ (40.41 - 44°S)	(0.4-33)	5.0	0.04-3.36	0.8	(1.8-16.3)	11
Feb	PFZ (44.1 - 50.4°S)	(0.9-4.4)	2.2	0.12-0.35	0.2	(5.1-18.9)	9.7
	AAZ (50.4 - 55.4°S)	(2.1-64.3)	19	(0.2-5.03)	1.4	(6.2-23.3)	14
	WG (55.4-70°S)	(20.1-88.3)	45	(1.66-4.06)	3.2	(6.6-38.9)	15

Table S2.2 Pigment concentrations in µg L^{-1} based on HPLC analysis for the Good Hope transect on this cruise (SANAE54). Resulting CHEMTAX phytoplankton community concentrations are given in the table below (Table S2.4) and displayed in Fig 2.3.

Latitude (N)	Longitude (E)	Date	Month	Chl-c3	Chl-c1c2	Peri	But	Fuco	Neo	Pras	Hex	Allox	Zea	Chl-b	Chl-a
-36.4249	**13.166**	12/6/2014	Dec	0.0000	0.0000	0.0000	0.0000	0.0000	0.0000	0.0000	0.0051	0.0000	0.0144	0.0000	**0.0303**
-39.0427	**11.4504**	12/7/2014	Dec	0.0000	0.0115	0.0058	0.0060	0.0126	0.0000	0.0000	0.0286	0.0000	0.0039	0.0075	**0.0962**
-41.7949	**8.6075**	2/14/2015	Feb	0.0000	0.0046	0.0000	0.0044	0.0096	0.0000	0.0000	0.0218	0.0000	0.0000	0.0000	**0.0480**
-44.4375	**7.1044**	12/9/2014	Dec	0.0046	0.0095	0.0000	0.0068	0.0183	0.0000	0.0000	0.0175	0.0000	0.0024	0.0000	**0.0742**
-44.6305	**6.2283**	2/13/2015	Feb	0.0050	0.0083	0.0041	0.0060	0.0130	0.0000	0.0021	0.0309	0.0000	0.0000	0.0000	**0.0840**
-46.0015	**7.3337**	1/12/2015	Jan	0.0089	0.0225	0.0093	0.0121	0.0816	0.0000	0.0000	0.0803	0.0000	0.0000	0.0000	**0.1828**
-49.1514	**2.4357**	12/10/2014	Dec	0.0196	0.0299	0.0114	0.0365	0.0335	0.0000	0.0000	0.0436	0.0000	0.0032	0.0109	**0.1826**
-49.1984	**2.137**	2/12/2015	Feb	0.0066	0.0146	0.0000	0.0027	0.0307	0.0000	0.0000	0.0208	0.0000	0.0000	0.0000	**0.1000**
-50.1477	**2.429**	1/14/2015	Jan	0.0000	0.0041	0.0000	0.0081	0.0177	0.0000	0.0028	0.0225	0.0000	0.0000	0.0052	**0.0725**
-52.1328	**-0.002**	12/11/2014	Dec	0.0079	0.0166	0.0000	0.0072	0.0443	0.0000	0.0000	0.0184	0.0000	0.0000	0.0071	**0.1190**
-52.8469	**1.541**	2/11/2015	Feb	0.0000	0.0122	0.0053	0.0000	0.0290	0.0000	0.0000	0.0075	0.0031	0.0000	0.0000	**0.0971**
-53.5562	**2.429**	1/14/2015	Jan	0.0204	0.0452	0.0518	0.0134	0.1492	0.0000	0.0000	0.0293	0.0000	0.0000	0.0083	**0.2861**
-54.6081	**2.828**	12/12/2014	Dec	0.0065	0.0151	0.0085	0.0046	0.0338	0.0000	0.0000	0.0130	0.0011	0.0000	0.0000	**0.1002**
-57.5542	**-1.7895**	1/1/2015	Jan	0.0087	0.0325	0.0000	0.0014	0.1018	0.0000	0.0000	0.0121	0.0000	0.0033	0.0000	**0.2079**
-58.3048	**-0.0017**	12/13/2014	Dec	0.0148	0.0404	0.0080	0.0083	0.1025	0.0000	0.0000	0.0265	0.0000	0.0000	0.0000	**0.2253**
-59.722	**-0.0027**	1/16/2015	Jan	0.0091	0.0188	0.0000	0.0067	0.0698	0.0000	0.0000	0.0272	0.0000	0.0000	0.0000	**0.1421**
-62.1655	**-3.069**	12/31/2014	Dec	0.0097	0.0289	0.0000	0.0026	0.0579	0.0000	0.0000	0.0543	0.0000	0.0039	0.0082	**0.1929**
-62.823	**-0.4718**	12/14/2014	Dec	0.0160	0.0456	0.0043	0.0056	0.1087	0.0000	0.0000	0.0300	0.0000	0.0000	0.0000	**0.2339**
-65.0015	**0.6542**	1/18/2015	Jan	0.0263	0.0650	0.0077	0.0054	0.1479	0.0000	0.0000	0.0582	0.0000	0.0000	0.0000	**0.2765**
-66.6125	**-1.4187**	12/15/2014	Dec	0.0000	0.0029	0.0000	0.0016	0.0150	0.0000	0.0000	0.0045	0.0000	0.0000	0.0000	**0.0437**
-67.638	**-0.0045**	1/19/2015	Jan	0.0567	0.1397	0.0075	0.0133	0.2211	0.0000	0.0000	0.2652	0.0000	0.0000	0.0000	**0.5704**
-69.792	**-1.9392**	1/20/2015	Jan	0.0192	0.0705	0.0039	0.0055	0.1833	0.0000	0.0000	0.0418	0.0000	0.0000	0.0000	**0.3773**
-70.034	**-2.6444**	12/16/2014	Dec	0.0080	0.0254	0.0000	0.0045	0.0965	0.0000	0.0000	0.0851	0.0000	0.0000	0.0000	**0.2597**
-70.09	**-1.5887**	1/23/2015	Jan	0.0035	0.0129	0.0000	0.0027	0.0410	0.0000	0.0024	0.0085	0.0015	0.0000	0.0128	**0.1140**

Table S2.3 Pigment:chla ratios used in CHEMTAX analysis of pigment data: **a**) initial ratios before analysis and **b**) final optimised ratios after analysis. Abbreviations: Chl, chlorophyll; Peri, peridinin; 19-But, 19'-butanoyloxyfucoxanthin; Fuco, fucoxanthin; Neo, neoxanthin; Pras, prasinoxanthin; 19-Hex, 19'-hexanoyloxyfucoxanthin; Allox, alloxanthin; Zea, zeaxanthin. Data sources for a): Chl-c1c2, Diatoms and Coccolithophores (Haptophytes-6; Gibberd et al., 2013: G3 and G4), 19-But, Zea and Pelagophytes (Mendes et al., 2015: SAZ), all other values (Wright et al., 2010).

a) Initial Pigment Ratios

Class / Pigment	Chl-c3	Chl-c1c2	Peri	19-But	Fuco	Neo	Pras	19-Hex	Allox	Zea	Chl-b
Cyanobacteria	0	0	0	0	0	0	0	0	0	1.742	0
Prasinophytes	0	0	0	0	0	0.07	0.09	0	0	0.042	0.55
Dinoflagellates	0	0.217	0.82	0	0	0	0	0	0	0	0
Cryptophytes	0	0.127	0	0	0	0	0	0	0.21	0	0
Phaeocystis-H	0.34	0.137	0	0.153	0.13	0	0	0.43	0	0	0
Phaeocystis-L	0.13	0.184	0	0.153	0.01	0	0	1.21	0	0	0
Coccolithophores	0.133	0.135	0	0.006	0.142	0	0	1.092	0	0	0
Pelagophytes	0.175	0.607	0	1.511	0.213	0	0	0	0	0	0
Chlorophytes	0	0	0	0	0	0.071	0	0	0	0.594	0.15
Diatoms	0.067	0.214	0	0	1.078	0	0	0	0	0	0

b) Final Optimized Pigment Ratios

Class / Pigment	Chl-c3	Chl-c1c2	Peri	19-But	Fuco	Neo	Pras	19-Hex	Allox	Zea	Chl-b
Cyanobacteria	0	0	0	0	0	0	0	0	0	0.635	0
Prasinophytes	0	0	0	0	0	0.031	0.052	0	0	0.024	0.317
Dinoflagellates	0	0.107	0.403	0	0	0	0	0	0	0	0
Cryptophytes	0	0.095	0	0	0	0	0	0	0.157	0	0
Phaeocystis-H	0.155	0.063	0	0.070	0.059	0	0	0.196	0	0	0
Phaeocystis-L	0.016	0.054	0	0.047	0.003	0	0	0.375	0	0	0
Coccolithophores	0.053	0.054	0	0.002	0.057	0	0	0.435	0	0	0
Pelagophytes	0.050	0.173	0	0.431	0.061	0	0	0	0	0	0
Chlorophytes	0	0	0	0	0	0.039	0	0	0	0.327	0.083
Diatoms	0.009	0.083	0	0	0.315	0	0	0	0	0	0

Table S2.4 Contribution of CHEMTAX phytoplankton groups to chla. Values represent the concentration of each phytoplankton group (µg L^{-1} chl-a), per sample.

Latitude (N)	Longitude (E)	Date	Month	Chl-a	Phorb	Diadino	Diato	Phyt	Phaeo	DDT	Fuco+Hex	DDT:FH	DDT:Chla	Phaeo:Chla
-36.4249	13.166	12/6/2014	Dec	0.0303	0.0000	0.0000	0.0000	0.0000	0.0000	0.0000	0.0051	0.0000	0.0000	0.0000
-39.0427	11.4504	12/7/2014	Dec	0.0962	0.0000	0.0048	0.0000	0.0000	0.0000	0.0048	0.0412	0.1165	0.0499	0.0000
-41.7949	8.6075	2/14/2015	Feb	0.0480	0.0000	0.0021	0.0000	0.0000	0.0000	0.0021	0.0314	0.0669	0.0438	0.0000
-44.4375	7.1044	12/9/2014	Dec	0.0742	0.0000	0.0040	0.0016	0.0000	0.0000	0.0056	0.0358	0.1564	0.0755	0.0000
-44.6305	6.2283	2/13/2015	Feb	0.0840	0.0000	0.0042	0.0000	0.0000	0.0000	0.0042	0.0439	0.0957	0.0500	0.0000
-46.0015	7.3337	1/12/2015	Jan	0.1828	0.0000	0.0144	0.0000	0.0000	0.0000	0.0144	0.1619	0.0889	0.0788	0.0000
-49.1514	2.4357	12/10/2014	Dec	0.1826	0.0000	0.0097	0.0038	0.0000	0.0000	0.0135	0.0771	0.1751	0.0739	0.0000
-49.1984	2.137	2/12/2015	Feb	0.1000	0.0000	0.0050	0.0000	0.0000	0.0000	0.0050	0.0515	0.0971	0.0500	0.0000
-50.1477	2.429	1/14/2015	Jan	0.0725	0.0000	0.0039	0.0000	0.0000	0.0000	0.0039	0.0402	0.0970	0.0538	0.0000
-52.1328	-0.002	12/11/2014	Dec	0.1190	0.0000	0.0061	0.0000	0.0000	0.0000	0.0061	0.0627	0.0973	0.0513	0.0000
-52.8469	1.541	2/11/2015	Feb	0.0971	0.0000	0.0037	0.0000	0.0000	0.0000	0.0037	0.0365	0.1014	0.0381	0.0000
-53.5562	2.429	1/14/2015	Jan	0.2861	0.0144	0.0179	0.0000	0.0051	0.0195	0.0179	0.1785	0.1003	0.0626	0.0682
-54.6081	2.828	12/12/2014	Dec	0.1002	0.0000	0.0036	0.0015	0.0000	0.0000	0.0051	0.0468	0.1090	0.0509	0.0000
-57.5542	-1.7895	1/1/2015	Jan	0.2079	0.0301	0.0147	0.0089	0.0000	0.0301	0.0236	0.1139	0.2072	0.1135	0.1448
-58.3048	-0.0017	12/13/2014	Dec	0.2253	0.0129	0.0092	0.0046	0.0000	0.0129	0.0138	0.1290	0.1070	0.0613	0.0573
-59.722	-0.0027	1/16/2015	Jan	0.1421	0.0000	0.0098	0.0000	0.0000	0.0000	0.0098	0.0970	0.1010	0.0690	0.0000
-62.1655	-3.069	12/31/2014	Dec	0.1929	0.0000	0.0100	0.0043	0.0000	0.0000	0.0143	0.1122	0.1275	0.0741	0.0000
-62.823	-0.4718	12/14/2014	Dec	0.2339	0.0229	0.0166	0.0033	0.0000	0.0229	0.0199	0.1387	0.1435	0.0851	0.0979
-65.0015	0.6542	1/18/2015	Jan	0.2765	0.0500	0.0202	0.0031	0.0042	0.0542	0.0233	0.2061	0.1131	0.0843	0.1960
-66.6125	-1.4187	12/15/2014	Dec	0.0437	0.0000	0.0035	0.0000	0.0000	0.0000	0.0035	0.0195	0.1795	0.0801	0.0000
-67.638	-0.0045	1/19/2015	Jan	0.5704	0.0157	0.0445	0.0000	0.0000	0.0157	0.0445	0.4863	0.0915	0.0780	0.0275
-69.792	-1.9392	1/20/2015	Jan	0.3773	0.0130	0.0196	0.0000	0.0080	0.0210	0.0196	0.2251	0.0871	0.0519	0.0557
-70.034	-2.6444	12/16/2014	Dec	0.2597	0.0000	0.0148	0.0029	0.0000	0.0000	0.0177	0.1816	0.0975	0.0682	0.0000
-70.09	-1.5887	1/23/2015	Jan	0.1140	0.0062	0.0034	0.0000	0.0000	0.0062	0.0034	0.0495	0.0687	0.0298	0.0544

Table S2.5 Additional pigment concentrations in µg L^{-1} not used in the group estimations, for specific pigment groupings and ratios sample. Phaeo = Phaeophorbide-a (Phorb) + Phaeophytin-a (Phyt), DDT = DD (Diadinoxanthin) + DT (Diatoxanthin), FH = Fucoxanthin (Fuco) + 19'-hexanoyloxyfucoxanthin (Hex).

Latitude (N)	Longitude (E)	Date	Month	Chl-a	Phorb	Diadino	Diato	Phyt	Phaeo	DDT	Fuco+Hex	DDT:FH	DDT:Chla	Phaeo:Chla
-36.4249	13.166	12/6/2014	Dec	0.0303	0.0000	0.0000	0.0000	0.0000	0.0000	0.0000	0.0051	0.0000	0.0000	0.0000
-39.0427	11.4504	12/7/2014	Dec	0.0962	0.0000	0.0048	0.0000	0.0000	0.0000	0.0048	0.0412	0.1165	0.0499	0.0000
-41.7949	8.6075	2/14/2015	Feb	0.0480	0.0000	0.0021	0.0000	0.0000	0.0000	0.0021	0.0314	0.0669	0.0438	0.0000
-44.4375	7.1044	12/9/2014	Dec	0.0742	0.0000	0.0040	0.0016	0.0000	0.0000	0.0056	0.0358	0.1564	0.0755	0.0000
-44.6305	6.2283	2/13/2015	Feb	0.0840	0.0000	0.0042	0.0000	0.0000	0.0000	0.0042	0.0439	0.0957	0.0500	0.0000
-46.0015	7.3337	1/12/2015	Jan	0.1828	0.0000	0.0144	0.0000	0.0000	0.0000	0.0144	0.1619	0.0889	0.0788	0.0000
-49.1514	2.4357	12/10/2014	Dec	0.1826	0.0000	0.0097	0.0038	0.0000	0.0000	0.0135	0.0771	0.1751	0.0739	0.0000
-49.1984	2.137	2/12/2015	Feb	0.1000	0.0000	0.0050	0.0000	0.0000	0.0000	0.0050	0.0515	0.0971	0.0500	0.0000
-50.1477	2.429	1/14/2015	Jan	0.0725	0.0000	0.0039	0.0000	0.0000	0.0000	0.0039	0.0402	0.0970	0.0538	0.0000
-52.1328	-0.002	12/11/2014	Dec	0.1190	0.0000	0.0061	0.0000	0.0000	0.0000	0.0061	0.0627	0.0973	0.0513	0.0000
-52.8469	1.541	2/11/2015	Feb	0.0971	0.0000	0.0037	0.0000	0.0000	0.0000	0.0037	0.0365	0.1014	0.0381	0.0000
-53.5562	2.429	1/14/2015	Jan	0.2861	0.0144	0.0179	0.0000	0.0051	0.0195	0.0179	0.1785	0.1003	0.0626	0.0682
-54.6081	2.828	12/12/2014	Dec	0.1002	0.0000	0.0036	0.0015	0.0000	0.0000	0.0051	0.0468	0.1090	0.0509	0.0000
-57.5542	-1.7895	1/1/2015	Jan	0.2079	0.0301	0.0147	0.0089	0.0000	0.0301	0.0236	0.1139	0.2072	0.1135	0.1448
-58.3048	-0.0017	12/13/2014	Dec	0.2253	0.0129	0.0092	0.0046	0.0000	0.0129	0.0138	0.1290	0.1070	0.0613	0.0573
-59.722	-0.0027	1/16/2015	Jan	0.1421	0.0000	0.0098	0.0000	0.0000	0.0000	0.0098	0.0970	0.1010	0.0690	0.0000
-62.1655	-3.069	12/31/2014	Dec	0.1929	0.0000	0.0100	0.0043	0.0000	0.0000	0.0143	0.1122	0.1275	0.0741	0.0000
-62.823	-0.4718	12/14/2014	Dec	0.2339	0.0229	0.0166	0.0033	0.0000	0.0229	0.0199	0.1387	0.1435	0.0851	0.0979
-65.0015	0.6542	1/18/2015	Jan	0.2765	0.0500	0.0202	0.0031	0.0042	0.0542	0.0233	0.2061	0.1131	0.0843	0.1960
-66.6125	-1.4187	12/15/2014	Dec	0.0437	0.0000	0.0035	0.0000	0.0000	0.0000	0.0035	0.0195	0.1795	0.0801	0.0000
-67.638	-0.0045	1/19/2015	Jan	0.5704	0.0157	0.0445	0.0000	0.0000	0.0157	0.0445	0.4863	0.0915	0.0780	0.0275
-69.792	-1.9392	1/20/2015	Jan	0.3773	0.0130	0.0196	0.0000	0.0080	0.0210	0.0196	0.2251	0.0871	0.0519	0.0557
-70.034	-2.6444	12/16/2014	Dec	0.2597	0.0000	0.0148	0.0029	0.0000	0.0000	0.0177	0.1816	0.0975	0.0682	0.0000
-70.09	-1.5887	1/23/2015	Jan	0.1140	0.0062	0.0034	0.0000	0.0000	0.0062	0.0034	0.0495	0.0687	0.0298	0.0544

Chapter 3

Manuscript prepared for submission to Deep Sea Research I

Winter biogenic silica and diatom distribution in the Indian Sector, Southern Ocean

Ian Weir[1], Sarah Fawcett[2], David Walker[3], Tommy Bornman[4,5], Susanne Fietz[1*],

[1]*Department of Earth Sciences, Stellenbosch University, 7600 Stellenbosch, South Africa*

[2]*Department of Oceanography, University of Cape Town, 7701 Cape Town, South Africa*

[3]*Department of Conservation and Marine Sciences, Cape Peninsula University of Technology, 8000 Cape Town, South Africa*

[4]*South African Environmental Observation Network, Elwandle Node, Grahamstown, South Africa*

[5]*Coastal & Marine Research Unit, Department of Botany, Nelson Mandela Metropolitan University, Port Elizabeth, South Africa*

**Corresponding author: Department of Earth Sciences, Stellenbosch University, 7600 Stellenbosch, South Africa, sfietz@sun.ac.za, +27218083117*

Keywords: macronutrients, chlorophyll-a, Polar Front, *Fragilariopsis spp.*

Geographic bounding coordinates: 61.58 °S 30.10 °E: 41.00 °S 29.60 °E

I.J. Weir contribution to manuscript: I.J. Weir is the lead author and was the main contributor in terms of analysis and writing. All authors contributed with ideas and S. Fietz helped edit the manuscript.

Abstract

Summer and spring phytoplankton communities in the Southern Ocean are well understood, but winter communities are often overlooked. Diatoms are a major contributor of biomass in the Southern Ocean and therefore when we consider a projected changing climate, understanding their spatial and seasonal distributions becomes fundamentally important in improving biogeochemical models. The results from our study suggest that winter communities are more productive than previously thought and warrant further investigation. Our study assessed nanophytoplankton distribution and their associated environments encountered along the 30 °E meridian in the Indian Southern Ocean oceanic zones. Winter waters had characteristic deep mixed layers (> 110 m) and cold surface waters with strong vertical mixing in the mixed layer. Winter macronutrient concentrations were comparable to previously published summer macronutrient concentrations, although slightly higher and homogenous in the upper 200 m. Chlorophyll-a concentrations of the Polar Frontal Zone and Antarctic Zone were comparable to previously published summer and spring studies, despite being coupled with slightly weaker nutrient depletion in surface waters. Biogenic silica (0.03 – 0.77 µM) and chlorophyll-a (0.04 – 0.6 µg/L) concentrations had an inverse relationship along the 30 °E meridian which was attributed to abundant, heavily silicified diatom species found furthest south as well as minor contribution of other phytoplankton groups to chlorophyll-a. The Polar Front was identified as an important biogeochemical boundary separating high chlorophyll-a, flagellate-dominated northern waters (Polar Frontal Zone and Subantarctic Zone) from southern waters (Antarctic Zone) characterized by low chlorophyll-a and high diatom biomass. The Antarctic Zone had the most diverse diatom community, although relative cell counts indicate that *Fragilaria* spp. were the dominant diatom genus. Heavily silicified *Fragilaria* spp. were important contributors to the estimated total diatom carbon and bSi contents. The findings from our study indicate that winter communities are no less important than summer or spring communities and that fully understanding seasonal progressions is fundamental in determining future diatom responses to changing ocean dynamics.

3.1. Introduction

Due to pronounced seasonality in the Southern Ocean, large environmental fluctuations such as seasonal fluctuations of irradiance (Deppeler and Davidson, 2017) exist in the region, greatly affecting phytoplankton productivity. While summer and spring diatom communities are well

understood (e.g. Fiala et al., 1998; Gibberd et al., 2013; Lasbleiz et al., 2016; Hoppe et al., 2017), winter communities are often overlooked, largely due to the inaccessibility of the Southern Ocean during the winter period. Consequently, our understanding of diatom distribution during the winter period is limited. Marine diatoms are a dominant phytoplankton group of the Southern Ocean and are documented as a major contributor to nutrient cycling and carbon export (e.g. Buesseler et al., 2005; Romero and Armand, 2010). Globally, diatoms contribute up to one fifth of global carbon fixation (Tréguer et al., 1995; Falkowski et al., 2000) and up to 40 % of total marine primary production (Tréguer and Pondaven, 2000). Diatoms use dissolved silicic acid from the water column in the construction of their frustules, which are comprised of amorphous biogenic silica. These mineralized, siliceous shells cause diatoms to sink more rapidly than other phytoplankton groups, contributing largely to the biological pump (Buesseler, 1998; Ducklow et al., 2001). This makes biogenic silica (bSi) an important indicator when considering diatom biomass and distribution.

Diatoms display a wide range of morphologies and can range from large, heavily silicified, chain-forming species such as *Fragilariopsis kerguelensis* (Nodder and Waite, 2001) or *Eucampia antarctica* in polar waters, to smaller, less silicified unicellular diatoms in tropical waters (Scharek et al., 1999; Cavender-Bares et al., 2001). Morphological characteristics such as cell size, often referred to as the "master trait", place important limitations on key organismal characteristics and biotic interactions, making cell size an important variable to consider particularly in terms of potential carbon export (Barton et al. 2013 and references therein). Diatom cell size and environmental variables such as iron (Fe) and light have been documented to affect the extent of silicification in diatoms (Brzezinski, 1985; Hutchins and Bruland, 1998; Takeda, 1998; Claquin et al., 2002). This has important implications for silicic acid cycling and will likely influence bSi concentrations in the water column. The majority of bSi studies in the Southern Ocean encompass the summer and spring period, focusing primarily on particulate export (Tréguer et al., 1988; Quéguiner et al., 1997; Buesseler et al., 2001) and bSi production/dissolution rates in the water column (Nelson and Gordon, 1982; Quéguiner, 2001). Furthermore, bSi in ocean sediments often serves to help understand dissolution kinetics (Rabouille et al., 1997; Van Cappellen and Qiu, 1997), and can be used as a paleo-reconstruction tool (Shemesh et al., 1995). Most commonly, bSi in the water column and sea-floor sediments

are studied in conjunction to provide insights into the marine silica budget both locally and globally (Nelson et al., 1995; Demaster, 2002). However, few studies have linked bSi distribution in the water column to the residing diatom community (Boyd et al., 2000; Buesseler et al., 2001; De La Rocha, 2002) and interpreted such observations in terms of the unique physical and biogeochemical environments encountered in the Southern Ocean.

Herein, we report, to our knowledge, the first vertical and latitudinal distributions of bSi and the residing diatom community structure for winter in this sector of the Southern Ocean. Furthermore, we provide a seasonal comparison by comparing our macronutrient data to existing summer data from several cruises between 1993-2008 and report the first winter macronutrient distribution in this sector. Studying diatom distribution and biomass in the winter alongside *in-situ* environmental conditions is essential in understanding future diatom community responses and improving biogeochemical models.

3.2. Methods

3.2.1. Study site and sampling

Samples were collected on the R/V *SA Agulhas II* (28 June - 13 July 2017) on the Winter Cruise 2017 (WC-17) conducted in the Indian sector of the Southern Ocean. The cruise consisted of three legs: leg S, which involved the ship steaming southwards from Cape Town to the Marginal Ice Zone (MIZ); leg M, the cruise track within the MIZ, and finally, the northbound leg IO in which sampling for this study took place at nine stations along a 30 °E meridian between 62 °S and 41 °S (Fig. 3.1). Frontal positions were estimated using conductivity-temperature-depth (CTD) cast temperature profiles, following frontal detection criteria outlined in Orsi et al. (1995). These estimates were compared with underway sea surface temperature (SST), ascertained from the temperature probe situated on the hull (Fig S3.2). Estimated frontal positions were further compared with known frontal positions (Belkin and Gordon, 1996; Gordon, 1971; Orsi et al., 1995) and leg S of the cruise as calculated by Smith et al. (*in prep*). Details on the calculation of frontal positions can be found in Supplementary Methods section S3.1 for leg IO used in this study and in Smith et al. (*in prep*) for comparison with frontal positions determined on leg S of the cruise. The MIZ was defined as waters covered by disjointed ice i.e. “pancake ice”. At the

beginning of leg IO the edge of the MIZ was crossed at 61.4 °S 30 °E (de Jong et al., 2018), marking the transition from ice-covered waters to ice-free waters. The Southern Boundary, which represents the northern-most limb of the Weddell Gyre, was crossed at 58.5 °S, while the Southern Antarctic Circumpolar Current front (SACCf) was estimated to be at 56.5 °S. Thereafter, the three major fronts of the Antarctic Circumpolar Current were crossed; the Polar Front (PF), Sub-Antarctic Front (SAF) and Sub-Tropical Front (STF), estimated to be located at 42.4 °S, 46.2 °S and 49.3 °S, respectively. The fronts separate five physically and geochemically distinct water masses; the Weddell Gyre, Antarctic Zone (AAZ), Polar Frontal Zone (PFZ), Sub-Antarctic Zone (SAZ) and Sub-Tropical Zone (STZ).

Seawater samples were collected from two separate casts at each station. Cast one was a deep cast (up to 4250 m) in which samples were collected for the analysis of macronutrients in GoFlo bottles strictly adhering to GEOTRACES protocols (Cutter et al., 2017). Cast two was a shallower, higher resolution cast taken from a maximum depth of 500 m to the surface with samples collected in Niskin bottles for analysis of bSi, chlorophyll-a (chla) and cell counting.

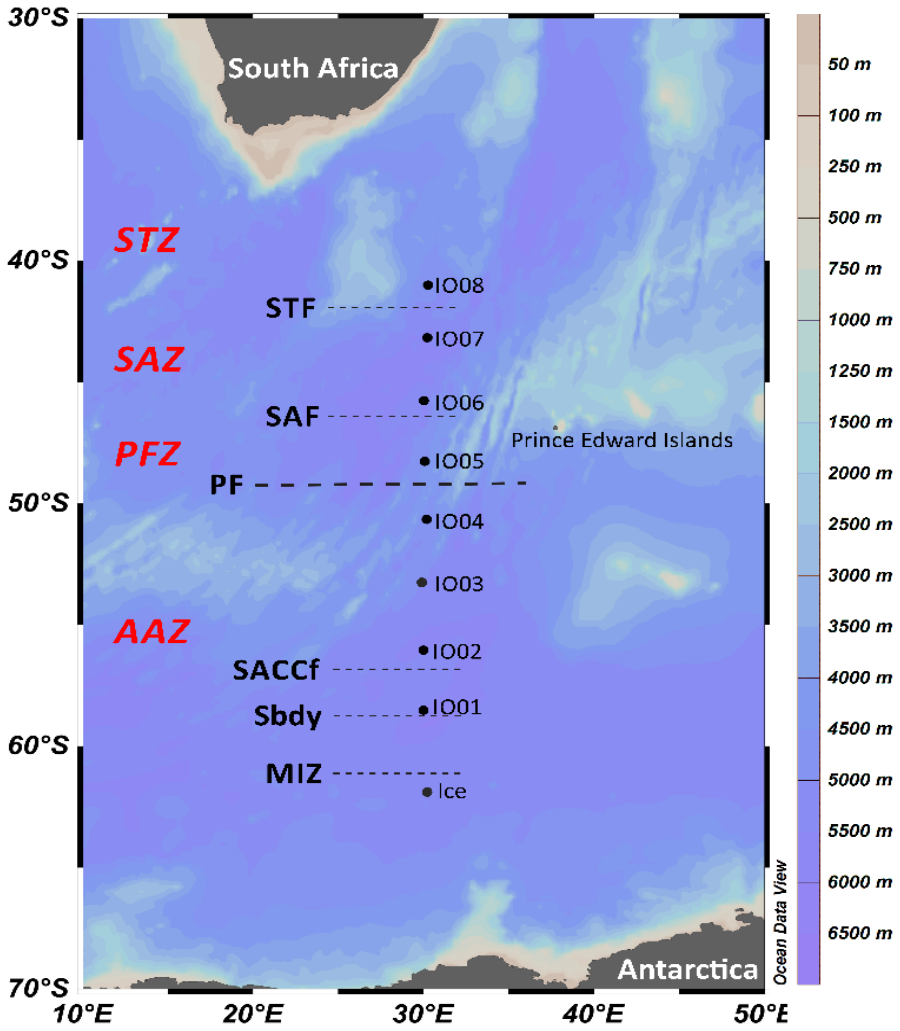

Figure 3.1 Location of the sampling stations during the WC-17 along the 30 °E meridian transect. Station "Ice" was a surface-only station (10 m) in which only bSi samples were collected for this study. The black dashed lines indicate the frontal positions and the oceanic zones are indicated by red text. Ocean bathymetry is specified by the colour bar on the right of the figure. Abbreviations: AAZ, Antarctic zone; MIZ, Marginal Ice Zone; PF, Polar Front; PFZ, Polar Frontal Zone; SAF, Subantarctic Zone; SAZ, Subantarctic Zone; SBdy, Southern Boundary; SACCf, Southern Antarctic Circumpolar front; PF, Polar Front; SAF, Subantarctic Front; STF, Subtropical Front.

3.2.2. Hydrography

Underway temperature was recorded continuously over 10-minute intervals by the hull-mounted thermosalinograph at around 8 m depth. Vertical profiles (0-200 m) of temperature, salinity, fluorescence and photosynthetically active radiation (PAR) were obtained by sensors mounted on the CTD. The same probes were used on both the GoFlo and Niskin CTD casts with profiles of the above-mentioned variables plotted in Supplementary Figures (Fig. S3.3). Temperature

profiles were used to calculate the depth of the mixed layer, by means of a 0.2 °C change in temperature threshold, following de Boyer Montégut et al. (2004). The depth of the euphotic zone was defined as the depth at which 1 % of surface irradiance was measured.

3.2.3. Macronutrients

Samples collected for macronutrient analysis were filtered, using a 0.2 µm syringe filter, into 50 ml Falcon® tubes and frozen at -20 °C immediately after sampling. Samples were analyzed three months later at the University of Cape Town. A Lachat Quick-Chem Flow injection autoanalyser was used for the analysis of NO_3^-+NO_2^- and $Si(OH)_4$ (Egan, 2008; Wolters, 2002). Phosphate and NO_2^- were analysed manually according to methods described by Grasshoff et al. (1983). The analytical error of the NO_3^- + NO_2^-, PO_4^{3-}, and $Si(OH)_4$ quantification is ± 0.04, ± 0.06, and ± 0.02 µM, respectively.

3.2.4. Particulate analysis

Chlorophyll-a: size fractionated chla determination was performed at all CTD cast stations between the surface and 150 m. The size fractionation was done by a parallel filtering of sub-samples (500 ml) through 0.3 µm and 2.7 µm Whatman glass fibre filters in dim light. Chlorophyll-a was extracted using 90% acetone for 24 hrs at -20°C and in darkness. Extracted chla was analysed using the non-acidified method on a desktop Turner Designs fluorimeter calibrated with a Sigma-Aldrich® chla analytical standard from *Anacystis nidulans*. The chla collected on the 0.3 µm filter will be referred to as "total chla". The chla which was collected on the 2.7 µm filter will be referred to as the "nanophytoplankton". To determine the picophytoplankton chla, the chla concentration obtained from the 2.7 µm filter was subtracted from the chla concentration of the 0.3 µm filter, defining picophytoplankton in the size range of 0.3 – 2.7 µm.

Biogenic silica: Approximately 2 L of seawater, sub-sampled into HDPE bottles, was collected for particulate silica analysis. Samples were filtered onto a 0.8 µm cellulose acetate membrane filter (Sartorius Stedim Biotech) with a diameter of 47 mm using a polyethylene filter holder. The filter was then folded and oven-dried for at least 12 hrs at 60°C. The dry filter was placed in a plastic petri dish, wrapped in tinfoil and stored at room temperature until analysis. The filtered bSi samples were analysed using an NaOH digestion method described by Ragueneau and Tréguer (1994). Biogenic silica was hydrolysed by a hot NaOH solution and analysed for silicic

acid using a modified colorimetric detection method of Grasshoff et al. (1983). The reduced silicomolybdic acid was measured on a Genesys 10-S UV Spectrophotometer at 810nm. Details of the adjustments from the Grasshoff et al. (1983) method are provided in Supplementary Methods Section (S3.2). Selected bSi samples were also analysed on the above-mentioned Lachat Quick-Chem autoanalyser to serve as an instrumental comparison with the analysis done as described above in section 3.2.3. Selected samples differed between 0.6 – 18 % in reported concentrations between the Lachat Quick-Chem autoanalyser and the Genesys 10-S UV Spectrophotometer analyses. A blank filter interference of 0.04 ±0.002 µM and 0.12 µM limit of detection is reported for the NaOH digestion and with the blank filter interference subtracted from the final reported bSi concentrations. Other analytical errors such as instrumental, pipetting and errors associated with the NaOH digestion were negligible (< 4 %). After NaOH extraction, filters were assayed for lithogenic silica by hydrofluoric acid (HF) addition following Ragueneau and Tréguer (1994). The lithogenic fraction was found to be below the detection limit (1.8 µM) of the HF digestion method, and therefore not reported herein.

Statistical correlation: To determine the relationship between bSi and chla in surface waters of the transect as well as the relationship between bSi and the carbon content of diatoms (see section 3.2.6), simple statistical correlation techniques were performed; the Pearson's Correlation Coefficient (*p*-value) and the Coefficient of Determination (R-value). Surface bSi concentrations were plotted against surface chla concentrations to determine the Pearson's Correlation Coefficient and the Coefficient of Determination using the statistical tools on Microsoft Excel.

3.2.5. Cell counts

Water samples (250 ml) were collected at the surface (ca.10 m) for phytoplankton and protozoan microscopic cell counts and identification at all CTD-cast stations. Samples were placed in amber glass-stoppered bottles and immediately fixed with 2% Lugol's solution. Samples were stored in the dark until analysis. Bottles were shaken and subsamples placed in a 15 ml Utermöhl settling chamber and left to settle for 24 hrs following the Utermöhl method (Hasle et al., 1996). Cell counts were done using an inverted Olympus microscope equipped with 10x, 40x and 100x oil-immersion objectives to identify and count phytoplankton. In order to do this, four random transects were performed across the slide where cells were identified, counted and grouped

according to the following categories: pennate diatoms, centric diatoms, flagellates, coccolithophores and ciliates. Using these counts the species per millilitre could then be calculated following Equation 1;

Species per mL = (species/no. of transects)(magnification factor/volume of sample) (Eq. 1)

Picophytoplankton counts were not done as limitations of magnification did not allow for the differentiation of picophytoplankton from detritus.

3.2.6. Estimation of diatom volume, carbon content and relative abundance

Surface samples (ca. 10 m) were collected at each station for Scanning Electron Microscopy (SEM) analysis to identify diatoms to a species level as well as to conduct cell measurements. Only diatoms > 0.8 µm were identified using this approach, as defined by the pore size of the membrane filter (0.8µm) and are assumed to represent the surface diatom community composition. Scanning electron micrographs were used to identify the cells to species level using taxonomic keys provided in Hasle et al. (1996) and Scott and Marchant (2005) as well as online resources on specific genera. Species names were verified using AlgaeBase (Guiry and Guiry, 2018). The cell dimensions were measured from SEM micrographs using image analysis software (ImageJ; https://imagej.net/). The cell volume was calculated for each diatom using an assigned geometric shape, where some assumptions were made based on hidden dimensions (see Hillebrand et al., 1999 and Sun and Liu, 2003 for details on the assumptions). The cell volume was then converted to carbon content according to the corrected equation of Eppley (Smayda, 1978):

$\log_{10}C$ (pg) = 0.76 $\log_{10}$ [cell volume (μm^3)] – 0.352 (Eq. 2)

The relative abundance of diatom species was calculated by sum of all species at each station. Diatom species that were identifiable, but not measurable due to fragmented cells, were included in the relative abundance count. Lastly, a cluster analysis was performed to produce a cluster dendrogram based on the distribution, occurrence and relative abundance of diatom species across the 30 °E transect. The analysis was performed using RStudio software implementing the hclust() function with the Unweighted Pair Group Method with Arithmetic Mean (UPGMA) and Euclidean distance to determine dissimilarity between stations.

3.3. Results

3.3.1. Hydrographic setting

Waters of the Indian Sector were characterized by deep mixed layers that shoaled northwards (Table 3.1). The AAZ maintained the deepest mixed layers in the study area (up to 160 m) while the most shallow mixed layers were recorded in the SAZ and STZ (< 120 m). Moreover, deepest euphotic depths (> 56 m) are recorded at St. 58.5 °S and 53 °S in the AAZ (Table 3.1). As expected, SST decreased southwards, with sub-zero temperatures recorded in the WG and MIZ (Fig. S3.2). Highest variability in SST among stations was observed in close proximity of the fronts and in the STZ. Similarly, salinity also decreased southward, although lowest salinities were recorded at St. 50.7 °S (Fig. S3.3). Most stations displayed little variation in temperature, salinity and fluorescence profiles within the mixed layer, but varied greatly below this depth (Fig. S3.3). Temperature and salinity largely increased below the mixed layer at all stations except at St. 50.7 °S and 41 °S. Station 50.7 °S showed a rapid decrease in temperature below the mixed layer followed by a gradually increasing temperature, whereas St. 41 °S, the northernmost station, shows a large continuous decrease in temperature below the mixed layer (Fig. S3.3).

Table 3.1 Summary of selected hydrographic and biogeochemical features encountered within the different oceanic zones along the 30 °E transect. Size-fractionated chla is reported as the integrated (%) of total chla in the water column (150 m). Biogenic silica and total chla concentrations are integrated over the water column (150 m). Diatom cell counts are reported from the surface (10 m). All mixed layer depths (MLD) are calculated from cast two, except St. 48 °S and 43 °S which are calculated from cast one (Fig. S3.3, Table S3.1). N.R. – not reported, N/A – not applicable.

Oceanic zone	Station	Latitude	MLD	Z_{eu}	> 2.7 µm	0.3 - 2.7 µm	Total chla	bSi	bSi:totalchla	Diatom cell count	bSi/cell	Estimated station carbon content/mL
		(°S)	(m)	(m)	(%)	(%)	(µg/m²)	(µmol/m²)	µmol/m² : µg/m²	(cells/ml)	(nmol/cell)	(pg C/mL)
STZ	I008	41	110	18	55	45	0.55	0.08	0.1	7	12	0.3
SAZ	I007	43	120	56	72	28	0.53	0.13	0.2	9	14	0.2
SAZ	I006	45.8	120	23	69	31	0.47	0.08	0.2	3	27	0.2
PFZ	I005	48	130	32	83	17	0.28	0.17	0.6	N.R.	N.R.	0.2
AAZ	I004	50.7	120	26	80	20	0.24	0.3	1.3	33	9	1.5
AAZ	I003	53	140	68	67	33	0.22	0.1	0.5	11	9	0.2
AAZ	I002	56	155	N/A	75	25	0.25	0.58	2.3	27	22	0.6
AAZ	I001	58.5	160	56	62	38	0.24	0.86	3.6	30	29	1.7
MIZ	Ice	61.3	N.R.	N.R.	N.R.	N.R.	N.R.	0.67	N.R.	N.R.	N.R.	N.R.

3.3.2. Macronutrients

Nitrite concentrations do not vary greatly with latitude and decrease in concentration with depth from values of > 0.15 µM in the surface (herein referred to as the upper 150 m of the water column) to below detection limit in deeper waters (Fig. 3.2). Nitrate and phosphate concentrations in surface waters displayed a southward increase, with highest concentrations reported farthest south in the AAZ (Fig. 3.2). Surface waters of the STZ are depleted in nitrate, and phosphate with concentrations of 7 and 0.6 µM, respectively. A clear transition in nitrate and phosphate concentrations from nutrient-deficient waters of the STZ to nutrient-rich waters of the ACC in the SAZ was observed (Fig. 3.2). Surface nitrate and phosphate concentrations increase southwards within the PFZ, with values increasing from 13 to 24 µM and 0.96 to 1.73 µM, for nitrate and phosphate, respectively. Highest surface nitrate (> 28 µM) and phosphate (> 1.7 µM) concentrations were found within the AAZ and, much like other stations, did not vary greatly within the upper 150 m of the water column. Below that, nitrate and phosphate concentrations steadily increase in concentration with depth (Fig. 3.2). Typically, the same southward increase in concentration was observed at depth as with surface nitrate and phosphate distributions, although there is a large phosphate pool below 1000 m at ca. 46 °S (Fig. 3.2).

A large nitrate pool was persistent in deeper waters below 1000 m of the AAZ (> 32 µM). The mixed layer appeared to control the vertical distribution of nutrients in the AAZ, resulting in a distinct gradient between nutrient-replete bottom waters and depleted surface waters (Fig. 3.2). For example, the mixed layer at 58.8 °S was ca. 160 m deep with homogenous nitrate (range 28 – 29 µM) and phosphate (1.7 – 2.0 µM) distributions. Below the mixed layer, macronutrient concentrations increased sharply to > 34 µM for nitrate and > 2 µM for phosphate (Fig. 3.2). This mixed layer and macronutrient relationship was far less pronounced, and almost non-existent at stations north of the PF. For example, at 47.6 °S, where the mixed layer was situated at 130 m, maximum nitrate concentrations in the upper 150 m were 23.5 µM, and gradually increased to a maximum of only 25.4 µM between 150 m and 250 m.

Low silicic acid concentrations (< 3.9 µM) persisted throughout the upper 150 m (surface) of the water column of the SAZ and PFZ (Fig. 3.2). The PF marks an important transition from northern silicic acid-depleted waters to silicic acid replete waters of the AAZ, where surface concentrations ranged between 24 - 78 µM. Deeper waters (> 1500 m) have high concentrations

of silicic acid (> 70 µM) across the water column, with concentrations as high as 132 µM reported in the AAZ. On a north to south transect, this large deep water silicic acid pool appears to shoal southwards, resulting in higher silicic acid concentrations in surface waters of the AAZ (Fig. 3.2).

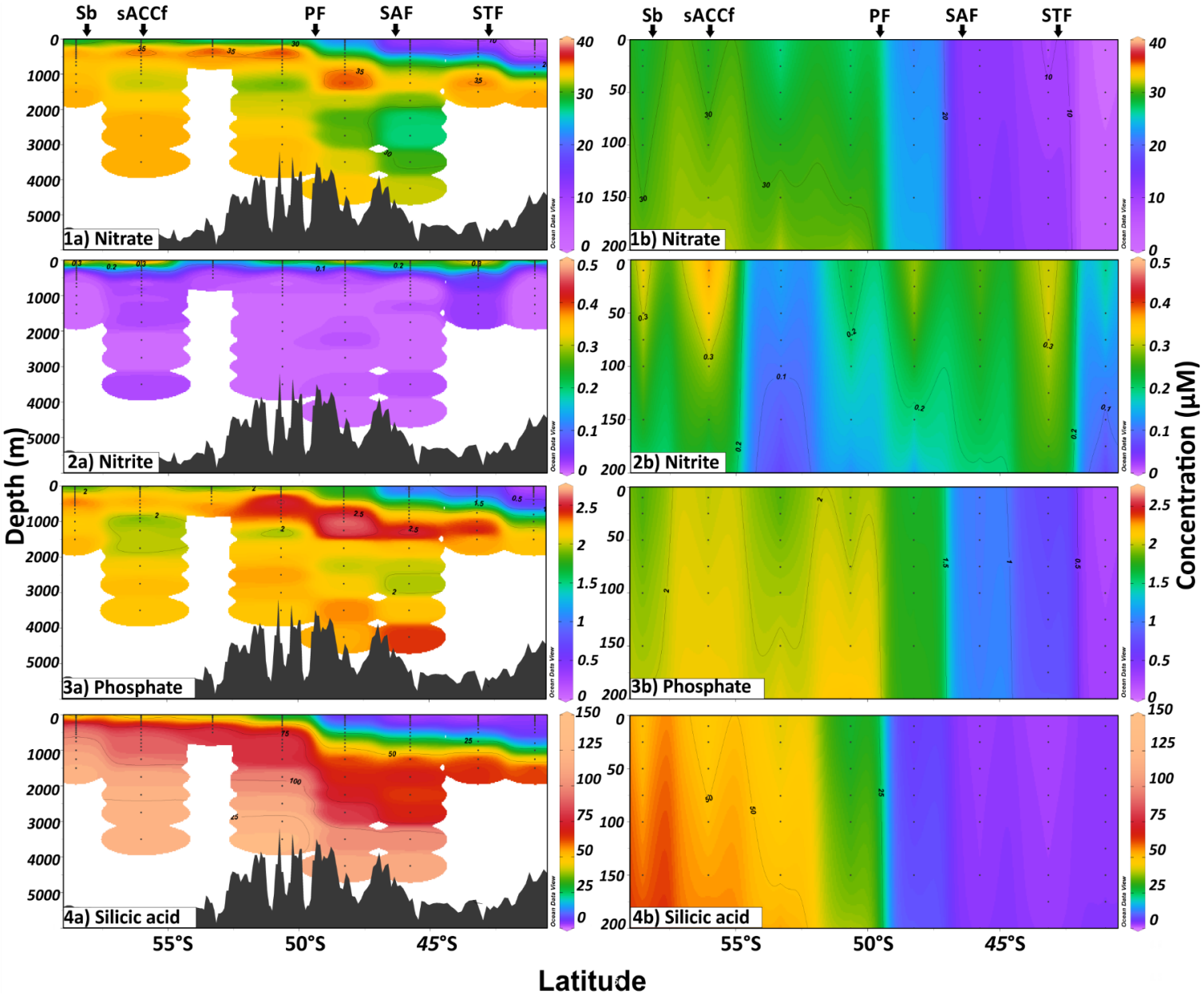

Figure 3.2 Depth profiles of macronutrients (nitrate, nitrite, phosphate, silicic acid) concentrations along a 30 °E transect with marked frontal positions (as indicated by black arrows above figure). Figures on the left are full depth profiles, while figures on the right are taken from the upper 200 m. The same interpolation was used in all figures. Small dots represent CTD sampling depths, while colours and contours correspond to concentrations. Plots created in Ocean Data View (ODV; Schlitzer, 2018).

3.3.3. Particulate distribution

Total chla and bSi concentrations show spatial variations between stations, although little vertical distinction within the upper 150 m of the water column (Fig. 3.3), much like macronutrient concentrations (Fig 3.2) and temperature and salinity distributions (Fig. S3.3). Total chla concentrations ranged between 0.03 – 0.61 µg/L in the upper 150 m, and displayed a general northward increasing trend, with highest concentrations recorded furthest north (Fig. 3.3, Table S3.2). The depth of the total chla maximum was seemingly shallow, varying between 10 – 100 m, with the majority of stations (56 – 45.8 °S) having chla maximums situated at above 25 m water depth (Fig. 3.3). Conversely, bSi concentrations (0.03 – 0.77 µM) displayed the opposite trend decreasing northward. As a result, bSi and total chla had a strong negative correlation ($R = -0.83$, $p = 0.001$).

Highest bSi concentrations were recorded in the MIZ (0.57 – 0.76 µM) and at St. 58.5 °S (0.68 – 0.77 µM) in the AAZ (Fig 3.3, Table S3.2). The AAZ generally displayed comparatively high bSi concentrations (0.22 – 0.77 µM), albeit comparatively low total chla concentrations (0.03 – 0.37 µg/L). Station 53 °S (IO03) was an exception to this observation, as this station displayed comparatively low bSi concentrations (0.05 – 0.14 µM) and comparatively low chla concentrations (0.02 – 0.27 µg/L). Ratios of bSi versus total chla integrated (µmol/m^2 : µg/m^2) over the mixed layer (individual mixed layer depths of each station) were highest in the AAZ (> 1.3 µmol/m^2 : µg/m^2), with the exception of St. 53 °S, and dropped to < 0.17 µmol/m^2 : µg/m^2 north of the PF (Table S3.1). Moreover, the highest bSi per cell ratio was found furthest south at 58.5 °S and 56 °S (22 – 29 nmol/cell) and at 45.8 °S (27 nmol/cell; Table 3.1).

The nanophytoplankton chla fraction (> 2.7 µm; see methodology 3.2.4) made up the bulk of the total chla at all stations, accounting for a minimum of 55% of the total chla integrated over the mixed layer at St. 41 °S and a maximum of 83% of the total chla integrated over the mixed layer at station 48 °S (Table 3.1). Surprisingly, both stations had relatively low bSi concentrations (0.04 – 0.16 µM). The contribution of nanophytoplankton to the total chla displayed no visible spatial trend with contributions > 70 % at several stations across the AAZ (56 °S, 50.7 °S), PFZ (48 °S) and SAZ (43 °S; Table 3.1). Consequently, the contribution of the picophytoplankton (0.3 – 2.7 µm) to the total chla displayed no clear spatial trend either and accounted for > 30 % of total integrated chla at several stations across the different water masses e.g. at 53 °S (AAZ), 45.8 °S (PFZ) and 41 °S (STZ; Fig. 3.3).

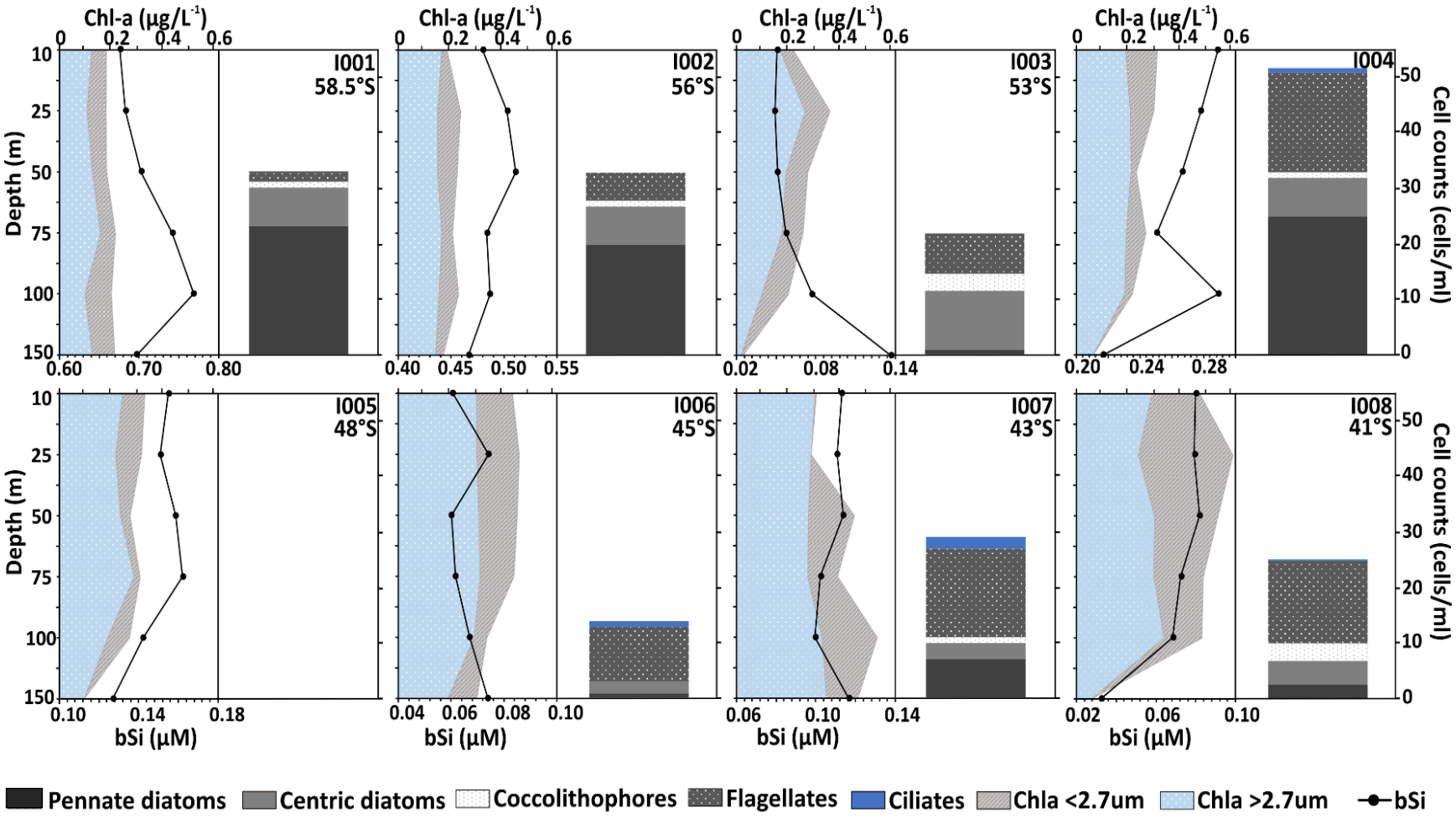

Figure 3.3 Size-fractionated chla and total bSi in the upper 150 m of the water column including all stations (58.5 – 41 °S) in conjunction with cell counts from 10 m water depth. Due to a seemingly well-mixed water column within the mixed layer (Fig. S3.3) a community of similar composition is assumed throughout the mixed layer and cell counts from 10m are assumed here to reasonably represent the community across the upper 150 m of the water column. Cell counts are not reported for station 48 °S (IO05). Station IO04 corresponds to a 50.7 °S latitude (not indicated on figure).

3.3.4. Nanoplankton group composition

Plankton cell counts were only conducted at a depth of 10 m[1] and will be assumed to represent the community within the mixed layer on the basis of a well-mixed water column as indicated by the temperature, salinity, macronutrients, chla, and bSi depth profiles discussed above. At all stations, light microscopic cell counts indicated a nanoplanktonic community dominated by diatoms and flagellates with minor coccolithophore and ciliate contribution (Fig. 3.3). Flagellates dominated stations north of the PF (48 – 41 °S) contributing > 55 % of the cells at these stations, which demonstrate comparatively high total chla concentrations. In the AAZ, plankton cell abundance was generally elevated, particularly at station 50.7 °S, while chla concentrations were low and bSi concentrations relatively high (Fig. 3.3). Plankton cell abundance were generally lowest farthest north (43 °S and 41 °S) and at 53 °S (< 25 cells/ml), with 43 °S and 41 °S coinciding with high chla concentrations, particularly of the picophytoplankton fraction (Fig. 3.3).

Pennate diatom cells greatly dominate the diatom cell count and were up to threefold more abundant than centric variations at certain stations (Fig. 3.3). Much like bSi distributions, pennate cell abundance generally decreased northward with some of the lowest counts recorded furthest north (48 – 41 °S; Fig. 3.3). Spatially, centric diatom variations were dissimilar to their pennate counterparts and did not follow the same general trend as bSi. North of the PF, centric diatom contribution was comparable to the pennate diatom contribution and in some instances exceeds the pennate diatom contribution, which generally corresponded with low bSi concentrations (Fig. 3.3). Focusing on the AAZ, diatom cells were the most abundant, particularly the pennate variation. Once again, station 53 °S (IO03) is an exception as it has relatively low diatom abundance with a concomitantly low pennate contribution (Fig. 3.3). Station 53 °S was further defined by centric cell counts exceeding pennate cells. A subsequent decline in centric cell numbers and concomitant rise in pennate cells was observed at station 50.7 °S. Diatom contribution to the community was lowest at station 45.8 °S (< 12 %), where flagellates greatly dominated the community (> 72 %), although diatom contribution did increase slightly at more northerly flagellate-dominated stations (Stations 43 °S and 41 °S, Fig. 3.3).

[1] Cell counts from 50 m, 100 m and PFZ to be included before final publication of paper

As expected, diatom cell counts were strongly correlated with bSi concentrations (R = 0.83, p = 0.001), while total cell counts were also correlated to bSi (R = 0.53, p = 0.04), although the correlation was not as strong. Highest biogenic silica per diatom cell (22 – 29 nmol/cell) was found furthest south in the AAZ (56 – 58.5 °S) and in the SAZ (27 nmol/cell) at 45.8 °S (Table 3.1).

3.3.5. Diatom species, cell volumes, and carbon contents

A total of 240 diatom cells and 29 diatom species were measured along the 30 °E transect (Table S3.3). Cluster analysis was performed to determine diatom community dissimilarity between stations (Fig. 3.4). It is evident that stations can be characterized into four major groups (Fig. 3.4); Group one comprised St. IO01 (58.5 °S), which had the most diverse diatom community (16 species), highest relative abundance, and the only occurrence of chain-forming species *Leptocylindrus* spp.; Group two consisted of St. IO02 (56 °S) and IO04 (50.7 °S) in the AAZ, which also had a diverse, abundant diatom community (13 species), with important contributions from *Fragilariopsis* spp.; Station IO03 (53 °S) did not group with other stations in the AAZ but rather in group four with stations north of the PF (St. 48 °S (IO05) and 45.8 °S (IO06)), which were associated with lower diatom community diversity, lower relative abundance and important contributions from *Nitzchia spp.* (Table S3.3); Group four consisted of the most northerly stations (St. 43°S (IO07) and 41 °S (IO08)) and had the lowest diatom diversity and relative abundance.

Cell biovolume and carbon content were highly variable among species (Table S3.3). For example, *Fragiliariopsis pseuodonana* was identified as the most abundant and ubiquitous species, although it did not occur at St. 41 °S (IO08). *F. pseuodonana* cells were small in comparison to other diatom species in the study and, as a result, the associated estimated carbon content of the cells was low (2 – 68 pg C cell^{-1}, Table S3.3), although slightly greater than global estimates (5 – 48 pg C cell^{-1}, Table S3.3). Micrographs of *F. pseuodonana* cells south of the PF indicated that a large number of these cells are heavily silicified (Fig. S3.4a). Moreover, heavily silicified, chain-forming *Fragiliaropsis kerguelensis* (Fig. S3.4b,c) only occurred south of the PF, dominating cell counts in this region and being one of the species with the highest estimated carbon content (6 – 246 pg C cell^{-1}). *Nitzschia* spp. were ubiquitous, becoming an important diatom species north of the PF, although they have a comparatively low carbon content (5 – 42

pg C cell^{-1}, Table S3.3). *Chaetoceros* spp. were also ubiquitous, although most abundant in the AAZ and PFZ with higher and more variable carbon content (2 – 309 pg C cell^{-1}) than *Nitzschia* spp. (Table S3.3).

Average diatom carbon content in the water column (upper 150 m) was estimated for each oceanic zone (Table 3.1; see Supplementary Methods S3.3 for details on calculations). The AAZ had by far the highest diatom carbon content in the study area, excluding St. 53 °S (IO03; Table 3.1). Concentrations were highest furthest south in the AAZ (St. 58.5 °S) reaching 1.74 pg C/mL with another important contribution at St. 50.7 °S (1.51 pg C/mL, Table 3.1). North of the PF, the STZ showed the highest diatom carbon content (Table 3.1). Average diatom carbon content distributions along 30 °E were correlated to bSi distributions ($R = 0.65$, $p = 0.01$).

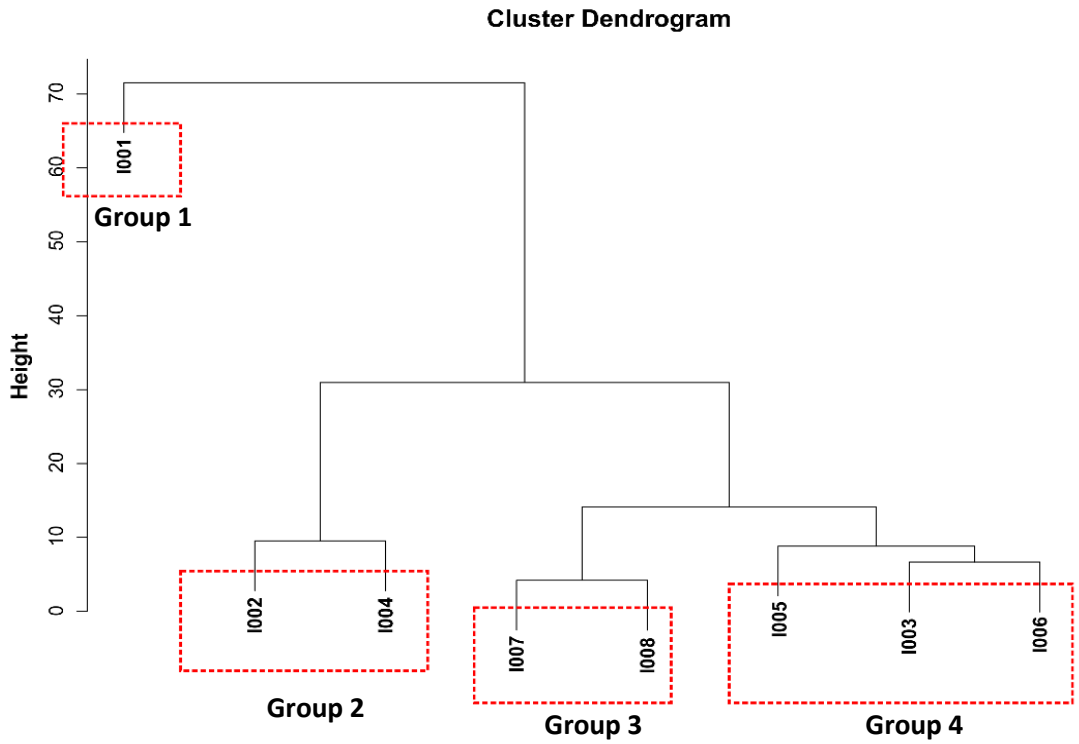

Figure 3.4 Cluster dendrogram of stations based on differences in occurrence and relative abundance of diatom species along a 30 °E transect, grouped according to the species composition at each station. The y-axis of the dendrogram represents the Euclidean distance or dissimilarity between clusters. Dashed red squares represent stations that are similar in diatom species composition. Cluster analysis was performed in RStudio software using the hclust() function with the Unweighted Pair Group Method with Arithmetic Mean (UPGMA) and Euclidean distance.

3.4. Discussion

Considering a changing climate, winter biogeochemical studies become more important as seasonal ice cover dynamics change and sea temperatures rise. Due to a paucity of winter data, biogeochemical models attempting to predict future environmental conditions in the Southern Ocean are limited, biasing biogeochemical models toward summer and spring. To better understand the residing diatom community of the winter Indian Southern Ocean, general relationships between physical and biogeochemical variables are investigated across a latitudinal gradient and are contrasted with summer/spring studies where available.

3.4.1. STZ, SAZ and PFZ

The winter SAZ and STZ are characterized by the lowest macronutrient concentrations in the study area and variable SST. The communities in these regions are flagellate-dominated with low diatom cell counts consistent with low bSi concentrations. Despite low macronutrient concentrations in the SAZ and near-limiting concentrations in STZ, these regions had the highest chla concentrations in the study area. Greater flagellate cell numbers in the SAZ and STZ may be linked to increasing irradiance and low silicic acid concentrations, limiting competing diatom growth in this region (Brzezinski, 1985; Weir et al., *in prep*). The picophytoplankton chla is also an important contributor to total chla concentrations in the STZ. Higher contribution of smaller phytoplankton groups in the STZ might be a result of a combination of warmer waters (Schlüter et al., 2011; Mendes et al., Weir et al., *in prep*), particularly low nitrate and phosphate concentrations (Hudson and Morel, 1990; Van Leeuwe et al., 2015) and unfavourable conditions for diatoms, such as low silicic acid concentrations as mentioned above.

The PFZ is separated from the AAZ by the PF, which marks an important physical boundary, particularly in terms of diatom distribution. The PF marks the extent of the AAZ, creating a strong silicic acid and temperature gradient (Freeman et al., 2016), which is evident in our study. The separation of diatom-dominated waters from flagellate-dominated waters by the PF is also evident in summer waters (Weir et al., *in prep*). An inverse relationship between chla and bSi is observed throughout waters north of the PF (including the PFZ, SAZ and STZ). Typically, early spring and late summer communities in the PFZ are also flagellate-dominated and account for, on average, 52 and 42 % of total phytoplankton biomass, respectively (Becquevort et al., 2000) and may be associated with low silicic acid concentrations. Moreover, published chla

concentrations did not exceed 0.36 and 0.30 µg/L in the spring and summer, respectively (Becquevort et al., 2000), similar to low chla concentrations observed in winter in this study (< 0.33 µg/L). This suggests that phytoplankton biomass in this (Indian) sector of the PFZ is maintained throughout spring to winter. Furthermore, on the basis of limited irradiance in the winter period of the PFZ and deeper winter mixed layers, we predict a similar flagellate-dominated community composition. Perhaps the flagellate community composition may be more diverse in winter, as flagellates such as *P. antarctica* have been shown to dominate over diatoms in waters associated with deeper mixed layers, such as those encountered in winter (Arrigo, 1999).

3.4.2. AAZ

The AAZ was characterized by well-mixed, relatively deep mixed layer waters (compared to the other ocean water studied here), and replete macronutrients. The nanophytoplankton community was strongly diatom-dominated with a high diatom biomass. As a result, the AAZ had the highest diatom carbon content per millilitre and proved to be the most important region for potential diatom carbon export.

High bSi concentrations observed in the AAZ are attributed to abundant diatom cells and especially heavily silicified *Fragilariopsis* spp. These high bSi concentrations and diatom cell counts are, however, accompanied by low total and nanophytoplankton (> 2.7 µm) chla concentrations, which may be a reflection of low contribution of other phytoplankton groups to total chla in the AAZ. Station 53 °S (IO03) was an exception to the general trends observed in the AAZ. In terms of bSi concentrations and the diatom community, St. 53 °S was more comparable to stations north of the PF (Fig. 3.4), even though physical and chemical variables were almost identical to other stations in the AAZ. On this basis, it is currently unclear what is driving the unusually low phytoplankton chla concentrations and low diatom biomass at St. 53 °S, although it must be noted that this study did not account for the potential of grazing pressures.

Our winter macronutrient concentrations in the AAZ are mostly comparable to macronutrient concentrations assessed from three World Ocean Circulation Experiment (WOCE) summer

cruises along the 30 °E transect (WOCE Global Data Resource, 2018; see example in Supplementary Figures (Fig. S3.5)). The similar deep water macronutrient concentrations (Fig. S3.5) point to minor seasonal and temporal variability. Macronutrient concentrations from our study are slightly higher and more homogenous in the upper 150 m than the WOCE summer data (Fig S3.5). The slightly weaker nutrient depletion in the surface waters in winter may result from a weaker biological uptake due to slower growth, most likely due to a combination of colder sea surface temperature and limiting light in the winter period, exacerbated by light attenuation through deep mixed layers. It is also possible that the unfavourable physical conditions are intensified by a depleted surface (150 m) trace metal (e.g. iron) pool, which is well documented throughout the Southern Ocean (e.g. de Baar et al., 1990; Klunder et al., 2011).

The winter phytoplankton community in the Indian AAZ may not be as unproductive as previously thought, as winter communities may in fact house similar phytoplankton biomass as summer and early spring. For example, summer studies found chla concentrations in the upper 150 m, to be in the range of 0.01 – 0.57 µg/L (Tréguer et al., 1988; Fiala et al., 1998; Becquevort et al., 2000), comparable to the ranges reported for winter conditions in this study (0.03 – 0.37 µg/L). Highest spring chla concentrations reported for the Indian Sector of the Southern Ocean did not exceed 0.36 µg/L (Becquevort et al., 2000). A further difference between summer and winter chla concentrations is the lack of a chla maximum in the winter period due to the deepening of the mixed layer, inducing a homogenous, vertical chla distribution throughout the mixed layer. Summer chla distributions of the Indian sector, in contrast, are defined by deep chla maximums and appeared to be closely associated with the temperature minimum (Fiala et al., 1998).

The community composition and cell characteristics appear to be different in summer and winter, possibly leading to the above-mentioned seasonal differences in the surface macronutrient depletion. For example, Fiala et al. (1998) showed that, in the summer AAZ, the picophytoplankton (defined as < 2 µm in their study) along with flagellate nanophytoplankton dominated the AAZ. In contrast, the relative contribution of picophytoplankton in winter, ascertained from our study, was minor across the AAZ. This suggests that the contribution of picophytoplankton may be more important in summer waters, possibly due to higher affinity for warmer waters and shallower mixed layers (Schlüter et al., 2011; Mendes et al., 2015, Weir et

al., *in prep*), and that diatom contribution is more important in winter. Furthermore, published summer bSi concentrations of 0.49 – 2.2 µM (Tréguer et al., 1988) are mostly higher than our winter bSi concentrations (0.05 – 0.77 µM), which, in the absence of indications of increasing diatom contribution in summer, may indicate stronger silicified cell walls in summer (leading to higher particulate summer bSi).

Fiala et al. (1998) reported diatom biomass to increase dramatically south of 58 °S (this was defined as the seasonal ice zone in their study). This could imply either a southward decrease in phytoplankton other than silicified diatoms (thereby decreasing the total chla without affecting the bSi) or increased silicification of the diatoms (thereby increasing the bSi without affecting the chla). In fact, we saw a southward decrease in chla and a strong increase in bSi, which along with the observed strong diatom dominance, supports the assumption of increased silicification in the AAZ towards the ice. Furthermore, high bSi per diatom cell furthest south in the AAZ corroborates the idea of higher silicification in this region. Increasing silicification with latitude may be linked to limited winter irradiance. Numerous incubation studies have further identified limiting trace nutrients along with light availability as important variables which increase silicification in diatoms (Brzezinski, 1985; Hutchins and Bruland, 1998; Takeda, 1998; Claquin et al., 2002). Changing silicification dynamics of diatoms in the Southern Ocean is thought to have large global biogeochemical implications for silicic acid cycling as well as climate regulation and led to the formulation of the Silicic Acid Leakage Hypothesis (SALH; Matsumoto et al., 2002). The SALH hypothesis postulates that the Last Glacial Minimum was brought about by iron fertilization in the Southern Ocean increasing diatom productivity (and CO_2 drawdown) while concurrently driving under-utilization of silicic acid by diatoms at high latitudes, allowing silicic acid "leakage" to lower latitudes. This will need to be investigated in further studies including micronutrient data.

3.4.3 Potential outputs for modelling

The applicability of our *in-situ* data set is outlined in a modelling manual by Vichi et al. (2015). The data generated from our study directly contributes to two of the four chief components considered in their Biogeochemical Flux Model;1) environmental parameters affecting biological rates and 2) Phytoplankton. More specifically, the Biogeochemical Flux Model will benefit from data relating to carbon dynamics, nutrient uptake and limitation, chlorophyll synthesis and

photoacclimation. Another global model, the biogeochemistry/ecosystem/circulation (BEC) model, makes use of several key phytoplankton functional groups, multiple limiting nutrients as well as other parameters and is run within a global ocean circulation model (Moore et al., 2004). The model aims at reproducing known eco-system dynamics in the upper ocean as well as basin-scale patterns such as primary and export production, biogenic silica production, chlorophyll and macronutrient concentrations. Our *in-situ* winter dataset, in conjunction with similar studies in the Southern Ocean, will serve as a good baseline for such a model. Our data will aid in validating the BEC model's reproducibility and assess the potential for seasonal bias.

3.5. Conclusion

The role of winter phytoplankton communities is more important than previously thought, with winter phytoplankton biomass comparable to both summer and spring. The PF marked an important transition between flagellate-dominated northern waters and diatom-dominated southern waters. However, our findings also suggest shifts in the communities. For example, in comparison to summer communities, diatoms become a more important group in the AAZ during the winter period, which may affect current biogeochemical models. In addition to seasonal progression, biogeochemical variables and biomass varied greatly within oceanic zones highlighting the importance of assessing individual water masses and their associated biogeochemical features. The PF exemplified this, marking an important transition between flagellate-dominated northern waters and diatom-dominated southern waters. Heavily silicified *Fragiliariopsis* spp. were important species south of the PF, contributing greatly to bSi and estimated diatom carbon biomass. Low phytoplankton biomass and heavily silicified diatoms in the AAZ may have been related to trace nutrient and light co-limitation, although this will need to be confirmed with corresponding trace metal data. Such findings have implications for silicic acid cycling and diatom carbon export. Thus, the results from our study indicate that winter waters are no less important than summer or spring and that understanding seasonal and spatial progressions is fundamental in improving biogeochemical modelling outputs.

Acknowledgements

The work leading to these results received funding from the National Research Foundation (NRF), under the SA/Norway Collaboration Program and the South African National Antarctic Program. I.J Weir acknowledges funding from NRF through Masters Project-linked Scholarship. The authors thank Captain Knowledge Bengu and the crew of the R/V SA Agulhas II, the Department of Environmental Affairs (DEA), and all the scientific cruise participants of the WC-17. The authors also acknowledge the NSF/NOAA-funded U.S. Repeat Hydrography Program for the WOCE macronutrient data. Furthermore, the authors acknowledge S. Smith and R. Flynn's (University of Cape Town) assistance in estimation of the frontal positions and macronutrient analysis, respectively.

References

Arrigo, K.R., 1999. Phytoplankton Community Structure and the Drawdown of Nutrients and CO2 in the Southern Ocean. Science 283, 365–367. https://doi.org/10.1126/science.283.5400.365

Barton, A.D., Finkel, Z. V., Ward, B.A., Johns, D.G., Follows, M.J., 2013. On the roles of cell size and trophic strategy in North Atlantic diatom and dinoflagellate communities. Limnol. Oceanogr. 58, 254–266. https://doi.org/10.4319/lo.2013.58.1.0254

Becquevort, S., Menon, P., Lancelot, C., 2000. Differences of the protozoan biomass and grazing during spring and summer in the Indian sector of the Southern Ocean. Polar Biol. 23, 309–320.

Belkin, I.M., Gordon, A.L., 1996. Southern Ocean fronts from the Greenwich meridian to Tasmania. J. Geophys. Res. C: Oceans 101, 3675–3696. https://doi.org/10.1029/95JC02750

Boyd, P.W., Watson, A.J., Law, C.S., Abraham, E.R., Trull, T., Murdoch, R., Bakker, D.C.E., Bowie, A.R., Buesseler, K.O., Chang, H., Charette, M., Croot, P., Downing, K., Frew, R., Gall, M., Hadfield, M., Hall, J., Harvey, M., Jameson, G., LaRoche, J., Liddicoat, M., Ling, R., Maldonado, M.T., McKay, R.M., Nodder, S., Pickmere, S., Pridmore, R., Rintoul, S., Safi, K., Sutton, P., Strzepek, R., Tanneberger, K., Turner, S., Waite, A., Zeldis, J., 2000. A mesoscale phytoplankton bloom in the polar Southern Ocean stimulated by iron fertilization. Nature 407, 695–702. https://doi.org/10.1038/35037500

Brzezinski, M.A., 1985. The Si:C:N ratio of marine diatoms: interspecific variability and the effect of some environmental variables. J. Phycol. 21, 347–357. https://doi.org/10.1111/j.0022-3646.1985.00347.

Buesseler, K.O., 1998. The decoupling of production and particle export in the surface ocean. Global Biogeochem. Cycles 12, 297–310. https://doi.org/10.1029/97GB03366

Buesseler, K.O., Andrews, J.E., Pike, S.M., Charette, M.A., Goldson, L.E., Brzezinski, M.A., Lance, V.P., 2005. Particle export during the Southern Ocean Iron Experiment (SOFeX). Limnol. Oceanogr. 50, 311–327. https://doi.org/10.4319/lo.2005.50.1.0311

Buesseler, K.O., Ball, L., Andrews, J., Cochran, J.K., Hirschberg, D.J., Bacon, M.P., Fleer, A., Brzezinski, M., 2001. Upper ocean export of particulate organic carbon and biogenic silica in the Southern Ocean along 170°W. Deep Sea Res. Part II Top. Stud. Oceanogr. 48, 4275–4297. https://doi.org/10.1016/S0967-0645(01)00089-3

Cavender-Bares, K.K., Karl, D.M., Chisholm, S.W., 2001. Nutrient gradients in the western North Atlantic Ocean: Relationship to microbial community structure and comparison to patterns in the Pacific Ocean. Deep Sea Res. Part I Oceanogr. Res. Pap. 48, 2373–2395. https://doi.org/10.1016/S0967-0637(01)00027-9

Claquin, P., Martin-Jezequel, V., Kromkamp, J.C., Veldhuis, M.J.W., Kraay, G.W., 2002. Uncoupling of silicon compared with carbon and nitrogen metabolisms and the role of the cell cycle in continuous cultures of *Thalassiosira pseuodonana* (Bacillariophyceae) under light, nitrogen, and phosphorous control. J. Phycol. 38, 922–930. https://doi.org/10.1046/j.1529-8817.2002.t01-1-01220

Cutter, G., Casciotti, K., Croot, P., Geibert, W., Geochemistry, M., Heimbürger, L.-E., Lohan, M., 2017. Sampling and Sample-handling Protocols for GEOTRACES Cruises. [http://www.geotraces.org/libraries/documents/Intercalibration/Cookbook.pdf].

de Baar, J.W., Buma, A.G.J., Nolting, R.F., Cadeé, G.C., Jacques, G., Tréguer, P.J., 1990. On iron limitation of the Southern Ocean: experimental observations in the Weddell and Scotia Seas. Mar. Ecol. Prog. Ser. 65, 105-122.

de Boyer Montégut, C., Madec, G., Fischer, A.S., Lazar, A., Iudicone, D., 2004. Mixed layer depth over the global ocean: An examination of profile data and a profile-based climatology. J. Geophys. Res. 109, C12003. https://doi.org/10.1029/2004JC002378

Deppeler, S.L., Davidson, A.T., 2017. Southern Ocean Phytoplankton in a Changing Climate. Front. Mar. Sci. 4, 40. https://doi.org/10.3389/fmars.2017.00040

de Jong, E., Vichi, M., Mehlmann, C., Eayrs, C., De Kock, W., Moldenhauer, M., Audh, R., 2018. Sea ice conditions within the Antarctic Marginal Ice Zone in winter 2017, onboard the SA Agulhas II. https://doi.pangaea.de/10.1594/PANGAEA.885211

De La Rocha, C.L., 2002. Measurement of silicon stable isotope natural abundances via multicollector inductively coupled plasma mass spectrometry (MC-ICP-MS). Geochem. Geophys. Geosys. 3, 1–8. https://doi.org/10.1029/2002GC000310

Demaster, D.J., 2002. The accumulation and cycling of biogenic silica in the Southern Ocean: revisiting the marine silica budget. Deep Sea Res. Part II, 49, 3155–3167.

Ducklow, H.W., Steinberg, D.K., Buesseler, K.O., 2001. Upper Ocean Carbon Export and the Biological Pump. Oceanogr. 14, 50-58.

Egan, L., 2008. Determination of nitrate and/or nitrite in brackish or seawater by flow injection analysis. Quickchem method® 31-107-04-1-C. Lachat Instruments, USA.

Falkowski, P., Scholes, R.J., Boyle, E.A., Canadell, J.G., Canfield, D., Elser, J., Gruber, N., Hibbard, K., Hogberg, P., Linder, S., Mackenzie, F.T., Moore III, B., Pedersen, T., Rosenthal, Y., Seitzinger, S., Smetacek, V., Steffen, W., 2000. The global carbon cycle; a test of our knowledge of Earth as a system. Science 290, 291–296.

Fiala, M., Semeneh, M., Oriol, L., 1998. Size-fractionated phytoplankton biomass and species composition in the Indian sector of the Southern Ocean during austral summer. J. Mar. Syst. 17, 179–194. https://doi.org/10.1016/S0924-7963(98)00037-2

Freeman, N.M., Lovenduski, N.S., Gent, P.R., 2016. Impact of Antarctic Polar Front Variability on Southern Ocean Biogeochemistry. Am. Geophys. Union, Fall Gen. Assem. 2016, Abstr. id. OS41D-06.

Gibberd, M.J., Kean, E., Barlow, R., Thomalla, S., Lucas, M., 2013. Phytoplankton chemotaxonomy in the Atlantic sector of the Southern Ocean during late summer 2009. Deep Sea Res. Part I Oceanogr. Res. Pap. 78, 70–78. https://doi.org/10.1016/j.dsr.2013.04.007

Gordon, A.L., 1971. Antarctic polar front zone. Antarct. Oceanol. I 15, 205–221. https://doi.org/10.1029/AR015p0205

Grasshoff, K., Kremling, K., Ehrhardt, M., 1983. Methods of Seawater Analysis. Verlag Chemie, Weinheim, Germany.

Guiry M.D., Guiry G.M., 2018. AlgaeBase [Internet]. Galway: World-Wide Electronic Publication, National University of Ireland; [cited 2018 Jul 25]. http://www.algaebase.org.

Hasle, G.R., Syvertsen, E.E., Steidinger, K.A., Tangen, K., 1996. Identifying Marine Diatoms and Dinoflagellates, United Kingdom Academic Press, London.

Hillebrand, H., Dürselen, C.D., Kirschtel, D., Pollingher, U., Zohary, T., 1999. Biovolume calculation for pelagic and benthic microalgae. J. Phycol. 35, 403–424. https://doi.org/10.1046/j.1529-8817.1999.3520403.

Hoppe, C.J.M., Klaas, C., Ossebaar, S., Soppa, M.A., Cheah, W., Laglera, L.M., Santos-Echeandia, J., Rost, B., Wolf-Gladrow, D.A., Bracher, A., Hoppema, M., Strass, V., Trimborn, S., 2017. Controls of primary production in two phytoplankton blooms in the Antarctic Circumpolar Current. Deep Sea Res. Part II Top. Stud. Oceanogr. 138, 63–73. https://doi.org/10.1016/j.dsr2.2015.10.005

Hudson, R.J.M., Morel, F.M.M., 1990. lron transport in marine phytoplankton: kinetics of cellular and medium coordination reactions. Limnol. Oceanogr. 35, 1002–1020. https://doi.org/10.4319/lo.1990.35.5.1002

Hutchins, D.A., Bruland, K.W., 1998. Iron-limited diatom growth and Si:N uptake ratios in a coastal upwelling regime. Nature 393, 561–564. https://doi.org/10.1038/31203

Klunder, M.B., Laan, P., Middag, R., De Baar, H.J.W., van Ooijen, J.C., 2011. Dissolved iron in the Southern Ocean (Atlantic sector), Deep Sea Res. Part II Top. Stud. Oceanogr. 58, 2678-2694. https://doi.org/10.1016/j.dsr2.2010.10.042.

Lasbleiz, M., Leblanc, K., Armand, L.K., Christaki, U., Georges, C., Obernosterer, I., Quéguiner, B., 2016. Composition of diatom communities and their contribution to plankton biomass in the naturally iron-fertilized region of Kerguelen in the Southern Ocean. FEMS Microbiol. Ecol. 92, 1–16. https://doi.org/10.1093/femsec/iw171

Leblanc, K., Arístegui, J., Armand, L., Assmy, P., Beker, B., Bode, A., Breton, E., Cornet, V., Gibson, J., Gosselin, M.-P., Kopczynska, E., Marshall, H., Peloquin, J., Piontkovski, S., Poulton, A.J., Quéguiner, B., Schiebel, R., Shipe, R., Stefels, J., van Leeuwe, M.A., Varela, M., Widdicombe, C., Yallop, M., 2012. A global diatom database – abundance, biovolume and biomass in the world ocean. Earth Syst. Sci. Data Discuss. 5, 147–185. https://doi.org/10.5194/essdd-5-147-2012

Matsumoto, K., Sarmiento, J.L., Brzezinski, M.A., 2002. Silicic acid leakage from the Southern Ocean: A possible explanation for glacial atmospheric pCO_2. Global Biogeochem. Cycles, 16. doi:10.1029/2001GB001442, 2002.

Mendes, C.R.B., Kerr, R., Tavano, V.M., Cavalheiro, F.A., Garcia, C.A.E., Dessai, D.R., Anilkumar, N., 2015. Cross-front phytoplankton pigments and chemotaxonomic groups in the Indian sector of the Southern Ocean. Deep Sea Res. Part II Top. Stud. Oceanogr. 118, 221–232. https://doi.org/10.1016/j.dsr2.2015.01.003

Moore, K.J., Doney, S.C., Lindsay, K., 2004. Upper ocean ecosystem dynamics and iron cycling in a global three-dimensional model. Global Biogeochem. Cycles 18 (4). doi:10.1029/2004GB002220

Nelson, D.M., Gordon, L.I., 1982. Production and pelagic dissolution of biogenic silica in the Southern Ocean. Geochim. Cosmochim. Acta 46, 491–501. https://doi.org/10.1016/0016-7037(82)90153-3

Nelson, D.M., Tréguer, P., Brzezinski, M.A., Leynaert, A., Quéguiner, B., 1995. Production and dissolution of biogenic silica in the ocean: Revised global estimates, comparison with regional data and relationship to biogenic sedimentation. Global Biogeochem. Cycles 9, 359–372. https://doi.org/10.1029/95GB01070

Nodder, S.D., Waite, A.M., 2001. Is Southern Ocean organic carbon and biogenic silica export enhanced by iron-stimulated increases in biological production? Sediment trap results from SOIREE. Deep Sea Res. Part II Top. Stud. Oceanogr. 48, 2681–2701. https://doi.org/10.1016/S0967-0645(01)00014-5

Orsi, A.H., Whitworth, T., Nowlin, W.D., 1995. On the meridional extent and fronts of the Antarctic Circumpolar Current. Deep Sea Res. Part I Oceanogr. Res. Pap. 42, 641–673. https://doi.org/10.1016/0967-0637(95)00021-W

Quéguiner, B., Tréguer, P., Peeken, I., Scharek, R., 1997. Biogeochemical dynamics and the silicon cycle in the Atlantic sector of the Southern Ocean during austral spring 1992. Deep Sea Res. Part II Top. Stud. Oceanogr. 44, 69–89. https://doi.org/10.1016/S0967-0645(96)00066-5

Quéguiner, B., 2001. Biogenic silica production in the Australian sector of the Subantarctic Zone of the Southern Ocean in late summer 1998. J. Geophys. Res. Ocean. 106, 31627–31636. https://doi.org/10.1029/2000JC000249

Rabouille, C., Gaillard, J., Tréguer, P., Vincendeaus, M., 1997. Biogenic silica recycling in surficial sediments across the Polar Front of the Southern Ocean (Indian Sector). Deep Sea Res. Part II 44, 1151-1176.

Ragueneau, O., Tréguer, P., 1994. Determination of biogenic silica in coastal waters: applicability and limits of the alkaline digestion method. Mar. Chem. 45, 43–51. https://doi.org/10.1016/0304-4203(94)90090-6

Romero, O.E., Armand, L.K., 2010. Marine diatoms as indicators of modern changes in oceanographic conditions. The diatoms: applications for the environmental and earth sciences. Academic press, London (Ed.2), Editors: Smol J.P. and Stoermer E.F., 373–400.

Scharek, R., Tupas, L.M., Karl, D.M., 1999. Diatom fluxes to the deep sea in the oligotrophic North Pacific gyre at Station ALOHA. Mar. Ecol. Prog. Ser. 182, 55–67. https://doi.org/10.3354/meps182055

Schlitzer, R., 2018. Ocean Data View, odv.awi.de.

Schlüter, L., Henriksen, P., Nielsen, T.G., Jakobsen, H.H., 2011. Phytoplankton composition and biomass across the southern Indian Ocean. Deep Sea Res. Part I Oceanogr. Res. Pap. 58, 546–556. https://doi.org/10.1016/j.dsr.2011.02.007

Scott, F.J., Marchant, H.J., 2005. Antarctic marine protists. Australian Biological Resources Study and Australian Antarctic Division, Canberra.

Shemesh, A., Burckle, L.H., Hays, J.D., 1995. Late Pleistocene oxygen isotope records of biogenic silica from the Atlantic sector of the Southern Ocean. Paleoceanography 10, 179–196. https://doi.org/10.1029/94PA03060

Smayda, T.J., 1978. From Phytoplankton to Biomass. Paris: UNESCO.

Smith, S., Altieri, K.E., Spence, K.A.M., Mdutyana, M., Burger, J., Rawatlal, M., Walker, D., Fawcett, S.E., *in prep*. Biogeochemical controls on ammonium accumulation in the surface ocean during winter in the Southern Ocean south of Africa.

Sun, J., Liu, D., 2003. Geometric models for calculating cell biovolume and surface area for phytoplankton. J. Plankton Res. 25, 1331–1346. https://doi.org/10.1093/plankt/fbg096

Takeda, S., 1998. Influence of iron availability on nutrient consumption ratio of diatoms in oceanic waters. Nature 393, 774–777. https://doi.org/10.1038/31674

Tréguer, P., Gueneley, S., Kamatani, A., 1988. Biogenic silica and particulate organic matter from the Indian sector of the Southern Ocean. Mar. Chem. 23, 167–180.

Tréguer, P., Nelson, D.M., Van Bennekom, A.J., DeMaster, D.J., Leynaert, A., Quéguiner, B., 1995. The Silica Balance in the World Ocean: A Re-estimate. Science 268, 375 LP-379.

Tréguer, P., Pondaven, P., 2000. Global change: Silica control of carbon dioxide. Nature 406, 358–359. https://doi.org/10.1038/35019236

Van Cappellen, P., Qiu, L., 1997. Biogenic silica dissolution in sediments of the Southern Ocean. II. Kinetics. Deep Sea Res. Part II Top. Stud. Oceanogr. 44, 1129–1149. https://doi.org/10.1016/S0967-0645(96)00112-9

van Leeuwe, M.A., Kattner, G., van Oijen, T., de Jong, J.T.M., de Baar, H.J.W., 2015. Phytoplankton and pigment patterns across frontal zones in the Atlantic sector of the Southern Ocean. Mar. Chem. 177, 510–517. https://doi.org/10.1016/j.marchem.2015.08.003

Vichi, M., Lovato, T., Lazzari, P., Cossarini, G., Gutierrez, M.E., Mattia, G., Masina, S., McKiver, W. J., Pinardi N., Solidoro, C., Tedesco, L., Zavatarelli, M., 2015. The Biogeochemical Flux Model (BFM): Equation Description and User Manual. BFM version 5.1. BFM Report series N. 1, Release 1.1, August 2015, Bologna, Italy, http://bfm-community.eu, pp. 104

Weir, I.J., Viljoen, J.J., Fietz, S., Cloete, R., Loock, J.C., Philibert, R., Roychoudhury, A.N., (*in prep*) Links between phytoplankton community composition and trace metal distribution in summer surface waters of the Atlantic Southern Ocean. Limnol. Oceanogr.

WOCE Global Data Resource, 2018. National Oceanographic Data Center Home Page. [Online] https://www.nodc.noaa.gov/woce/wdiu/

Wolters, M., 2002. Determination of silicate in brackish or seawater by flow injection analysis. QuickChem® method 31-114-24-1-D. Lachat Instruments, USA.

Supplementary to Chapter 3

Winter biogenic silica and diatom distribution in the Indian Sector, Southern Ocean

Ian Weir[1], Sarah Fawcett[2], David Walker[3], Tommy Bornman[4,5], Susanne Fietz[1*]

S3. Supplementary Methods

S3.1. Calculation of frontal positions

The frontal positions at the time of water sampling were identified based on temperature sections from eight CTD cast stations along the 30 °E transect (Fig. S3.1), following the frontal identification criteria outlined in Orsi et al. (1995). The low-resolution temperature data set made frontal determination tedious, particularly as an eXpendable BathyThermograph (XBT) probe was not used as outlined in Orsi et al. (1995). A vertical section of temperature across the transect was generated on Ocean Data View (Fig. S3.1) and compared with the hull-mounted thermosalinograph temperature profiles (Fig. S3.2), which were recorded every 10 minutes. The above-mentioned temperature plots were then compared with those found in literature (Belkin and Gordon, 1996; Gordon, 1971; Orsi et al., 1995) and with those determined on leg S of the cruise, as calculated by Smith et al. (2018), allowing frontal estimation to be accurate to one decimal place. The following criteria were used in identifying the frontal positions;

STF: θ increase from 10 °C – 12 °C at 100 m

SAF: θ > 4-5 °C at 400 m

PF: θ < 2 °C along the θ-min at Z < 200 m

PF: θ > 2.2 °C along the θ-max at Z < 800 m

SACCf: θ > 1.8 °C along θ-max at Z > 500 m

Sb: θ < 0 °C along θ-min at Z < 150 m

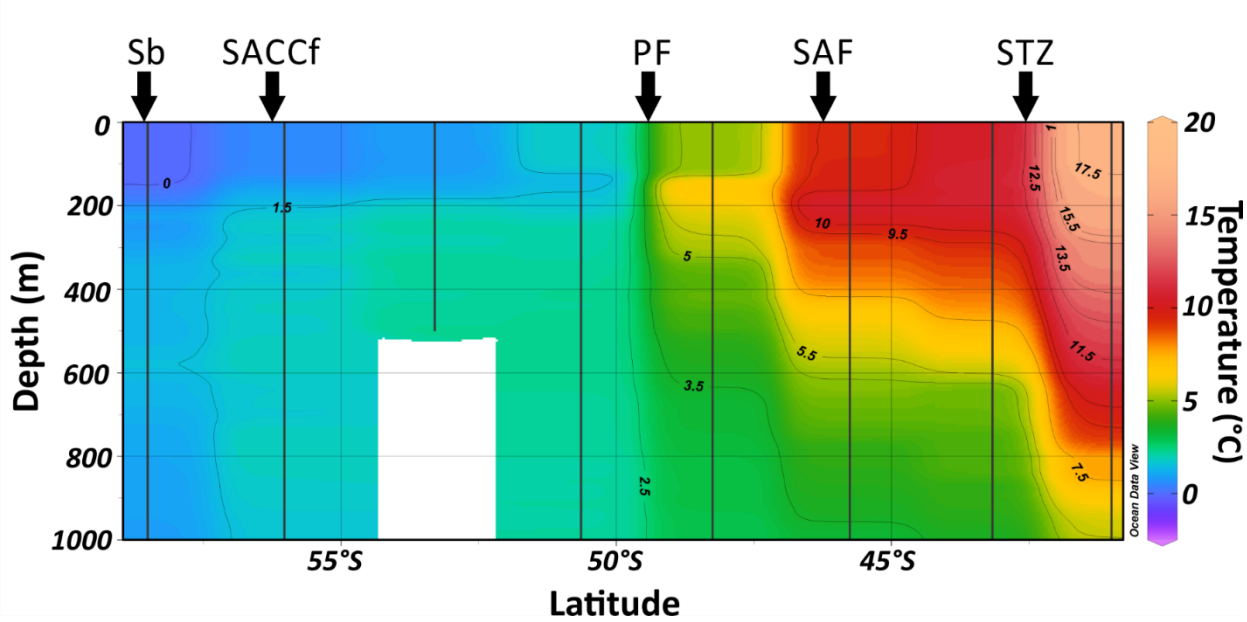

Figure S3.1 Temperature depth profile (upper 1000 m) used in the estimation of the frontal positions. Vertical black lines indicate sampling sites and arrows indicate the estimated frontal positions.

S3.2 Modified colorimetric detection of silicic acid

Concentrations of certain reagents differed slightly from the original method described by Grasshoff (1983). Following the modified method, sulphuric acid (3.6 M) was added to a solution of ammonium molybdate terathydrate (20g/100ml) instead of to sulphuric acid (4.5 M) and ammonium molybdate tetrahydrate (12.7g/100ml) as recommended by Grasshoff (1983). A modified solution of ascorbic acid (1.75g/100ml) was also used, which differed from the 2.8g/100ml recommended by Grasshoff (1983).

S3.3 Calculation of average carbon content in the water column (pg C/mL) in each ocean zone

For each oceanic zone all the observations of diatoms and their associated carbon contents are summed together (pg C cell^{-1}). The sum of all observations in a particular ocean zone is then divided by the volume of water filtered through the SEM stub to provide average diatom carbon content in surface waters (pg C/mL) for each oceanic zone.

S3. Supplementary Figures

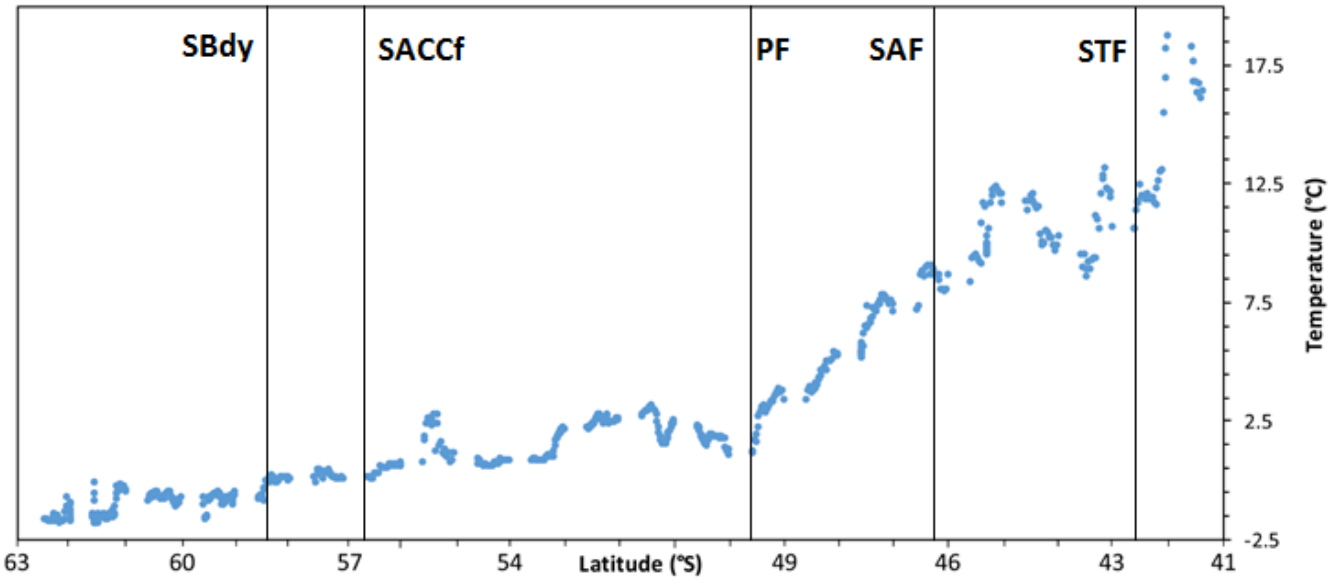

Figure S3.2 Sea surface temperature along the WC-17 30°E transect recorded from the hull-mounted thermosalinograph (ca. 8 m). Estimates of the positions of the major fronts are indicated. STF – Subtropical Front, SAF – Subantarctic Front, PF – Polar Front, SACCf – Southern Antarctic Circumpolar front, SBdy – Southern Boundary.

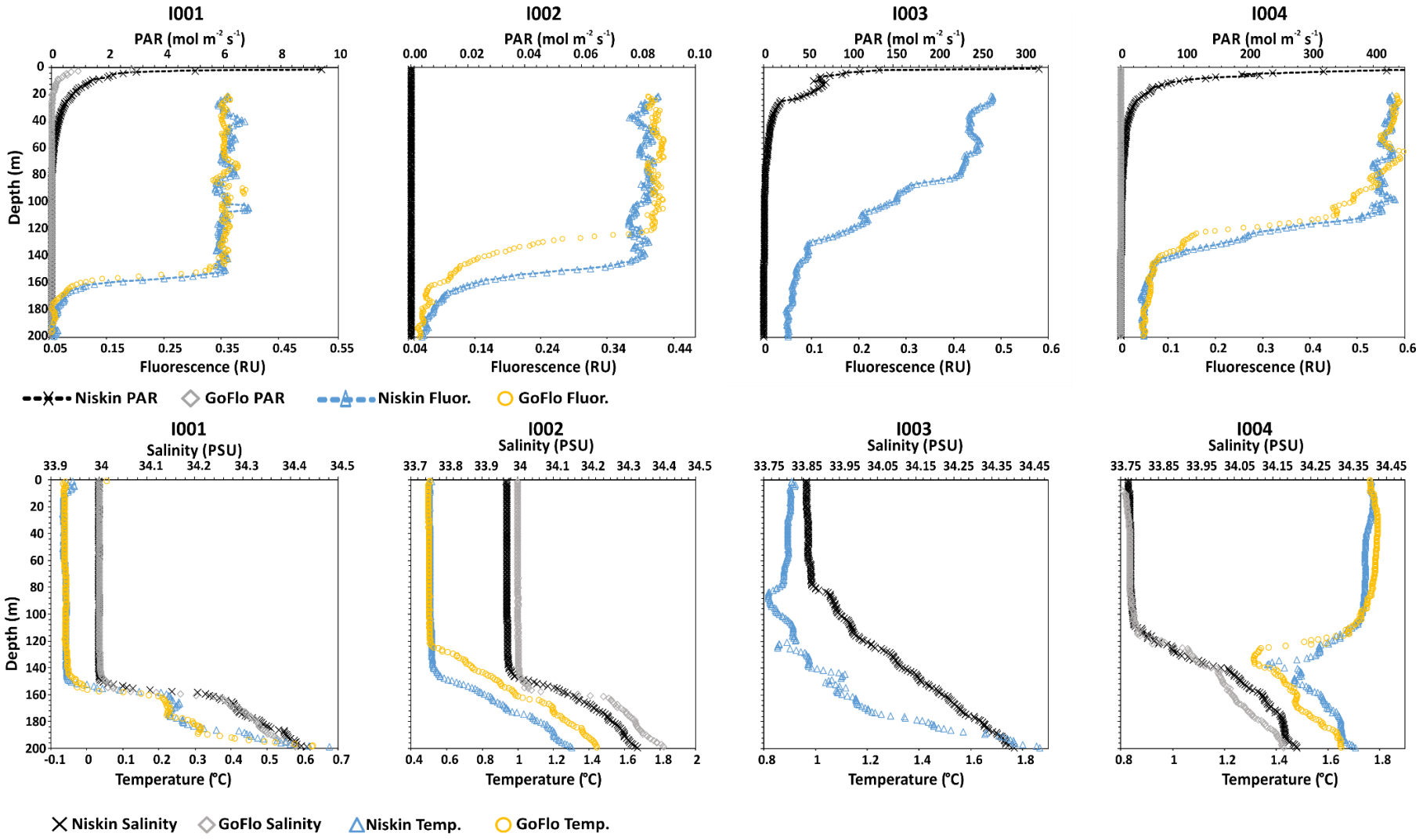

Figure S3.3 (Continued on next page) Temperature and salinity profiles compared with PAR and fluorescence profiles in the upper 200 m at each station. Profiles are taken from cast one (GoFlo cast) and cast two (Niskin cast) to serve as a comparison. The same CTD probes were used on both casts. Fluorescence (in relative units, RU) reported only from below a depth of 20 m to account for surface quenching and reported as a 10 point moving average. Station 58.5 °S (IO01) was the southernmost station and St. 41 °S (IO08) was the northernmost station along the 30°E transect. Station locations can be found in Figure 3.1 and Table 3.1.

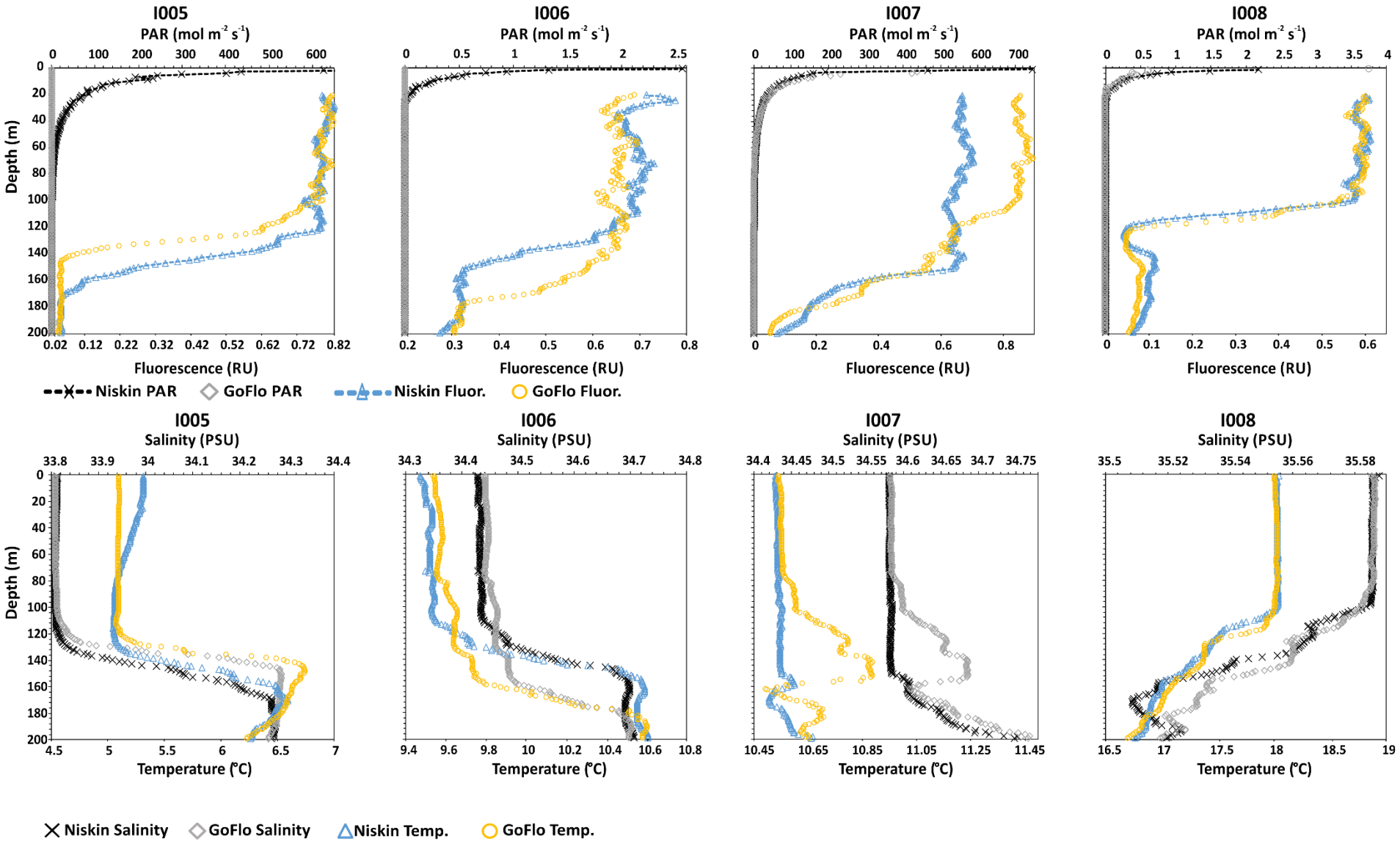

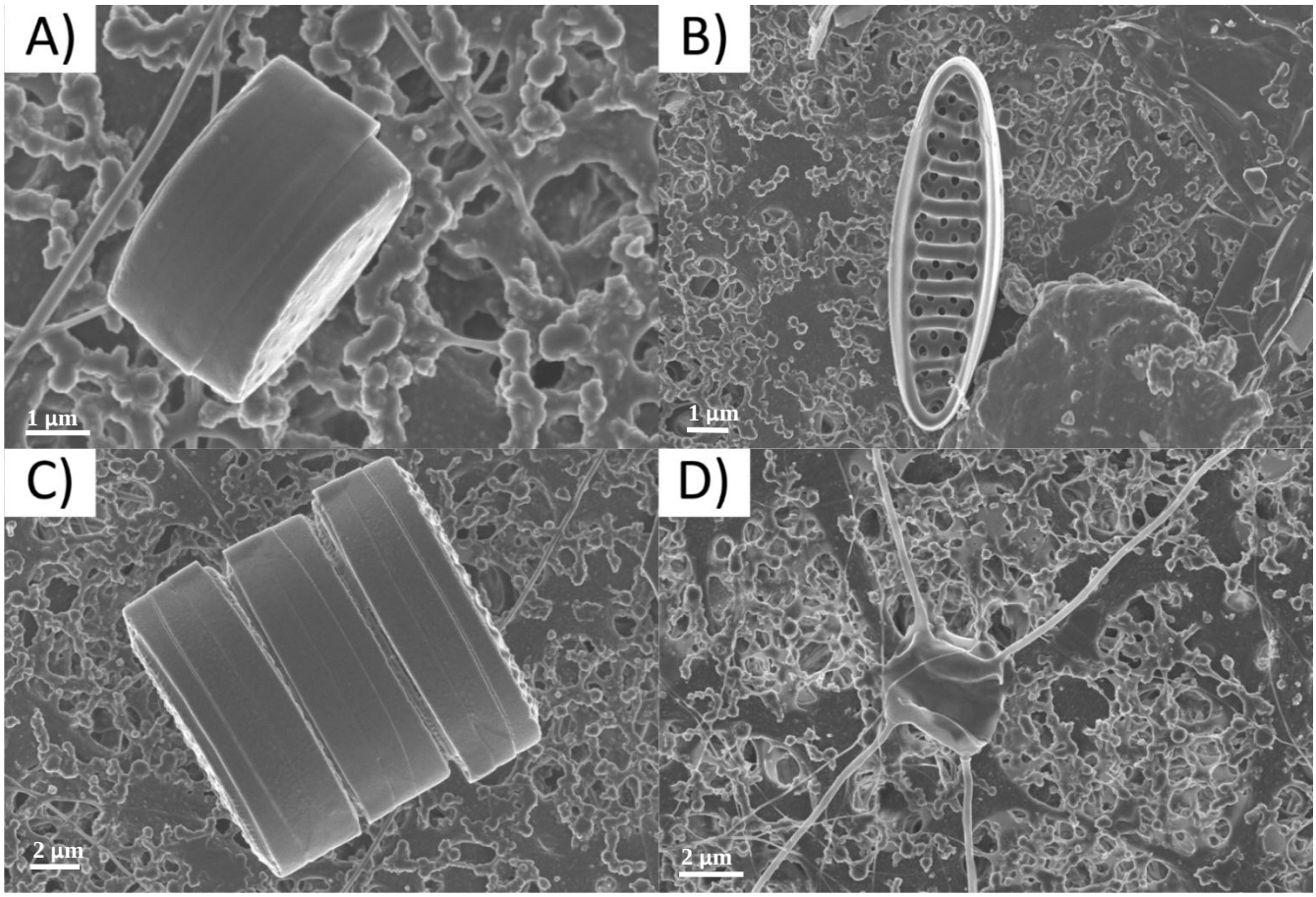

Figure S3.4 Scanning Electron micrographs of selected diatom species. **A)** heavily silicified *F. pseuodonana* at 56 °S, **B)** *F. kerguelensis* (solitary form) at 58.5 °S, **C)** heavily silicified chain-forming *F. kerguelensis* at 58.5 °S, **D)** *Chaetoceros neglectus* at 53 °S.

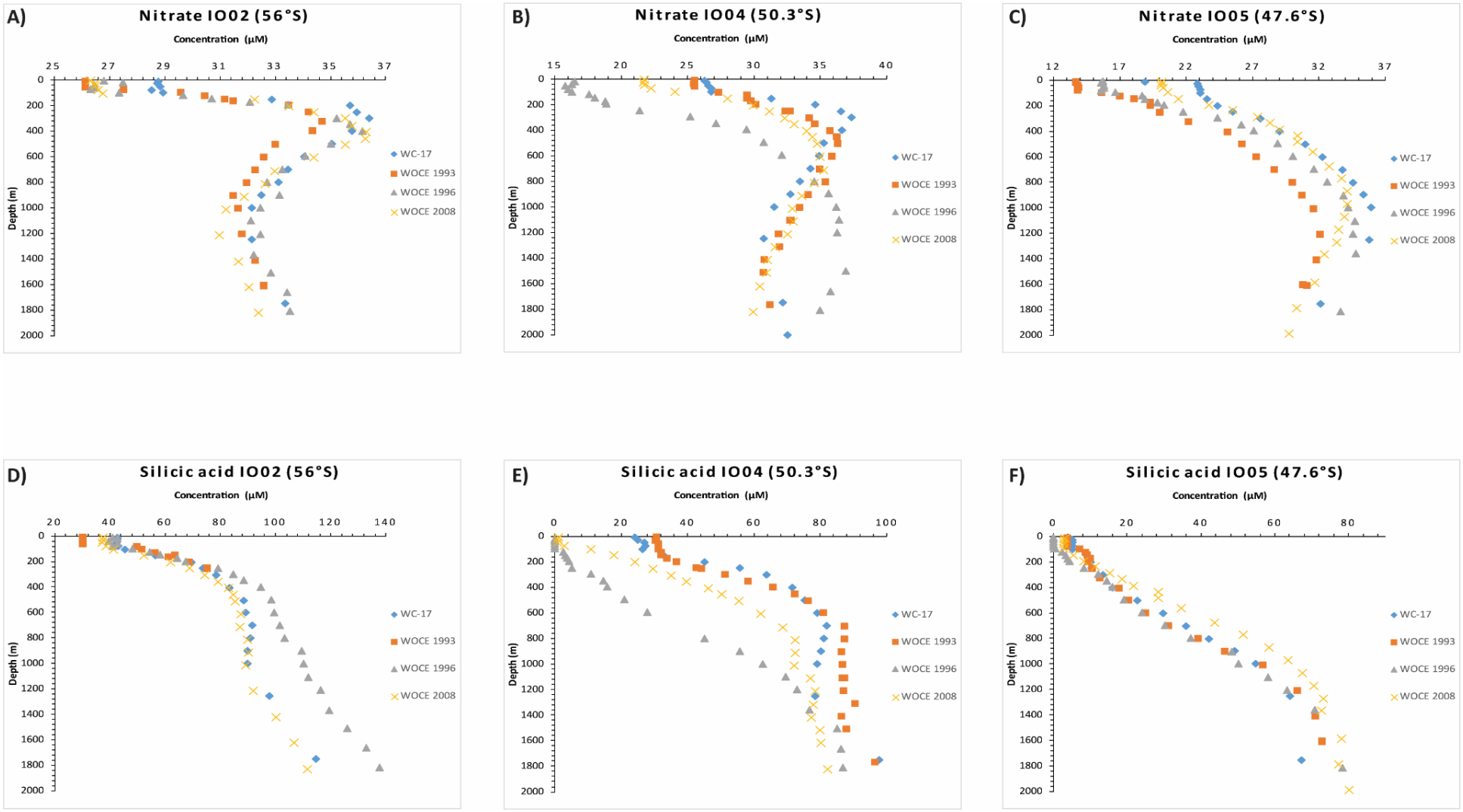

Fig. S3.5 Comparison of winter nutrient concentration determined during winter 2017 with summer concentrations determined between 10-25 years ago during three WOCE cruises along the 30 °E transect. Shown are example depth profiles of nitrate concentrations (**A-C**) and silicic acid concentrations (**D-F**) from selected stations. Panel **A**) and **D**) represent St. IO02 at latitude 56 °S (this study) compared with WOCE data from 1993 at latitude 56.3 °S; WOCE 1996, at latitude 56.3 °S and WOCE 2008, at latitude 56 °S. Panel **B**) and **E**) represent St. IO04 at latitude 50.3 °S (this study) compared with WOCE 1993, at latitude 50.4 °S; WOCE 1996, at latitude 50 °S, and WOCE 2008, at latitude 50.2 °S. Panel **C**) and **F**) compares station IO05 at latitude 47.6 °S (this study) with WOCE1993, at latitude 47.5 °S; WOCE 1996, at latitude 47 °S and WOCE 2008 at latitude 47.5 °S.

S3. Supplementary Tables

Table S3.1 Mixed layer depth and euphotic zone. The mixed layer is calculated from cast one (GoFlo cast) and cast two (Niskin cast). The euphotic zone was not calculated for the GoFlo cast, as most GoFlo casts were done at night. N/A – not applicable, irradiance was zero as station was sampled during the night.

Station	Niskin MLD (m)	GoFlo MLD (m)	Niskin Z_{eu} (m)
I008	110	120	18
I007	250	120	56
I006	120	150	23
I005	70	130	32
I004	120	120	26
I003	140	145	68
I002	155	135	N/A
I001	160	160	56

Table S3.2 (Continued on next page) Biogenic silica and size fractionated chla concentrations along the 30 °E transect across the major zones. Chlorophyll-a was size fractionated and reported as nanophytoplankton (>2.7 µm) and picophytoplankton (0.3 – 2.7 µm). The bSi was not size fractionated.

Sub-system	Station	Latitude	Depth (m)	bSi (µmol/L)	> 2.7 µm (µg/L)	0.3 - 2.7 µm (µg/L)	Total chl-a (µg/L)	% > 2.7 µm	% 0.3 – 2.7 µm
STZ	IO08	41°S	10	0.08	0.29	0.19	0.48	61	39
STZ	IO08	41°S	50	0.08	0.24	0.37	0.61	40	60
STZ	IO08	41°S	75	0.08	0.30	0.25	0.55	55	45
STZ	IO08	41°S	100	0.07	0.30	0.19	0.50	61	39
STZ	IO08	41°S	125	0.07	0.34	0.15	0.49	70	30
STZ	IO08	41°S	150	0.03	0.06	0.00	0.06	100	0
SAZ	IO07	43°S	10	0.11	0.31	0.01	0.31	98	2
SAZ	IO07	43°S	25	0.11	0.29	0.00	0.29	100	0
SAZ	IO07	43°S	50	0.11	0.28	0.18	0.46	61	39
SAZ	IO07	43°S	75	0.1	0.28	0.12	0.40	71	29
SAZ	IO07	43°S	100	0.1	0.33	0.22	0.55	60	40
SAZ	IO07	43°S	150	0.12	0.35	0.12	0.47	74	26
SAZ	IO06	45.8°S	10	0.06	0.31	0.14	0.45	69	31
SAZ	IO06	45.8°S	25	0.07	0.31	0.17	0.47	65	35
SAZ	IO06	45.8°S	50	0.06	0.32	0.15	0.47	67	33
SAZ	IO06	45.8°S	75	0.06	0.32	0.13	0.45	71	29
SAZ	IO06	45.8°S	100	0.07	0.30	0.05	0.35	86	14

SAZ	IO06	45.8°S	150	0.07	0.19	0.11	0.31	63	37
PFZ	IO05	48°S	10	0.15	0.25	0.09	0.33	74	26
PFZ	IO05	48°S	25	0.15	0.22	0.10	0.32	69	31
PFZ	IO05	48°S	50	0.16	0.24	0.04	0.28	87	13
PFZ	IO05	48°S	75	0.16	0.29	0.02	0.32	92	8
PFZ	IO05	48°S	100	0.14	0.19	0.08	0.27	70	30
PFZ	IO05	48°S	150	0.13	0.10	0.00	0.10	100	0
AAZ	IO04	50.7°S	10	0.29	0.19	0.12	0.32	61	39
AAZ	IO04	50.7°S	25	0.28	0.21	0.09	0.30	69	31
AAZ	IO04	50.7°S	75	0.25	0.19	0.08	0.27	72	28
AAZ	IO04	50.7°S	100	0.29	0.19	0.03	0.22	87	13
AAZ	IO04	50.7°S	150	0.22	0.07	0.00	0.07	100	0
AAZ	IO03	53°S	10	0.05	0.17	0.05	0.22	76	24
AAZ	IO03	53°S	25	0.05	0.27	0.10	0.37	73	27
AAZ	IO03	53°S	50	0.05	0.19	0.08	0.28	70	30
AAZ	IO03	53°S	75	0.06	0.18	0.08	0.26	69	31
AAZ	IO03	53°S	100	0.08	0.10	0.10	0.20	49	51
AAZ	IO03	53°S	150	0.14	0.02	0.01	0.03	69	31
AAZ	IO02	56°S	10	0.48	0.17	0.02	0.19	89	11
AAZ	IO02	56°S	25	0.5	0.15	0.09	0.24	63	37
AAZ	IO02	56°S	50	0.51	0.16	0.07	0.23	68	32
AAZ	IO02	56°S	75	0.48	0.17	0.04	0.21	79	21
AAZ	IO02	56°S	100	0.49	0.16	0.08	0.24	68	32

AAZ	IO02	56°S	150	0.47	0.15	0.03	0.18	83	17
AAZ	IO01	58.5°S	10	0.68	0.13	0.06	0.19	68	32
AAZ	IO01	58.5°S	25	0.68	0.11	0.07	0.18	59	41
AAZ	IO01	58.5°S	50	0.7	0.13	0.06	0.19	69	31
AAZ	IO01	58.5°S	75	0.74	0.16	0.06	0.22	73	27
AAZ	IO01	58.5°S	100	0.77	0.10	0.10	0.20	50	50
AAZ	IO01	58.5°S	150	0.7	0.13	0.09	0.22	59	41
ICE	Ice	61.6°S	10	0.57	n.d	n.d	n.d	n.d	n.d
ICE	Ice	61.6°S	10	0.76	n.d	n.d	n.d	n.d	n.d

Table S3.3: (Continued on next page) List of diatom species cell sizes, cell volumes and carbon per cell along the 30 °E transect. The columns from left to right (A to H) denote: A - diatom species, B - length range of cell [µm], C - width range of cell [µm], D - number of cells measured, E - range of cell volume [μm^3], F - range of carbon per cell [pg C $cell^{-1}$], G - carbon per cell range from global diatom database (Leblanc et al., 2012) H- stations at which species were found. N.R. – not recorded. Details on calculations can be found in the Methods under section 3.2.6

A	B	C	D	E	F	G	H
Achnanthes brevipes	11	8	2	638	60	16-1190	I001
Asteromphalus hyalinus	21	7	1	2363	163	77-149	I001
Chaetoceros atlanticus	4-8	2-9	4	19-523	4-233	180-747	I001, I005
Chaetoceros convolutus	10-19	10-19	2	854-5495	75-309	25-30	I002
Chaetoceros dichaeta	4-12	1-8	20	7-907	2-79	41-50	I001, I002, I003, I004, I006
Chaetoceros neglectus	3-10	4-5	16	67-166	8-23	60-110	I001, I002, I003, I004, I005, I007
Dactyliosolen antarcticus	73	N.R.	N.R.	N.R.	N.R.	185-1483	I002, I005
Fragilariopsis cylindrus	1-17	1-2	15	2-39	1-7	4-71	I001,I004, I007, I008
Fragilariopsis kerguelensis	9-49	2-10	28	33-4072	6-246	57-351	I001, I002, I003, I004
Fragilariopsis pseudonana	3-11	2-8	55	6-748	2-68	5-48	I001, I002, I003, I004, I005, I006, I007
Fragilariopsis rhombica	7-26	3-11	8	50-2712	9-181	49-329	I001, I002, I003, I004
Leptocylindrus spp.	11-13	3-4	42	604-626	55-59	5-2827	I001
Navicula directa var *directa*	12	5	1	203	25	159-500	I001
Nitzchia lecointei	10-17	2	6	24-48	5-8	156	I001, I002
Nitzschia acicularis	33-49	2-3	5	87-197	13-25	29-72	I002, I003, I004

Nitzschia bicapitata	19	6	1	403	42	6-36	I004
Nitzschia sicula var *bicuneata*	26	6	1	457	47	33-237	I002, I003, I004
Pseudonitzschia prolongatoides	52	5	1	547	54	1-27	I003
Pseudonitzschia spp.	N.R.	N.R.	N.R.	N.R.	N.R.	N.R.	I004
Pseudonitzschia subcurvata	40	4	1	297	34	9-38	I004
Pseudostaurosira brevistriata	19	3	1	133	18	N.R.	I008
Thalassionema nitzschioides	19-20	3	2	129-133	18	10-220	I007, I008
Thalassiosira gracilis var *gracilis*	8-13	3-4	3	122-535	17-21	10-100	I001
Thalassiosira lentiginosa	24-41	8-9	4	3385-5332	214-734	271-286	I001, I004
Thalassiosira maculata	22	7	1	2711	181	N.R.	I001
Thalassiosira perpusilla	8-10	2-3	14	6-420	4-44	N.R.	I001, I002, I003, I004, I006, I007
Thalassiosira poroseriata	6	2	1	50	9	N.R.	I002
Thalassiosira symmetrica	17	6	1	1310	104	N.R.	I008
Thalassiothrix antarctica	N.R.	N.R.	N.R.	N.R.	N.R.	81-4832	I002, I005

Conclusion

A multi-variable approach, which combined an array of chemical and physical variables, was implemented in this study to account for phytoplankton community variability and to aid in the understanding of associated *in-situ* environmental conditions. Phytoplankton communities in this study were found to vary both spatially and temporally, with variability driven by a combination of biogeochemical variables. The Polar Front proved to be an important biogeochemical boundary in both summer and winter waters, separating silicic acid replete diatom-dominated southern waters from northern waters associated with lower silicic acid concentrations and greater flagellate contribution. Such findings support the notion of studying waters of the Southern Ocean in terms of their associated oceanic zones due to large physical and environmental fluctuations between these regions.

Similarly, it was established that seasonality brought about large physical and environmental variations such as changes in temperature, macro- and micronutrient concentrations, water column mixing, light, and the depth of the mixed layer, which were found to shape the phytoplankton community. Environmental changes mentioned above exerted a strong influence on the phytoplankton community with seasonal shifts in community structure even a few months apart. The phytoplankton community was also shown to influence biogeochemical cycles, imparting distinctive macronutrient ratios in the water column. The intrinsic link between the phytoplankton community and nutrients is further demonstrated by an influx of micronutrients, which was linked to community diversification and could not be explained by macronutrient concentrations and physical variables. Studying a suite of trace metal distributions proved to be an important additional variable when considering phytoplankton variability, as certain metals seemed to be preferentially utilized, possibly driving underutilization of other metals. Furthermore, it allowed for the association of certain trace metals to phytoplankton groups e.g. Zn, Mn and silicic acid were strongly correlated in the water column suggesting simultaneous uptake of the two metals and silicic acid, most likely driven by a group such as diatoms.

Another important association established by this study was the inverse relationship between chlorophyll-a and biogenic silica in the winter period, which was attributed to the increasing southward abundance of heavily silicified diatom species as well as limited contribution to

chlorophyll-a from other phytoplankton groups in diatom-dominated waters. Heavy silicification is thought to be related to iron and light co-limitation, however, this is yet to be confirmed – pending the release of the trace metal dataset.

Further findings indicate low biomass in winter waters, although comparable to both summer and spring. This suggests seasonal variations in biomass may not be as great as previously thought, warranting further investigation. Such findings may have profound implications for biogeochemical models, which are typically bias toward summer and spring communities. The winter Antarctic zone was identified to have the highest nanophytoplankton biomass and was the most significant in terms of diatom distribution. In comparison to summer waters, such findings indicate that diatom community contribution is more important in the winter than the summer, while picoplankton contribution may be more important in summer waters. The low biomass phytoplankton community was homogenously distributed within the mixed layer as a result of a well-mixed water column typical of the winter period, while low biomass was associated with colder sea surface temperatures and limited irradiance, exacerbated by deeper mixed layers. This may have been intensified by widespread micronutrient limitation but will have to be confirmed in the future.

Recommendations for future work

Winter Cruise 2017 trace metal data are expected to be released shortly and will greatly compliment the work done in this study and may provide additional insights into silicification and the unusually low biogenic silica and chlorophyll-a concentrations encountered at St. IO03. Therefore, a recommendation from this study would be to couple trace metal data with observed chla and bSi concentrations. Unexpectedly high biomass in the winter season warrants future investigation as this may have important implications for biogeochemical models. As such, findings from this study have sparked an interest in coupling winter biogenic silica, chlorophyll-a and SEM micrographs from beneath the seasonal ice and may shed light on diatom silicification further south, it would be nice to see such a project come to fruition. In terms of future trace metal/phytoplankton work, trace metal isotopes are expected to be analysed and will greatly compliment the work already done in this study and more accurately infer biological uptake of

trace metals. Lastly, this study has highlighted the need to critically assess seasonal phytoplankton progressions and their associated environments. However, in the future, the same regions (sectors of the Southern Ocean) need to be compared to fully assess seasonal progressions.